Copyright Warning & Restrictions

The copyright law of the United States (Title 17, United States Code) governs the making of photocopies or other reproductions of copyrighted material.

Under certain conditions specified in the law, libraries and archives are authorized to furnish a photocopy or other reproduction. One of these specified conditions is that the photocopy or reproduction is not to be "used for any purpose other than private study, scholarship, or research." If a, user makes a request for, or later uses, a photocopy or reproduction for purposes in excess of "fair use" that user may be liable for copyright infringement,

This institution reserves the right to refuse to accept a copying order if, in its judgment, fulfillment of the order would involve violation of copyright law.

Please Note: The author retains the copyright while the New Jersey Institute of Technology reserves the right to distribute this thesis or dissertation

Printing note: If you do not wish to print this page, then select "Pages from: first page # to: last page #" on the print dialog screen

ABSTRACT

Quantitative Maesurement of Pyrolysis and Combustion Species Concentration by Molecular-Beam-Sampling-Mass-Spectrometry

by
Xian Zhong

A molecular-beam-sampling apparatus utilizing both a time-of-flight mass spectrometer with vacuum ultraviolet (VUV) photoionization and a quadrupole mass spectrometer with electron impact ionization is described. These systems are used to analyze reactants and products, as well as reactive intermediates, from flow tube experiments at reduced pressures and elevated temperatures. It is shown that the quadrupole signal sensitivity can be predicted using literature cross sections which are based upon the atom hybridization within the various molecules. Measurements of the VUV photoionization sensitivity for stable species led to development of a group additivity approach to predict cross sections. This approach was extended to reactive intermediates, and detailed comparisons of quadrupole and TOF data shows a very good agreement between the two techniques. The two techniques are compensation of each other and provide the full information we need. It is also shown how the minimal fragmentation achieved with the VUV source leads to much more accurate species concentration measurements for reactive intermediates.

Quantitative Measurement of Pyrolysis and Combustion Species Concentration by Molecular-Beam-Sampling-Mass-Spectrometry

by

Xian Zhong

A Thesis
Submitted to The Faculty of New Jersey Institute of Technology
in Partial Fulfillment of The Requirements for The Degree of
Master of Science
Department of Applied Physics
October 1992

APPROVAL PAGE

Quantitative Measurement of Pyrolysis and Combustion
Species Concentration by
Molecular-Beam-Sampling-Mass-Spectrometry

by
Xian Zhong

Distinguished Professor of Chemistry.
Dr. Bozzelli, Joseph W., Thesis Adviser
New Jersey Institute of Technology

Associate Professor of Physics
Dr. Chin, K.Ken, Committee Member
New Jersey Institute of Technology

Principal Investigator, Senior Research Chemistry
Dr. Anthony M. Dean, Committee Member
Exxon Research and Engineering Company
Annandale, New Jersey

BIOGRAPHICAL SKETCH

Author: Xian Zhong

Degree: Master of Science in Applied Physics

Data: October, 1992

Undergraduate and Graduate Education:

. Master of Science in Applied Physics, New Jersey Institute of Technology, Newark, New Jersey, 1992

. Master of Science in Physical Chemistry Graduate School, Dalian Institute of Chemical Physics, Academia Sinica, P.R. China. 1985

. Bachelor of Science in Physics Hebei University, P.R. China. 1982

Major: Applied Physics

Publication:

Xian Zhong "Measurement of Pyrolysis and Combustion Species Concentration by Molecular beam sampling with VUV Ionization / TOF and Quadrupole Mass Spectromric Analysis" Chemical and Physical Progresses in Combustion 1991 Fall Technical Meeting. The Eastern Section of the Combustion Institute. October 14-16

Xian Zhong "Quantitative Measurement of Pyrolysis and Combustion Species Concentration by Molecular beam Sampling Mass Spectromtry" accepted by J. Chemical Physics.

ACKNOWLEDGEMENT

The financial support for this work was provided by Exxon Research and Engineering Company. I also wish to thank my advisors, Dr. Anthony M. Dean and Prof. Joseph W. Bozzelli for their encouragement and guidance during my work in Exxon.

I also wish to thank Dr. R.L.Woodin for the early training in this research area.

I also wish to thank Professor Chin, K. Ken for his encouragement during my study in NJIT.

I particularly want to thank my friend, Dr. A. Paul, and Mr. S.Dougal, who helped in many ways, in both work and life. I hope our friendship can continue in the years to come.

I wish to thank my parents for their faith in my ability and their support and encouragement through all my life.

Finally, I wish to thank my family for putting up with the long hours and frustrated waiting over the past years. I hope I will be able to spend more time with Fun My only daughter. My wife, Ju, has been instrumental in this work. Without her love and support I would have never even attempted, much less completed, anything worthwhile in my life.

TABLE OF CONTENTS

LIST OF FIGURES

LIST OF TABLES

CHAPTER 1
INTRODUCTION

Complementary advance in theory and experiment as well as fast computer have provided significant new insights into the complex chemistry occurring during the high temperature pyrolysis and combustion. Examples of modelling successes include recent work in flames [1], engines [2] and pyrolysis [3]. Such detailed model are generally considered to be more reliable if they can successfully describe the behavior of reactive intermediates, since these are usually much sensitive to subtle details of the chemistry than either the reactants or products. In particular, accurate knowledge of the concentration-time profiles of these intermediates provide a rigorous test of the accuracy of the proposed kinetic model. We demonstrate methods for accurate determination of these (free radical) intermediates, as well as the stable species, in this paper. These data should allow further validation of detialed reaction mechanisms as well as provide key insights to reaction pathways. The elimination of post reactor-zone loss and surface artifacts on measurements of reactive species will also allow more accurate determination of species rate constants for important elementary reactions. A successful model can lead to pathways to improve a product yield or eliminate an undesired byproduct.

New laser-based optical probes [4,5,6,7] and molecular beam mass spectroscopic sampling techniques [8,9,10,11,12,13] allow precise measurement of reactive intermediate (i.e., free radical as well as reactive stable species such as epoxdes) concentrations.

Accurately quantifying stable species and free radical intermediates during pyrolysis and combustion is important because these intermediates are involved in many of the reaction steps, even through some radical concentrations are rarely exceed the o.1 percent level. Comparison between theoretical and experimental measurement provides an iterative route to meaningful rate constant and improved reaction models.

There are two common examples of most experimental kinetic studies. One type of chemical kinetic study in the literature utilizes a specific diagnostic technique e,g. laser fluorescence or absorption to monitor one specific radical or active species in a reaction system such as a flame, shock tube, tubular flow or photo chemical reactor. A second series of experimental measurements utilize similar reactors to those indicated as above but monitor only stable reactants, intermediates and final products.

Present modeling studies on the relevant reaction systems illuminate a number of significant problems associated with the different types of experiments. The monitoring of a single species, whether it be a reactive radical or important product / intermediates is that the concentrations of many important species are completely uncharacterized. The problem here is that significant interactions with species which are not monitored can occur and never be incorporated into the model.

The stable species monitoring experiments typically take the reactants our of the actual reactor environment, essentially quenching the reaction, where the active intermediates are completely lost. The radicals lost are frequently converted to stable

species, which are then incorrectly characterized as products or intermediates. This quenching occurs by reaction in the cooler zones after the reactor and in/on surfaces of a variety of sampling probes. These is very little which can be done in these classical experiments to preserve the integrity of the radical pool.

The problems with the monitoring of only stable products and intermediates are particularly harmful in the case of radical species which are relatively nonreactive, e,g. resonantly stabilized radicals, where their concentration can build up to significant level - similar to those of some the stable intermediates. Obviously this artifice can dramatically interfere with development of accurate mechanisms to model the reaction system.

This paper details the use and capabilities of a molecular beam mass spectrometer (MBMS) to study specific hydrocarbon pyrolysis reactions. The instrument design allows considerable flexibility in choice reactive system probed. Any reaction generating gas phase intermediates and / or products can be examined using MBMS techniques. The reactor and analytical equipment, which are constructed and operating, allow simultaneous monitoring of both stable intermediates and reactive species. In addition the species flow directly from the reactor through a molecular beam sampling interface to the dual mass spectrometer analyzers without collisions.

The major reasons for using mass spectrometric detection are the high sensitivity and universality. All atoms and molecules have a mass spectrum and thus can be identified. The electron impact (EI) quadrupole mass spectrometer has the advantage that the energetic

electron can ionize all the molecule with high sensitivity. The 70 eV electron impact ionization cross section is easy to calculate from the group theory and used to measure the relative concentration of various species in the mixture beam. On other hand, the high energy electron can easily break the molecular bonds and dissociate the large polyatomics to lower molecular weight fragments, which in turn can obscure the low concentration free radical at the same mass / charge ratio. If one species has no appreciable parent ion the whole data is ruined. The lost information make it impossible to quantitative determine the concentrations of all species in the mixture. This disadvantage can be compensated by the soft photoionization technique.

The vacuum ultraviolet (VUV) photoionization Time-of-Flight Mass Spectrometer system is highly sensitive to the radicals, olefins and arene species. In addition the photoionization technique is operated so that only the parent ions are formed from the radicals and stable species, [Fig. 1.1 a, b] which are subject to ionization at the energy of these photons. In the hydrocarbon pyrolysis and combustion reaction only high IP species such as OH, C2H2 and CH4 are undetectable by our vacuum ultraviolet (VUV 10.5 eV) photoionization Time-of-Flight Mass Spectrometer. However these lost information are provided by the conjugate quadrupole mass spectrometer. The relative 118.2 nm photoionization cross section of radicals are not in the literature. This is the major motivation of this work. We have determinate the ionization cross section of gas phase olefins and small hydrocarbon radicals and assigned the

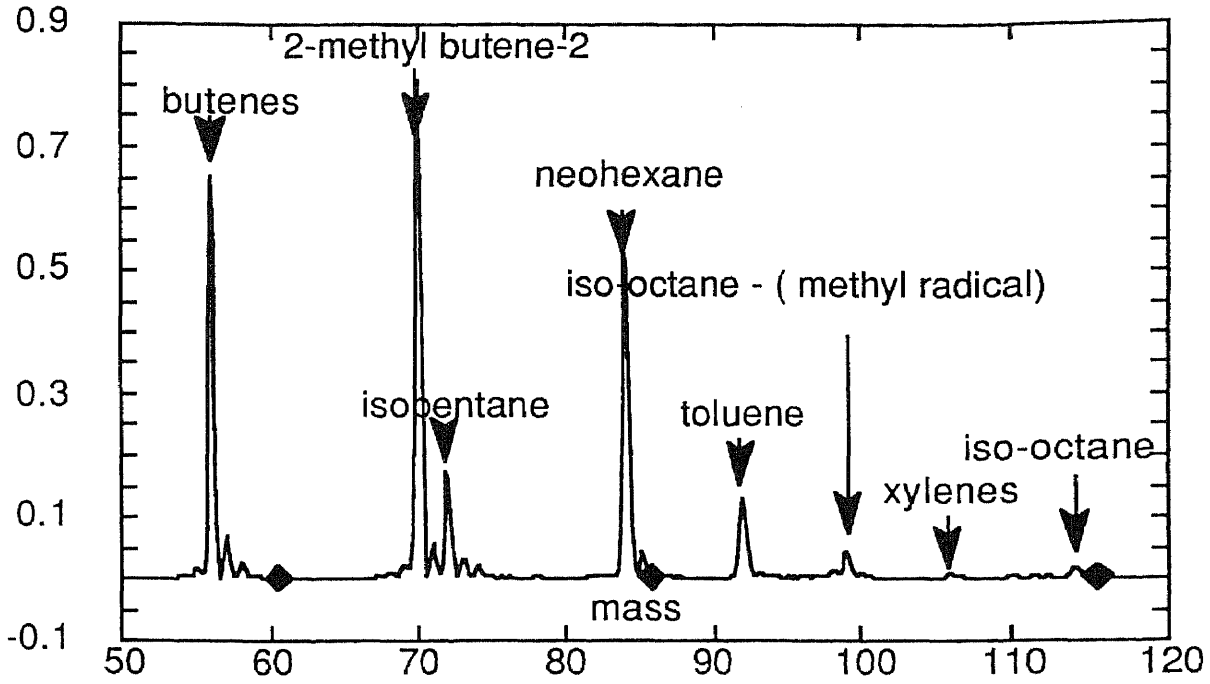

Fig.1.1 a Fuel HC-2 VUV (10.5 eV) photionization TOF spectrum

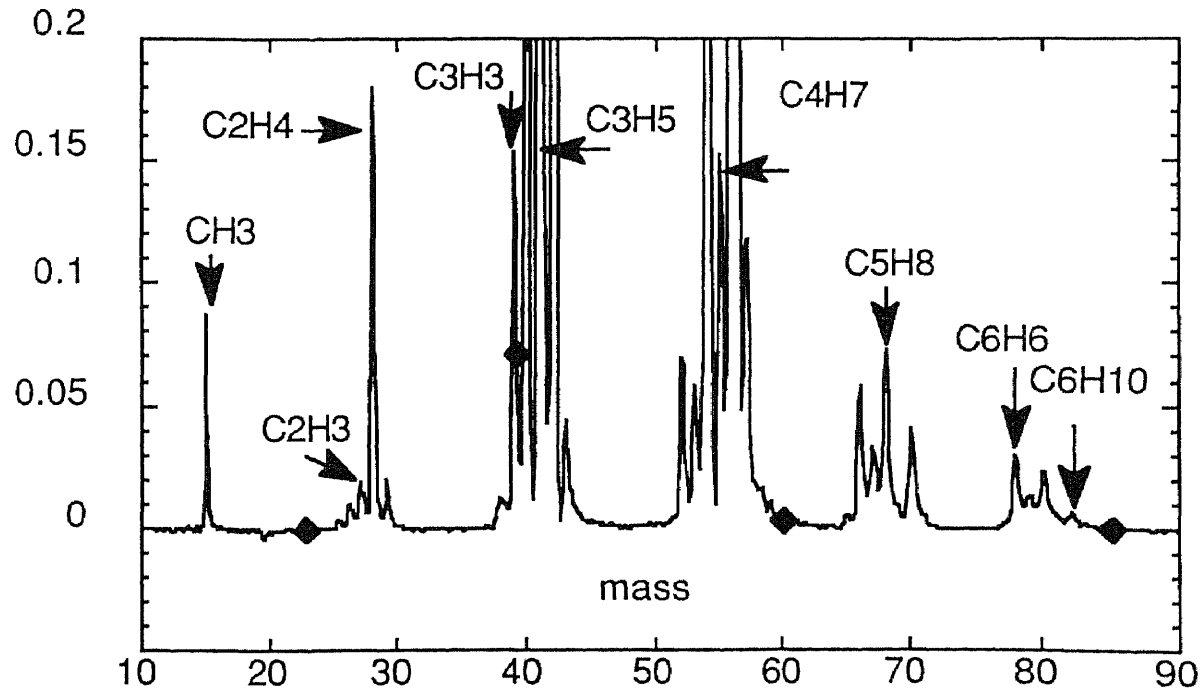

Fig.1.1 b 1-butene pyrolysis products at 1331K 10 Torr in Sapphire reactor

coefficient of unpaired 2p electron on the carbon atom as well as the hybridization groups to the total ionization cross section.

CHAPTER 2
DESCRIPTION OF APPARATUS

Our Molecular Beam Mass Spectrometer, MBMS is designed to measure radicals and stable species in an on-line molecular beam sampling which being exstracted from high temperature reactors. This MBMS was build up in Exxon research and engineering company in 1984. In this work, we added a new design of tubular reactor and an 118 nm laser-based VUV light source. The quadrupole mass detector and VUV photonionization time-of-flight, TOF detector work together as an hybrid mass spectrometer to obtain the whole information we need in hydrocarbon pyrolysis and combustion reactions.

The following description is intended to serve both as an introduction of this apparatus and its fundamental properties as well as a " road map " for a possible user of this instrument.

2.1 Overall Description

A schematic of the molecular beam mass spectrometer (MBMS) is shown in Fig.2.1 The system consist of three vacuum chambers. According to their working function we distinguish them as source chamber, Time-of-flight (TOF) chamber and Quadrupole (Quad.) chamber. The low pressure gas flows though a high temperature, short residence time tubular reactor and expands into the source chamber forming a free jet. The core of this jet is selected by a conical skimmer mounted between source chamber and TOF chamber.

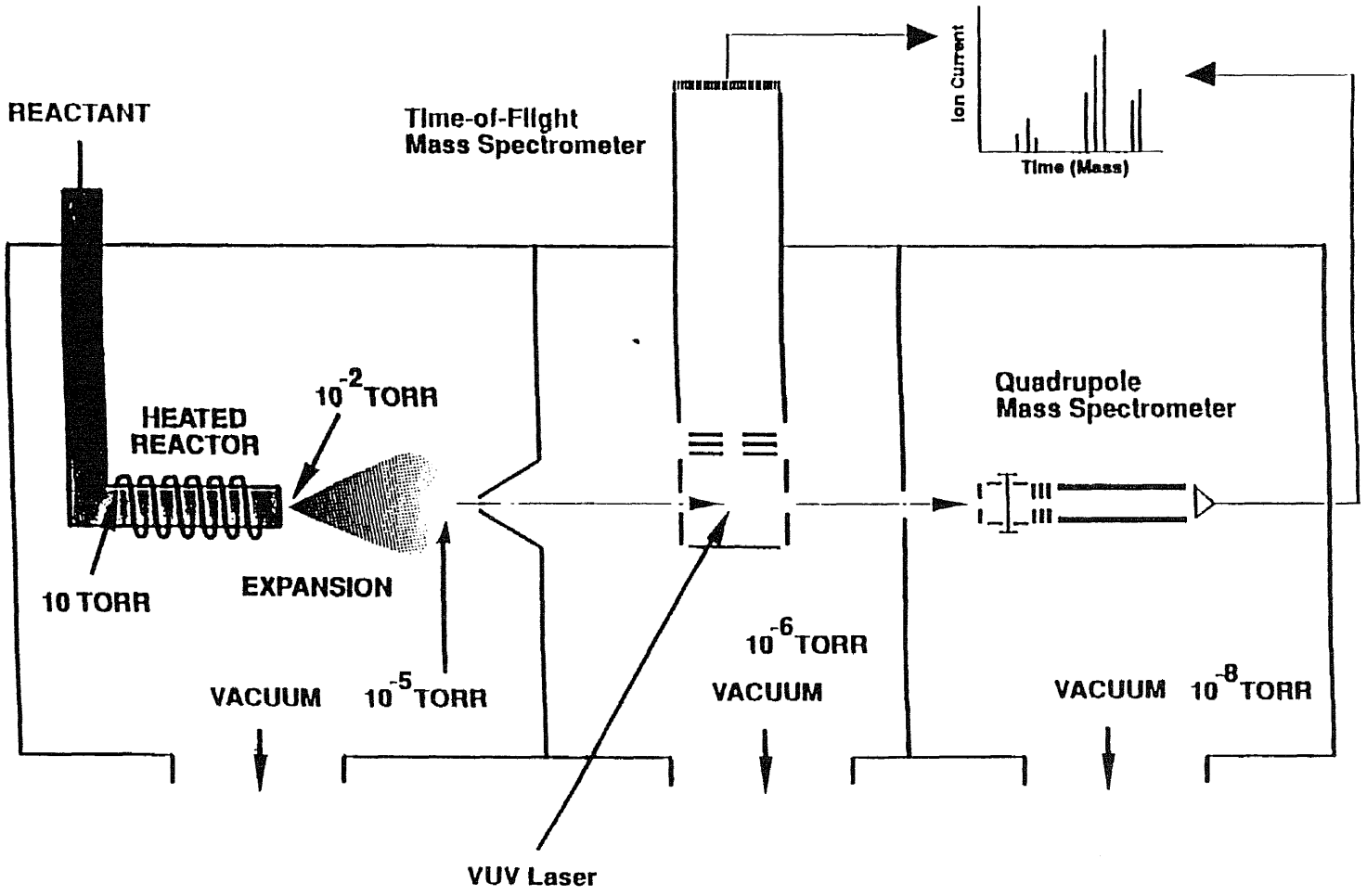

Fig. 2.1 A hybrid molecular beam mass spectrometer MBMS

The resulting molecular beam enters the TOF chamber and Quad. chamber for diagnosis. In TOF chamber the beam is crossed with VUV light beam in the preacceleration zone and the produced ions are separated and detected by TOF mass spectrometer according to their mass. The molecular beam continue reaches to Quad. chamber for simultaneous analysis by a quadrupole mass spectrometer. Both of these two data sets are collected by computer controlled programs.

2.2 Source Chamber

The source chamber is pumped by a VHS-10 diffusion pump (Varian Inc) and a roughing pump (Welch 1375). Because the reactor is directly open to this chamber 99% gas flow is pumped out from this chamber. To maintain a 10^{-4} Torr operating pressure in this chamber with the maximum pump speed 5000 L/s of diffusion pump VHS-10 the maximum gas flow rate is about 60 sccm. The pressure in the foreline is monitored by a thermocouple vacuum gauge and the pressure in the chamber is monitored by a cold cathode vacuum gauge (TPG 300 Blazers Inc) and an ionization gauge. When the gas flow is shut down this chamber can be pumped to 3×10^{-7} Torr. We usually use 6 to 20 sccm total flow rate which gives a 4×10^{-5} Torr background pressure in the source chamber. This high vacuum is a critical condition for free jet formation.

2.3 Mass Flow Control and Pressure Measurement of Reactor

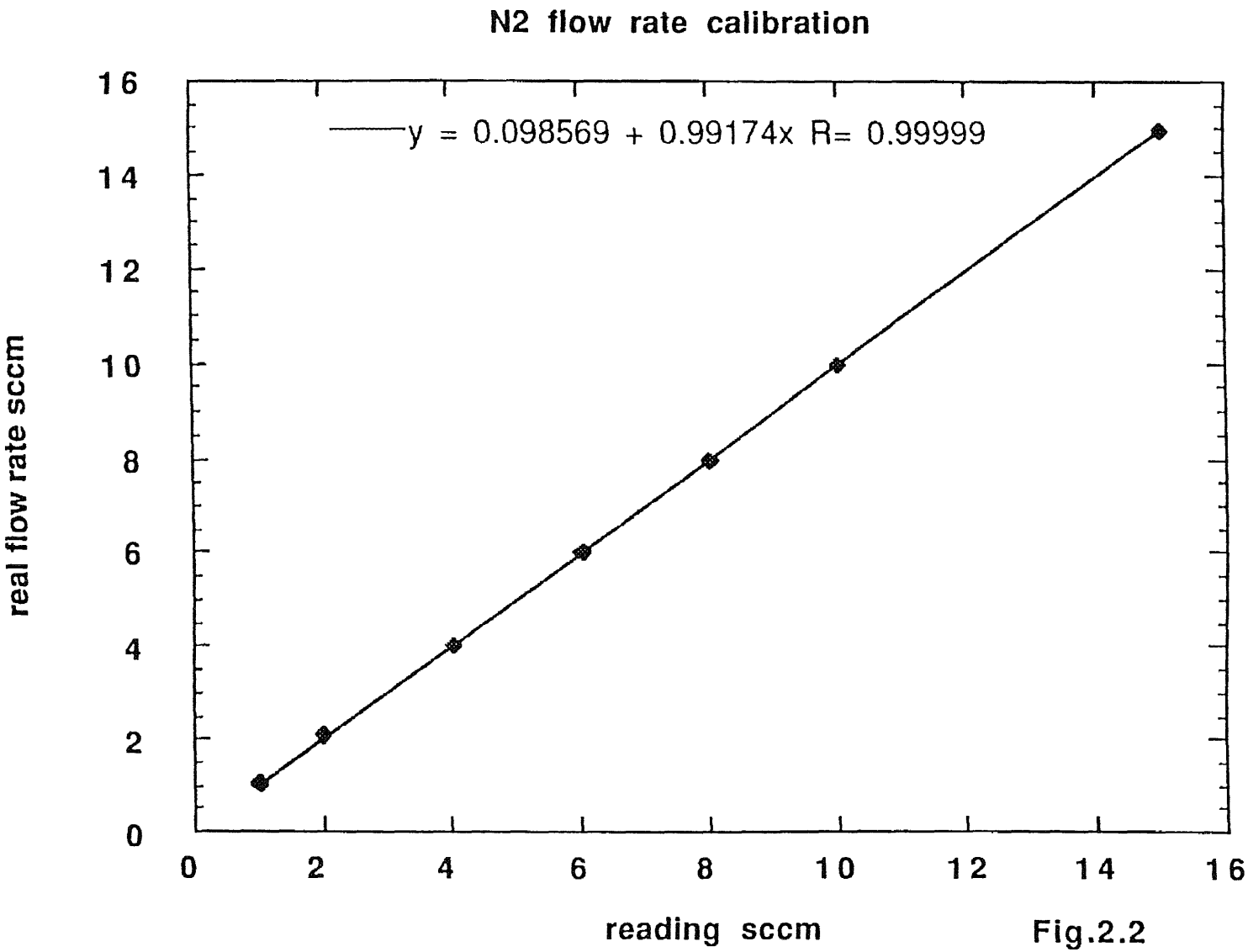
N2 flow rate calibration
y = 0.098569 + 0.99174x R= 0.99999
real flow rate sccm
reading sccm
0
2
4
6
8
10
12
14
16

Fig.2.2

The gases are fed through a digital mass flowmeter (MKS Inc) and mixing tee. The gases are fully mixed before feeding into reactor. The mass flowmeters are adjusted and recalibrated every three months or before the multicomponets experiment by a saop bubble flow meter according to its manual. Water pressure is take into account.

$$Q = Q_m (P_r - P_{H2O}) / P_r \qquad \text{Eq 2.3.1}$$

But the deviation is still present between individual flowmeters. The major reason of this deviation is the Gas Correction Factor which is dependent on the molecular heat capacity and temperature. However the estimated maximum uncertainty is about 5%. Using nitrogen as calibration gas we get a good agreement between reading and real flow rate FIG.2-2. For multicomponents experiment we directly calibrate the individual gas flow rate. The pressure of gas in the pipe line is monitored by manometer (MKS Baratron) at two points, one point is just behind the reactor and the second point is far away from the reactor. The pressure drop between these two point is very small. With a constant flow rate the pressure increases with the reactor temperature.

2.4 High Temperature Small Tubular Reactor

For many years high temperature flow reactor have been widely used on simple reaction systems for obtaining kinetic data [14, 15, 16, 17]. We use the similar reactor as molecular beam source to study

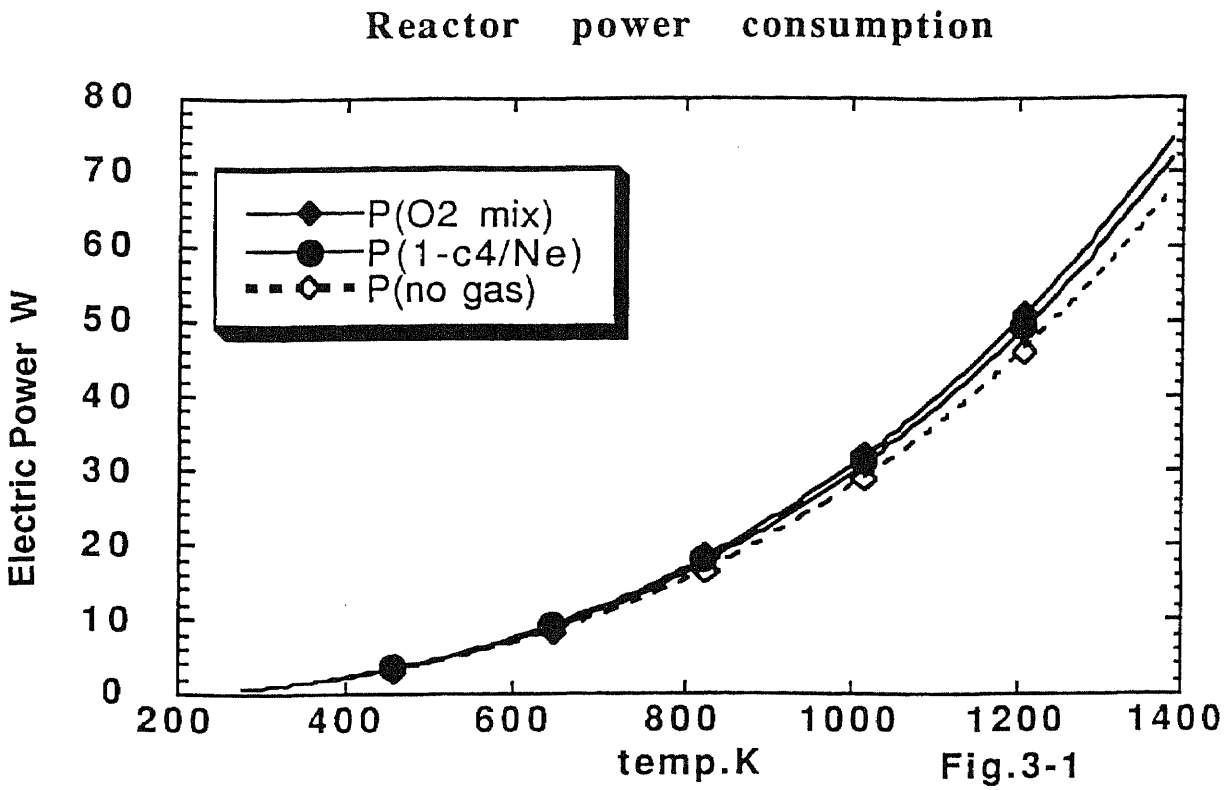
Reactor power consumption
Electric Power W
80
70
60
50
40
30
20
10
0
200
400
600
800
1000
1200
1400
temp.K
P(O2 mix)
P(1-c4/Ne)
P(no gas)

Fig.3-1

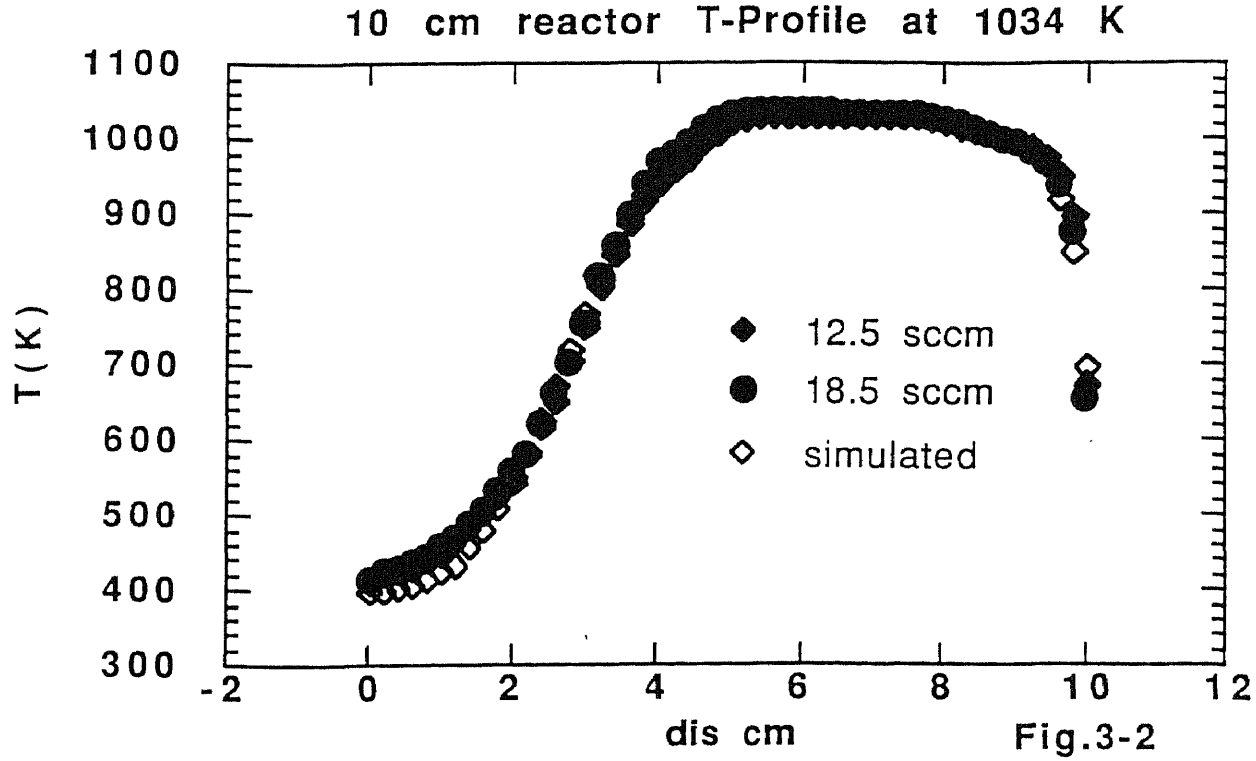
10 cm reactor T-Profile at 1034 K
T(K)
1100
1000
900
800
700
600
500
400
300
-2
0
2
4
6
8
10
12
dis cm
12.5 sccm
18.5 sccm
simulated

Fig.3-2

the pyrolysis reaction and oxidation of hydrocarbons. A typical pyrolysis process will accur in a 500 K temperature interval around 1200 K in a couple of millisecond time scale. This short resident time, low pressure flow tubular reactor as molecular beam source is favorable to preserving reactive intermediates which are very important to explain the whole reaction mechanism. The basic idea is that the mixture gas was heated up rapidly to a high temperature level in a well known dynamical properties flow tube, chemical reaction take place in the high temperature region within a couple of ms and when the mixture expands along the reactor, the reaction is slowed down because the collision frequency is reduced with the pressure drop. In the vacuum chamber there are no collision in the molecular beam thereby freezing all reactants, products and intermediates. Molecular beam sent this sample into mass spectrometer for analysis. This sample is a good representative of mixture at the end of the reactor. Surface effect can be studied by using different material reactors.

A theory of subsonic compressible flow in a small tubing is well known. G.Rotzoll [18, 19] presented this theory with friction, heat transfer and chemical reaction kinetics and bring it into a suitable form for numerical calculation. He shows a good agreement between theory prediction and experimental results for small diameter reactor (ø 0.02 cm) and a appreciable temperature lag for larger diameter reactor (ø 0.05 cm).

Hydrocarbons pyrolysis reaction produce a lot of soot which were easily block small diameter reactor. This situation forced us to looking for a cheap and larger diameter reactor.

2.4.1 Tubular Reactor

Our tubular reactors are made by alumina, quartz and sapphire tubing with the length, diameter ratio about 70. The heating region is about 75% of total reactor length. The unwired end is mounted in a stainless steal union to connect with inlet gas system. The diameter of these reactors are ø 0.75 , ø1 and ø1.5 mm. With tungalloy heating wire these reactors can heat up to 1400 K.

2.4.2 Temperature Profile

The heat balance was set up by the radiation heat loss, reactor material heat transfer and electric heat power. The heat carried out by the gas flow was negligible for small gas flow rate Fig.3-1. Typically the gas may carry out less than 5% total electric heat power and this only effect the rising edge of reactor temperature profile Fig.3-2. We have measured the temperature profile at various reactor temperature T_r for alumina and sapphire reactors. From these experimental results we find out that if we start from a typical temperature profile which has a reactor temperature T_{ro} at 1000 K , then we can generate other temperature profile at other reactor temperature Tr by the formula :

$$T(T_r,x) = 300+(T(T_{ro},x)-300)*(T_r-300)/(T_{ro}-300) \quad \text{Eq 2.4.2.1}$$

where 300 K is the room temperature, or initial gas temperature. we choose 1000 K as reference temperature because it nears pyrolysis

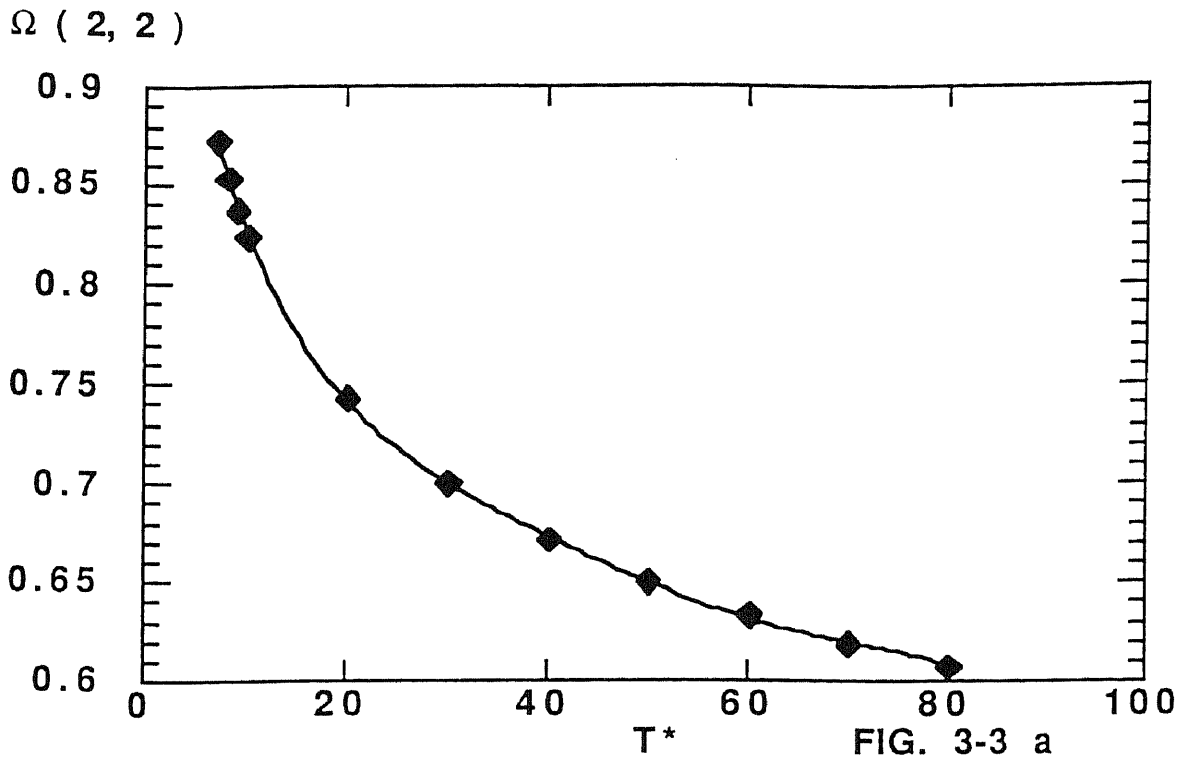

FIG. 3-3 a

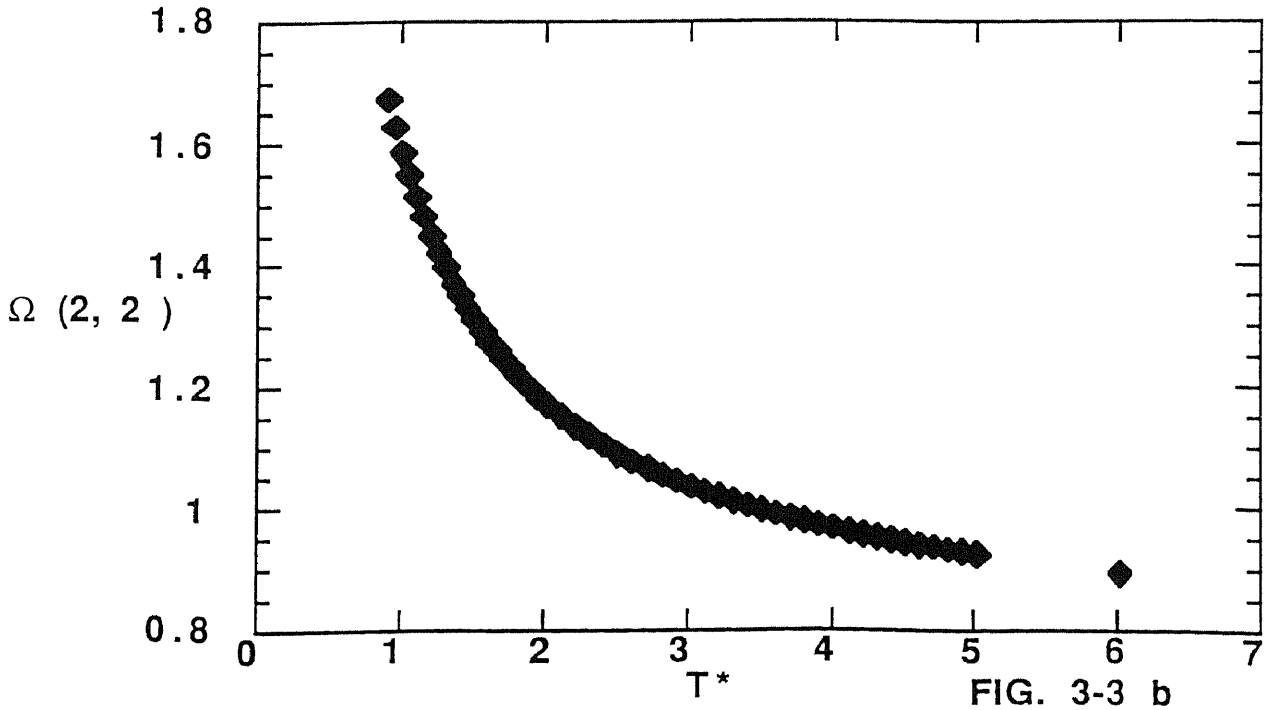

FIG. 3-3 b

temperature of butenes. Fig.3-2 . This reactor has a good behavior of temperature profile, a rapid heating up part , a flat high temperature plateau and drop down exit. A simulated temperature profile can macth experimental data very well.

When $x < 7.55$ cm

$$T(x) = (0.0507675Tr/D-1.65/D)\ \exp(-((x-2.8)/10\ D)^2) \quad \text{Eq 2.4.2.2}$$

with a boundary condition $T(7.55) = Tr$

When $x > 7.6$ cm

$$T(x) = (0.00015\ Tr + 0.1002)\ Tr/D\ \exp(-((x - 10.48)/0.64)^2) - 0.033925\ Tr + 9.244 \quad \text{Eq 2.4.2.3}$$

This analytic-function and it's derivative are used to calculate the reactor dynamics properties.

2.4.3 Tubular Reactor Dynamics Properties

Reynolds has found that if the dimensionless quantity $Re = (D\ v\ ) /(\pi\ \mu\ )= 4m'/(\ \pi\ D\ \mu)$ is less than 2000 the flow is in stable state and be defined as laminar flow. For the given components mixture gas we can choose the mass flow rate and reduce the Reynold number less than 20. Although the developed laminar flow has radially nonuniform flow velocity, it is a good practice to use the radially averaged temperature, concentration and velocity as laminar flow

dynamics properties in small diameter tubing and treated it as one dimension compressible flow. Starting from the conservation equations of total mass flow, momentum, energy and individual species, G. Rotzoll gives a mach number equation for the fully developed laminar flow .

$$dM/dx = rM^3/(M^2-1)\ f/D\ (\ (r-1)^2M^2\ \ (T-1)/Cp*dCp/dT+2*(1-M^2)/(1-rM^2)) + (\ 2/(1-rM^2)+(r-1)/Cp*dCp/dT\ -1)M/2\ \ dT/dx/T \qquad \text{Eq 2.4.3.1}$$

where M is the mach number, x the axial coordinate, r the specific heat ratio, T the absolute temperature, Cp the heat capacity, f denote the friction coefficient and D the tube diameter. The temperature profile is known from the experiment as a function of axial coordinate and the various independent quantities appearing in the equation can be calculated as the function of axial coordinate and averaged temperature by the following algebraic relations.

$$Cp = \Sigma\ n_j\ Cp_j \qquad \text{Eq 2.4.3.2}$$

where n_j is the mole fraction of i'th species in the mixture, Cp_j is the heat capacity of i'th species in the mixture and a function of temperature best fitted by a polynomial, for hydrocarbon the heat capacity is given by group additivity theory.

$$r = Cp/\ (\ Cp - R\ ) \qquad \text{Eq 2.4.3.3}$$

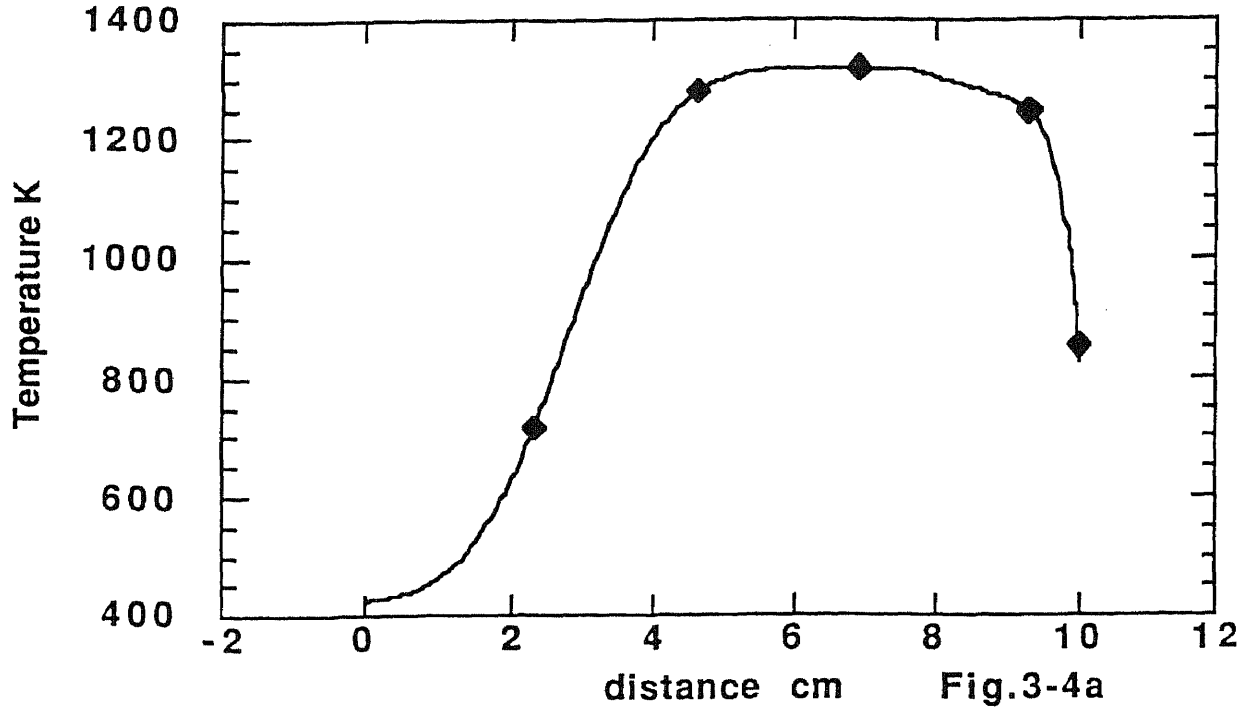

Fig.3-4a

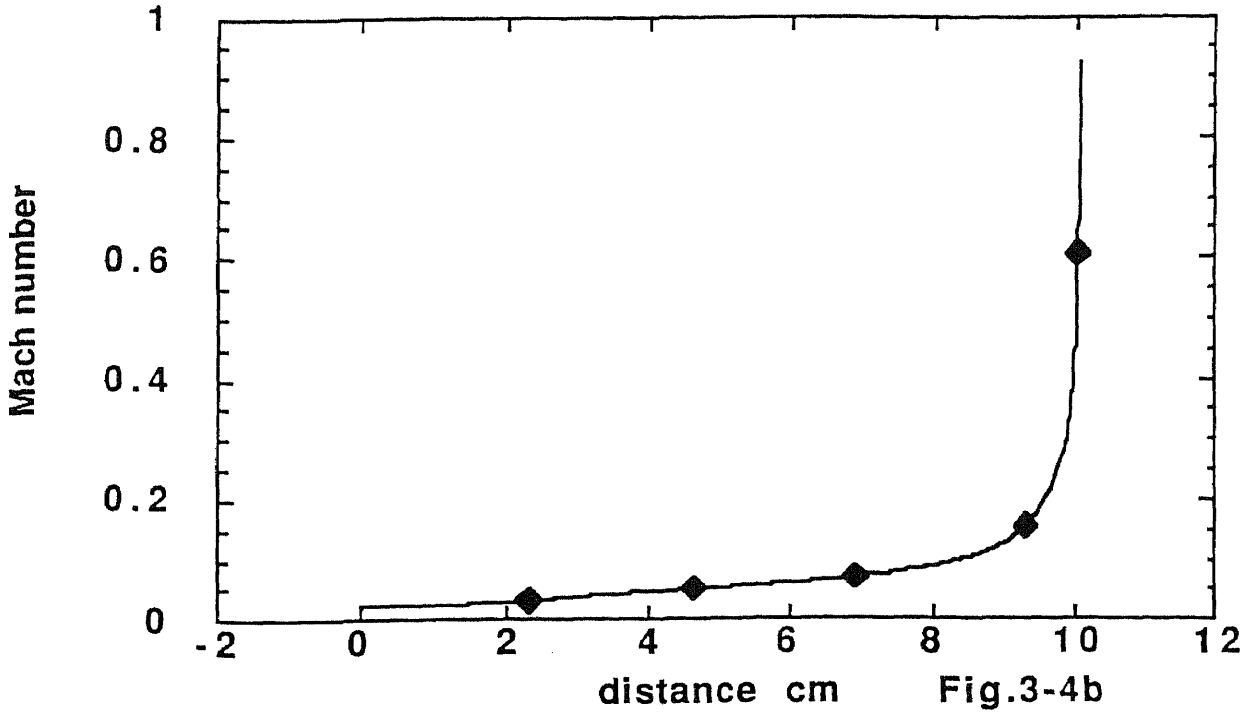

Fig.3-4b

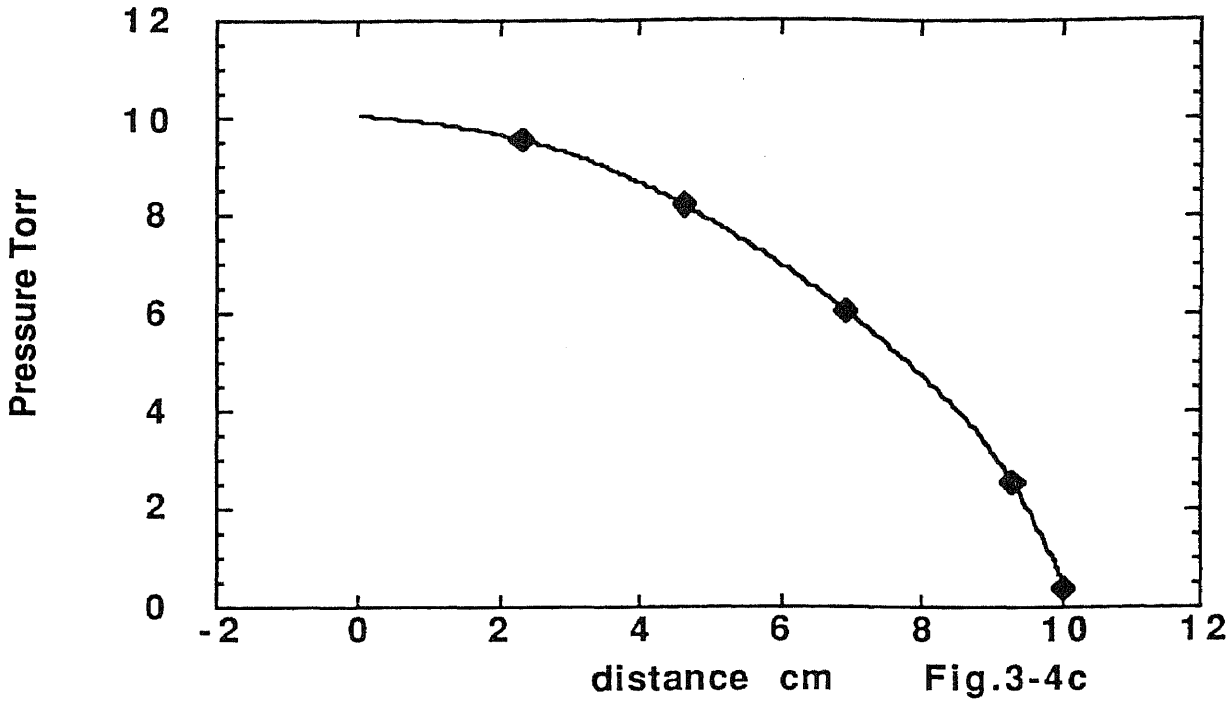

Fig.3-4c

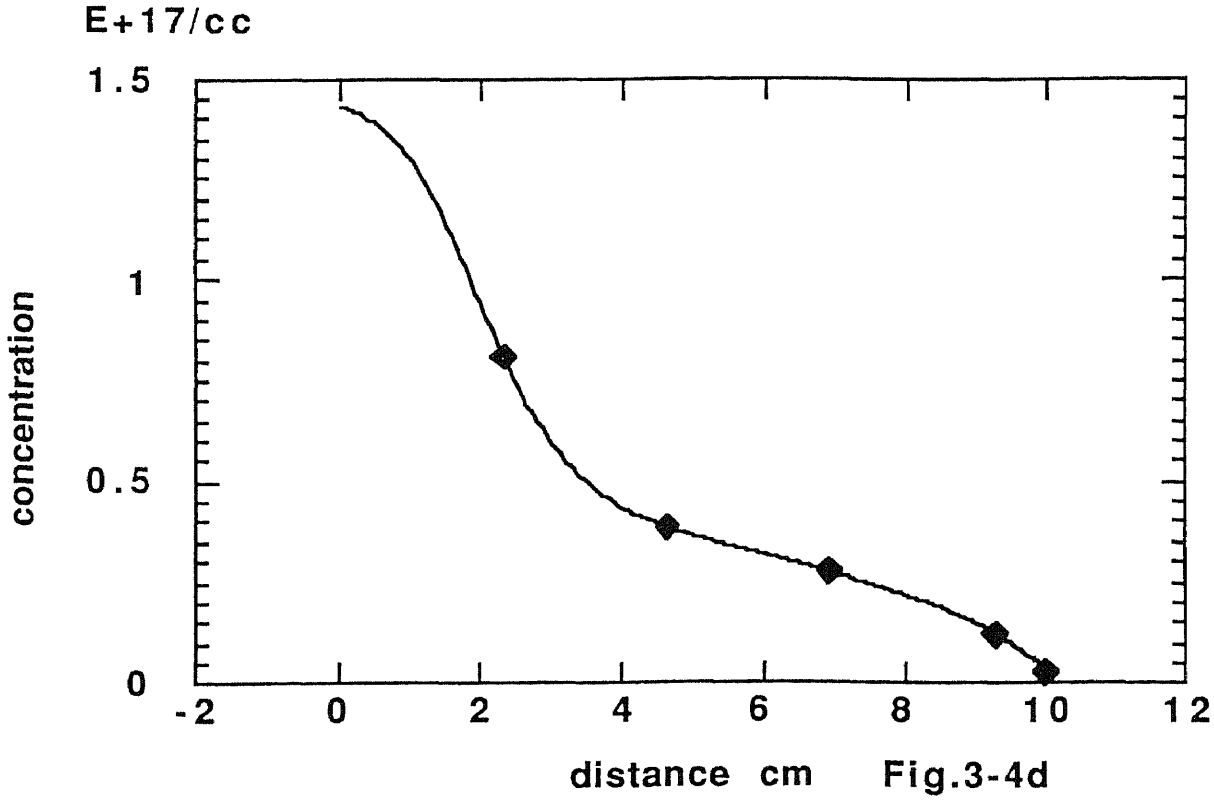

Fig.3-4d

12 sccm Ne/1-butene flow residence time via reactor temperature

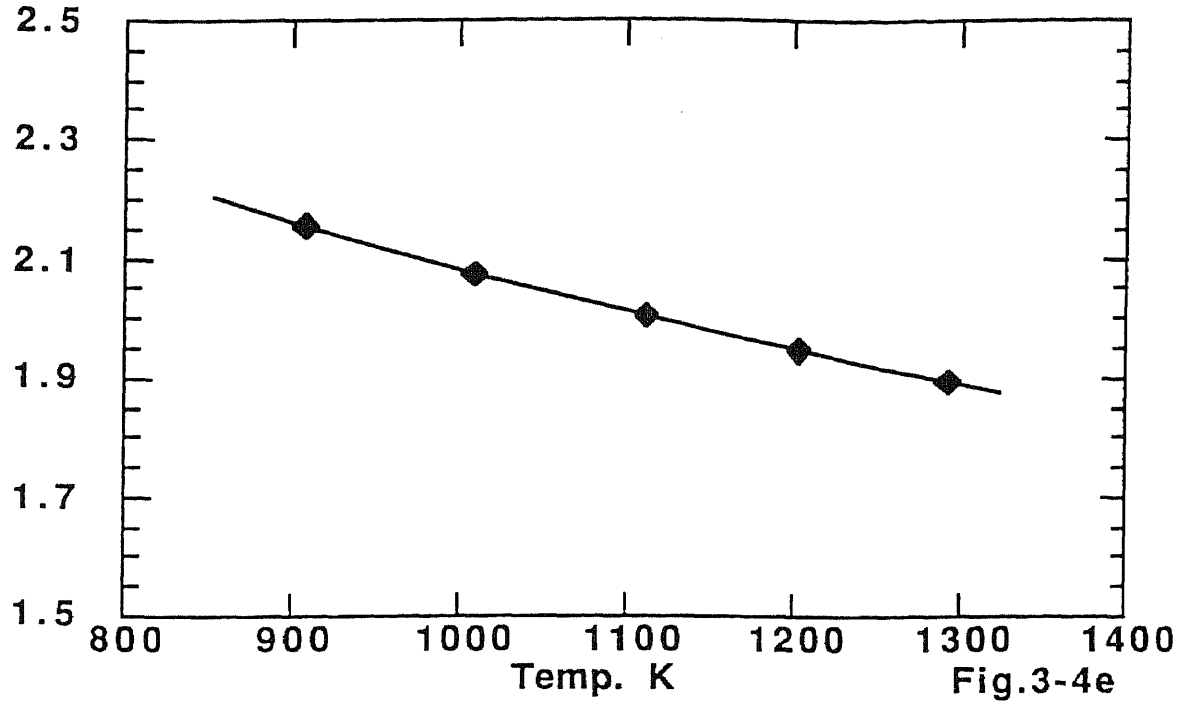

Fig.3-4e

12 sccm Ne/1-butene flow average pressure at reaction zone

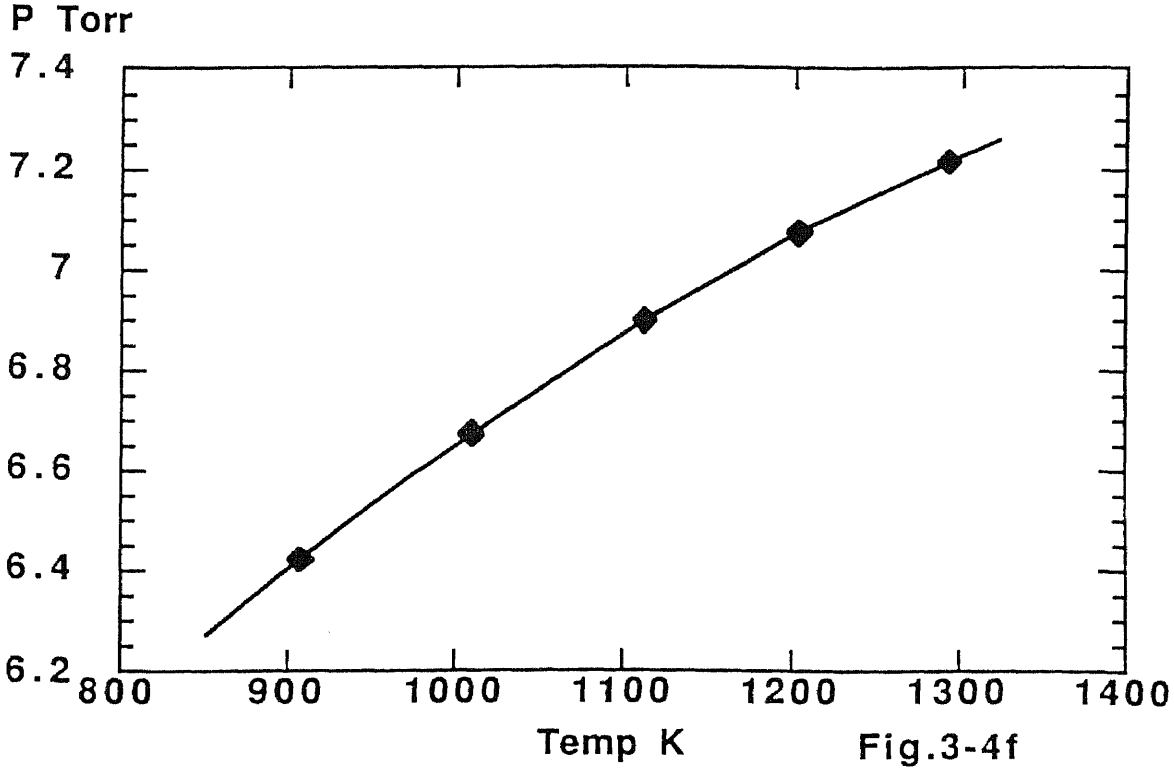

Fig.3-4f

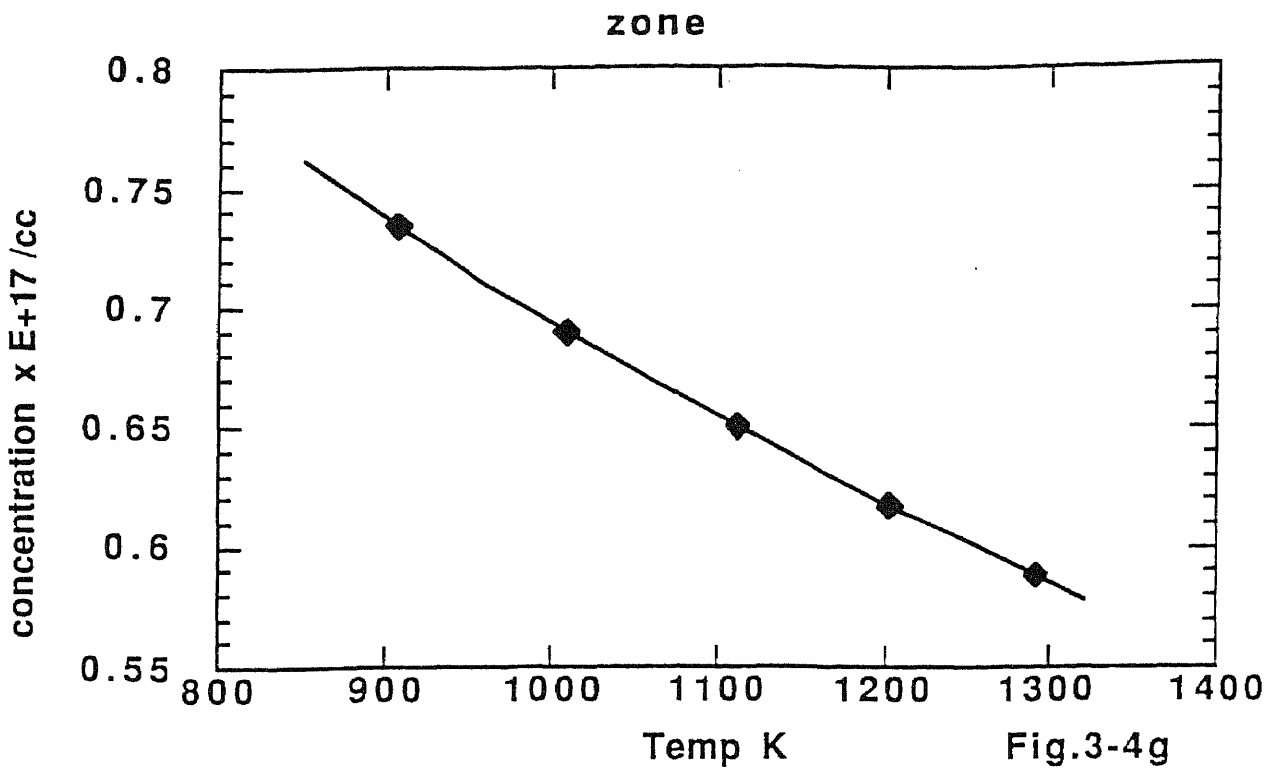

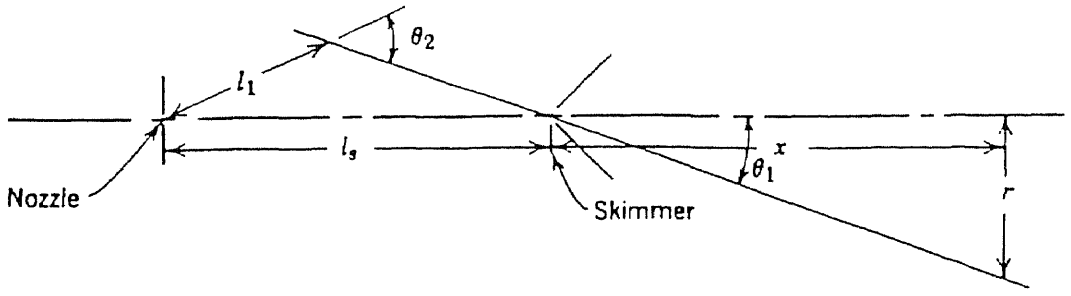

FIG.3-5 Schematic diagram indicating the geometry and dimensions used in the development of expression for theoretical intensity.

This is the mixture specific heat ratio.

For the fully developed laminar flow, the friction coefficient is given by

$$f = 16/Re = 4\pi D\ \mu\ /\ m' \qquad \text{Eq 2.4.3.4}$$

or more convenient form

$$f/D = 16/ReD = 4\pi\mu/m' \qquad \text{Eq 2.4.3.5}$$

here m' is the total mass flow rate and μ is the mixture viscosity. Because there is no completely rigorous computational scheme to calculate the multcomponent viscosity. We simply use the algebraic mean.

$$\mu = \Sigma\ ni\ \mu i \qquad \text{Eq 2.4.3.6}$$

and the μi is easy to find from other literature.

$$\mu i \times 10^6 = 26.69 \times \text{sqrt}\ (\ Mi\ T\ )\ /\ \partial^2\ \Omega i\ (2,2\ ) \qquad \text{Eq 2.4.3.7}$$

where the ∂ is the collision diameter in angstroms, and the Ωi (2,2) is the reduced collision integral. These integrals in turn dependent upon the intermolecular forces of the gas molecules, so that the potential energy of interaction of colliding molecule must known. Lennard-Jones (12-6) potential was used to get a tabulated collision integral as a function of reduced temperature.

$$T^* = T / (e/k) \qquad \text{Eq 2.4.3.8}$$

where k has is regular meaning and e is the well depth in Lennard-Jones (12-6) potential.

$$ø (r) = 4 e ((∂/r)^{12} - (∂/r)^6) \qquad \text{Eq 2.4.3.9}$$

For the different reduced temperature intervals we use polynomial to fit the collision integral. FIG.3-3a, b.

However the deviation of viscosity from it algebraic mean is expected, and can be used to judge the entrance pressure Pe do not violate the pressure drop in the upstream inlet pipe. The mach number differential equation is solvable by numerical method under boundary conditions.

At the exit the tube is open to very low pressure vacuum chamber the flow is choked and the mach number is reach to unity. At the inlet, on other hand, there is a unlaminar flow region because the pipe cross section change. the distance of the laminar flow redeveloping is the order of

$$x \approx D/20 \text{ Re Pr} \qquad \text{Eq 2.4.3.10}$$

Pr is the Prandtl number ($Pr = \mu Cp / k$) For gases this number is about unity. When Re is less than 20 this distance is the same order as the tube diameter. But the uncertainty is still present and leave the initial mach number be determined only by the mach number equation and exit boundary condition.

$$Me = v/v_s = 4\ m'/\pi\ D^2\ R\ T_e / P_e M_w\ (r\ R\ T_e / M_w)^{-1/2} \quad \text{Eq 2.4.3.11}$$

This parameter is understood as the interpolation result. The physical meaning of this parameter is that the turbulence flow changes the mach number . This data will be used to calculate the density distribution in the reactor, which obey the differential equation :

$$dç/dx = ç\ (\ 2\ r\ M^2\ f\ /\ D + dT\ /\ dx\ /\ T\ )/\ (\ r\ M^2\text{-}1) \quad \text{Eq 2.4.3.12}$$

the boundary condition is $ç_e = m'/(\ A\ vs\ Me)\ To/Te$. vs is the local sound speed and A the cross section of reactor. The axial velocity and radially averaged pressure distribution along the reactor are given by the ideal gas law and the definition of the mach number.

$$V(x\ ) = (\ r\ R\ T/\ M_w)^{1/2}\ M \quad (\ R\ 8.31441x10^7\ erg\ K^{-1}\ mol^{-1}\ ) \quad \text{Eq 2.4.3.13}$$

where the M_w is the mole weigh of the mixture and given by the arithmetic formula

$$Mw = \Sigma\ ni\ Mwi \quad \text{Eq 2.4.3.14}$$

Pressure distribution is

$$P(x\ ) = ç/Mw\ RT \quad \text{Eq 2.4.3.15}$$

because the density is given by g/cc and the pressure given by the

Torr the union transfer factor is need and the equation become

$$P\ (\text{Torr}) = \rho\ (\text{g/cc}) / M_W(\text{g}) \times 7.6 \times 10^5 \times RT \qquad \text{Eq 2.4.3.16}$$

$$R = 0.082$$

A simple program in Excel is written to calculate the Mach number profile, pressure drop distribution, residence time, average pressure and density under operating conditions [FIG.3-4 a, b, c ,d]. Residence time and average concentration are temperature dependent. [FIG.3-4 e, f,]

2.4.4 Molecular Beam Sampling

Molecular beam sampling technique is used to transfer the mixture from the low pressure flow reactor to the detector without further collisions. It is well known that the dynamical properties of a molecular beam are dependent on the beam source, nozzle geometry and beam forming condition. Our molecular beam apparatus is a nozzle-skimmer beam system, FIG.2-1. Collisions on the downstream of the skimmer is negligible because the pressure in this TOF chamber is around 10^{-7} Torr (l = 1000 m). The molecular beam dynamic properties are simply determined by the density and velocity distribution of free jet at the skimmer entrance [20]. In the following treatment we will neglect the collision between the jet and background molecules in the source chamber and the reflected molecules from the skimmer surface. This assumption is

true as long as the pressure in the source chamber is lower than 10^{-4} Torr (l = 1 m) and use special designed skimmer. Kantrowizt and Grey [21] assumed the thermal velocity distribution in the jet is given by the equation ;

$$dn = n \left(m/2\pi kT \right)^{3/2} \exp\left(-m/2kT \left(v-u \right)^2 \right) d^3v \qquad \text{Eq 2.4.4.1}$$

where n,T and u are the density, translation temperature and beam velocity. m is the mass of a molecule, k is the boltzmann constant and v the molecular therm velocity. In the nozzle beam n, T and u dependent on the extent of expansion of the free jet before the skimmer. If the density in the jet become low enough, the jet will transit to a free molecular flow before it reaches to the skimmer. The transition distance L_1 is dependent on the pressure drop at nozzle region. With the help of geometry lengths and angles defined by the FIG 3-5. The theoretical flux of a molecular beam through an orifice coaxial with free jet is given by the equation

$$I(r,x) = n_1 \pi rs^2 \left(m/2\pi kt_1 \right)^{3/2} \int \exp\left(- m/2kT[\left(v-u\cos \phi_2 \right)^2 + u^2 \right.$$

$$\left. \sin^2\phi_2]\right) v^3 \, dv \cos^4\phi_1 / x^2 \qquad \text{Eq 2.4.4.2}$$

$$\sin\phi_2 = L_s/L_1 \sin\phi_1 \qquad \text{Eq 2.4.4.3}$$

The integral was carried out by J.B.Anderson [20] and on the beam axial the beam flux is given by

$$I = n_s (r_s/x)^2 u (L_s/L_1)^2 (r M^2 + 3)/2 \qquad \text{Eq 2.4.4.4}$$

For the adiabatic free expansion the jet velocity and density are given by

$$u(z) = [2 r /(r-1) k / m (T_n - T)]^{1/2} \qquad \text{Eq 2.4.4.5}$$

$$n(z) = N_n (D_n/L_z)^2 (2/(r+1))^{(1/(r-1))} ((r-1)/(r+1)^{1/2} (T_n/(T_s-T))^{1/2}$$

plug in the beam flux equation Eq 2.4.4.4 we get

$$I (r=0,x) = N_n [rkT_n/m]^{1/2} (D r_s/L_1 x)^2 (2/(r+1))^{(1/(r-1))} (2/(r+1))^{1/2} (r M^2 + 3)/2 \qquad \text{Eq 2.4.4.6}$$

where N_n is the density at nozzle and T_n the nozzle temperature. For a fully developed laminar flow it's mach number will reaches to unity at reactor exit and it's temperature profile shows a rapid temperature drop at nozzle region ΔL = 2-3 D , which indicate a fast gas expansion. This expansion is truly a adiabatic free expansion. The beam flux equation is valid for our molecular beam. The beam velocity at the nozzle is the local sound velocity $V_s = (rkT/m)^{1/2}$ as the basic assumption of laminar flow in a tubular reactor. We can rewrite this equation for experiment convenience;

$$I (x) = m'/ç /x^2 F (r_s, D, P, r, T) \qquad \text{Eq 2.4.4.7}$$

where m' is the total mass flow rate ç is the flow density and x is the distance from skimmer to the detection point. F () is a function of beam system geometry and the laminar flow dynamic properties. This simplified model can serves as a convenient standard by which to judge the actual behavior of real beams. Because the laminar flow expand into the vacuum chamber, the flow tube in the jet is like to be laminar flow, so the molecular beam will be a homogeneous beam, the mole fraction in the beam is a true reflection of the flow rate in the reactor. However the real molecular beam properties will be only revealed by the experiment.

2.5 TOF Mass Spectrometry

Photoinization time-of-flight (TOF) mass spectrometer is mounted in the second vacuum chamber, in which the operating pressure is less than 10^{-6} Torr. This apparatus consist of a short puls VUV light source, VUV photogalvanic detector, photoinizer, acceleration electrodes assembly, free drift tube and microchannel plate detector. A fast preamplifier provides an addition gain of 10 to the TOF signal. The TOF signal was recorded by a transient waveform recorder Biomation 8100 with the dwell time of 10 ns per channel. The real time base data was sent to a Macintosh computer and corrected by the VUV photon flux fluctuation signal monitored from photogalvanic cell shot by shot. The detection sensitivity is about 10^8 molecules per cubic centimeter and the resolution is about 300 at M/e = 128 and the relative fluctuation is less than 5 % after 50 shots average FIG.4-1a. Because the VUV laser pulse width is about

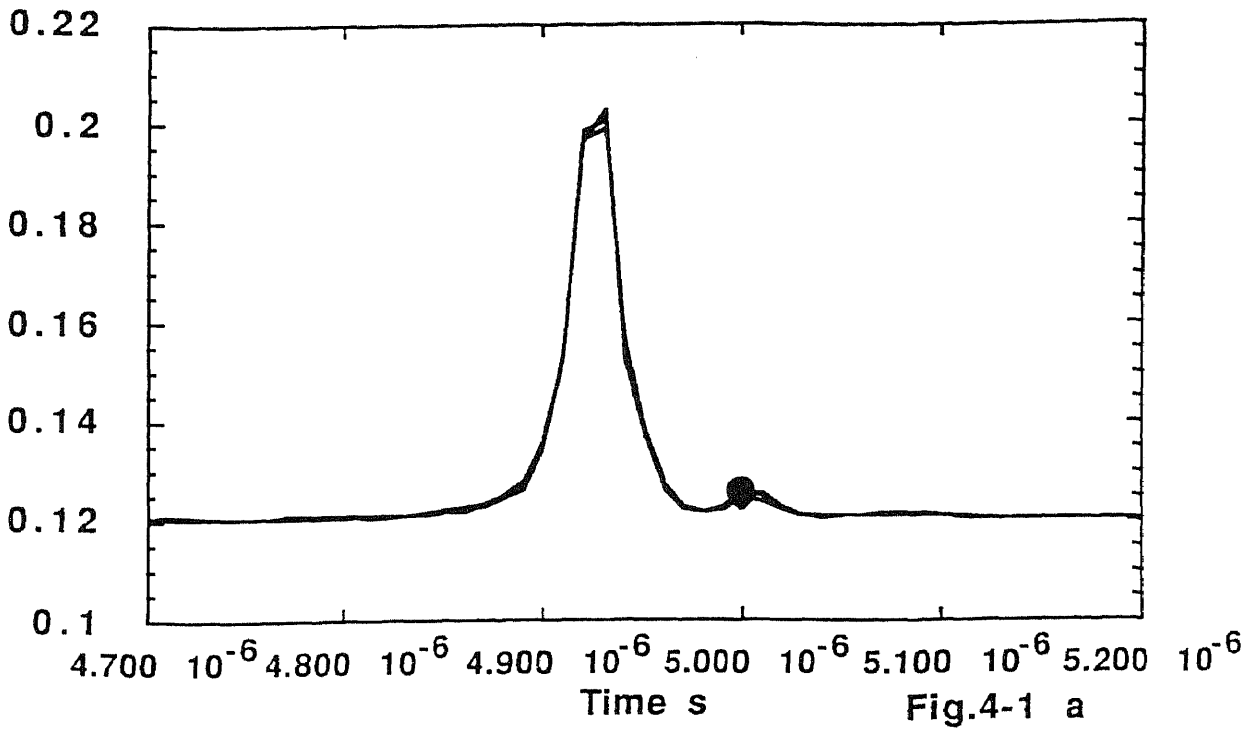

Fig.4-1 a

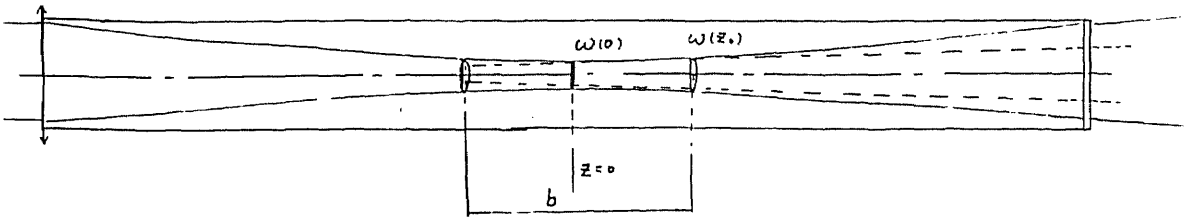

$$\omega(z) = \omega(0)\left[1 + \left(\frac{\lambda z}{\pi\,\omega(0)^2}\right)^2\right]^{1/2}$$

$$I_{third} \propto I_{first}^3\, N_0^2\, \chi^2\, (b\Delta k)^2 \exp\left(\frac{b\Delta k}{2}\right)$$

$$b = 2z_0$$

$$\Delta\vec{k} = \vec{k}_3 - 3\vec{k}_1$$

$$\omega(z_0) = \sqrt{2}\ \omega(0)$$

FIG. 4-2

5 ns, in this time scale the molecular beam is stationary in the ionizer, so the laser can only see the density of the molecular beam . The TOF signal FIG. 4-1 b,c. is proportional to the molecular beam density only. After corrected by the VUV photogalvinic signal the TOF signal can be written as

$$S_i = k\, \partial_i\, n_i \qquad \text{Eq 2.5.1}$$

where the ∂ is the 118.2 nm photoionization cross section, the n is the species number density in the molecular beam, i represent the i'th species and k the experiment constant.

2.5.1 Short Pulse VUV Light Source

The short pulse VUV light source consist of a freqency-tripled Nd:YAG laser (Quanta Ray DCR II) and an one meter nonlinear freqency-tripling inert gases cell. The Nd:YAG laser provides 10 Hz, 354.6 nm laser with donut beam profile. The laser beam is directly focusing through a quartz lens (f = 50 cm) into the tripling cell, there the four wave mixture process generates frequency-tripling photons under the phase-match condition. Third-harmonic generation in phase-matched mixture of metal vapors and inert gases is a convenient technique to provide high power VUV light. Under the tight focusing condition. the focusing length b is much less than the tripling cell. The dominant four wave mixture process occurs in the focusing region, [Fig. 4-2] in which electromagnetic

wave can be treated as plane wave and the ratio of generated third-harmonic power to incident fundamental power is given by

$$P(\text{third}) \approx P(\text{fund.})^3 N^2 x^2 (b\Delta k)^2 \exp(b\Delta k/2) \qquad \text{Eq 2.5.2.1}$$

where N is the gas number density, x is the third nonlinear susceptibility, $\Delta k = k_3 - 3k_1$ is the the phase mismatch of the gas. K_j is the i'th order wave-vector. The peak power is achieved when the phase match condition $b\Delta k = -4$ is satisfied. To get the negative Δk the medium must has negative dispersion for the third order wave vector. for the 118.2 nm light, we chose Xenon as the nonlinear medium and the negative dispersion is contributed dominantly by the short wavelength wing of Xenon 119.2 nm 5p,5d transition. In the practice the focus length is fixed by the tripling cell focusing lens and the incident wavelength. For more flexibility we use Ar as buffer gas to compensate Δk . The Rayleigh scatting and window absorption are the main loss factor of VUV light. To reduce the laser fluctuation we can work at the saturated condition. When 1 Torr Xeon and 11 Torr Ar are put in the cell, the conversion efficiency is about 10^{-5} for the 30 mJ/pulse of 5 ns duration laser. Only 10% VUV light passes through a 1 x 10 mm slits and crosses the molecular beam in ionizer. This VUV beam design can optimizes the time resolution of TOF measurement and reduces possible fluctuation in the molecular beam. We are not separate the 354.6 nm and 118.2 nm laser. The fundamental laser (354.6 nm) doesn't take part in the ionization process. A typical VUV photoionization TOF spectrum is show in the FIG. 4-1a,b.

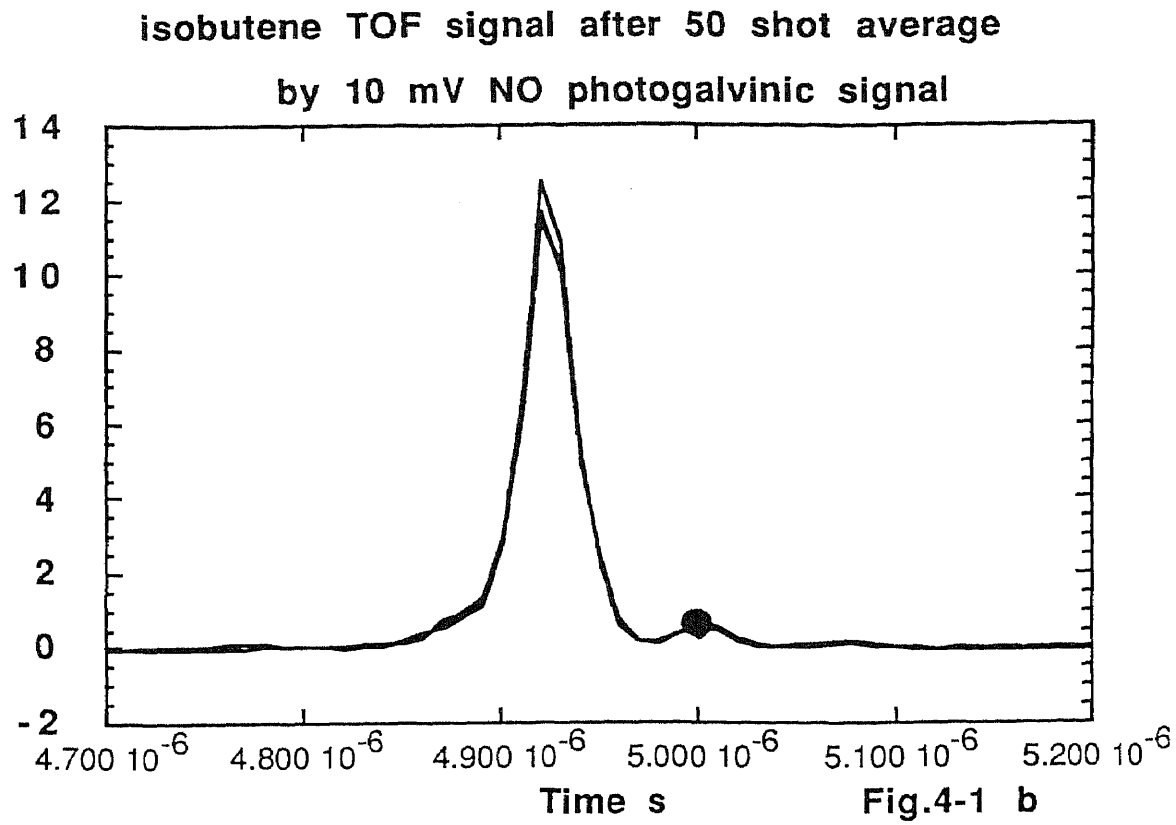

Fig.4-1 b

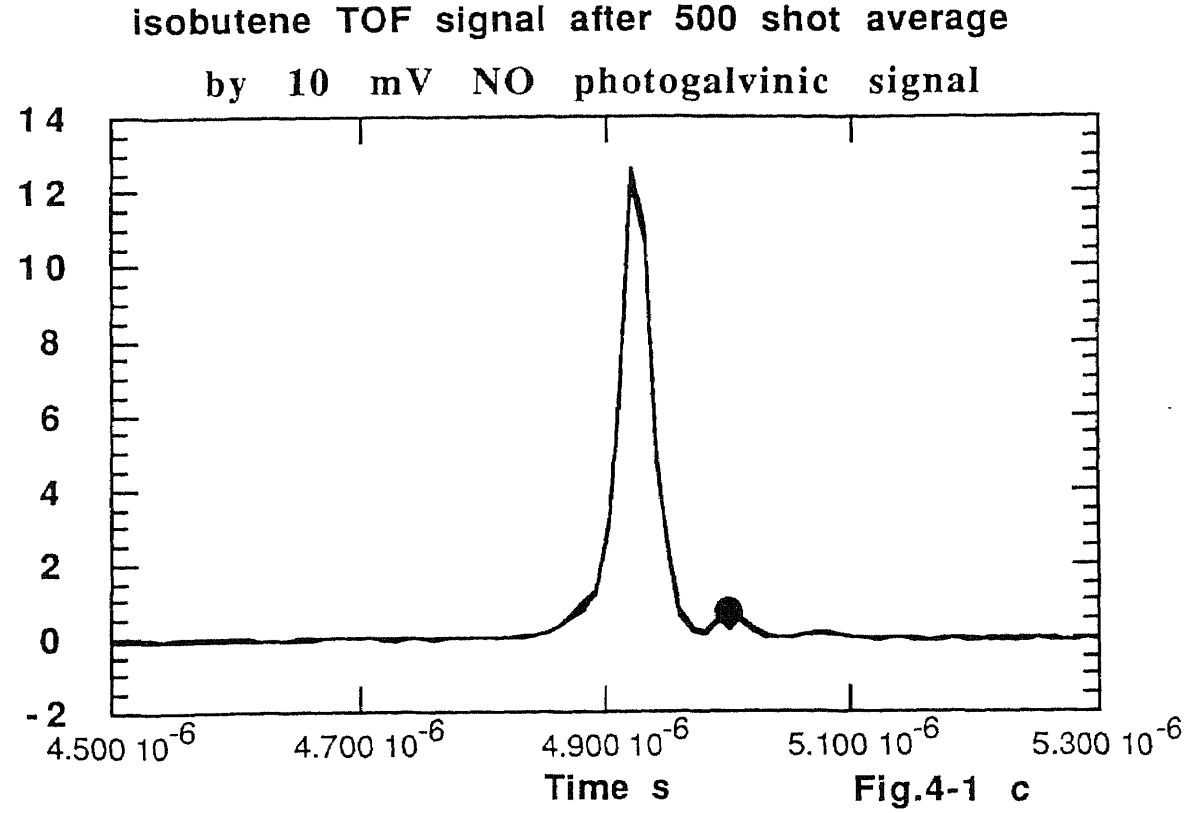

Fig.4-1 c

2.5.2 VUV Photogalvanic Detector

VUV photogalvanic detector is a nitric oxide photonionization cell. The ionization potential if NO is 9.6 eV. Nitric oxide is inert for 345.6 nm (3.5 eV) laser and can ionized by 118.2 nm photon (10.5 eV). Photoions are collected by an electrode and the photogalvanic signal is linearly proportion to the intensity of VUV light. $S = k\ I$. Here the I is the 118.2 nm light intensity, k is an experimental constant including the instrument response constant. This signal will be sent to computer to normalize TOF signal shot by shot.

2.5.3 TOF Assembly

The TOF assembly consist of photoionizer-preaccelaration zone, acceleration zone and free field shift tube FIG2-1. molecular beam and VUV light beam cross in the photoionizer-preacceleration zone and produce ions. These ions are accelerated to 3500 ev kinetic energy before going into free field shift tube. The total flight time of ions with mass-charge ratio m/e is given by the equation

$$t = \beta\ m^{1/2} \qquad \text{Eq 2.5.3.1}$$

The resolution is $R = M/\Delta m = t/2\Delta t$. The high kinetic energy ions of mass charge ratio from 12 to 200 are detected by the microchannel plate assembly with an unity probability [22]. The detection probability of ions can be represented as

$$P = 1 - e^{-r} \qquad \text{Eq 2.5.3.2}$$

where r is a parameterization variable, the secondary electron coefficient. A nonlinear least-squares analysis produced the following expression:

$$r = 2.58 \times 10^{-7}\ m\ \exp(\ 2.31 \times 10^{-4}\ v\ ) \qquad \text{Eq 2.5.3.3}$$

where m is the ion mass (u) and v is the ion velocity (m s^{-1}). The velocity of an ion with mass, m, (u) and energy, E, (KeV) is given below: $v = 4.39 \times 10^5 \sqrt{(\ E/m)}$

2.5.4 TOF Time-Mass Transfer and Signal Fluctuation

In the TOF mass spectrometer the signal is recorded in real time domain and has a Gaussin distribution. When a pulse ion assembly generated in the preacceleration electric field, all the ions will gain the same kinetic energy after they leave the electric field.

$$E_k = \Delta V\ e = m/2\ v^2 \qquad \text{Eq 2.5.4.1}$$

where ΔV is the potential difference and v the final velocity of ion. The flight time is proportional to the square root of ion's mass.

$$T_m + T_o = \beta \sqrt{m} \qquad \text{Eq 2.5.4.2}$$

where T_m is measured time and T_o is the delay time. This formula is the time-mass conversion equation. The peak area in the time domain spectrum is proportion to the ion number generated by the laser. In a short time period the laser and VUV light intensity are very stable and the deviation between individual data sets are less then 5 % after 50 shot average. After 500 shot average the result is similar FIG.4-1b, c. We choice 200 shot average in our measurement. For the long time period we need photogalvinic signal from NO cell to reduce the changing of VUV intensity.

2.6 Quadrupole Mass Spectrometer

Extranuclear C50 mass spectrometer with an axial ionizer is used to detect the species in the molecular beam. A computer program controls the mass scan typically from 10 to 100 amu with in 0.3 second (1000 amu/s). The stable species cracking pattern are collected first. The experimental ß factor defined by the parent ion yield to the total ion yield is used to calculate the relative concentration of various species in the molecular beam. After corrected by the indevidual species velocity which is propertional to the reciprocal of molecular weight square root. The relative electron (70 eV) impact ionization cross section is calculated from the group theory. [23]

CHAPTER 3
EXPERIMENT AND RESULTS

3.1 MOLECULAR BEAM MOLE FRACTION ENRICHMENT INDEX

3.1.1 Introduction

Molecular beam sampling is widely used as an interface in analysis instrument such as GC/MS and as well as our MBMS. Mixture from high pressure source expands into a multistage vacuum system. The centre part of this free jet was pick up by a series skimmers and forming a Molecular beam. The molecular beam dynamical properties such as velocity, intensity and mole fraction are dependent on the beam source temperature, pressure drop at exit and mixture initial component. It is found that in a supersonic molecular beam the mole fraction of heavier molecules in the beam was different with the mole fraction in the source, this is so called mole fraction enrichment. The enrichment is caused by the different diffusion rate of molecules with different mass, so the ratio is a function of relative molecular mass. We define this ratio by equation

$$\log R = x \log(mi/mj) \qquad \text{Eq 3.1.1.1}$$

where x is the enrichment index which is dependent on the beam forming condition and mixture components. In the "seed" ideal beam x = 1 [20]. We measured this index for our molecular beam forming

from a fully developed laminar flow. For the nitric oxide, allene, trans-2-butene and benzene four component mixture at 400 K source temperature, the averaged index is about 0.02. This result implied that the light molecules are more easily be cooling down by the expansion and have lower local temperature in the molecular beam.

3.1.2.Experiment

Our MBMS is mentioned above. The relative mole fraction of source mixture is measured by the static cell photogalvanic technique. Mixture is introduced into the TOF chamber through a leak valve. The molecules are distributed in the chamber homogeneously. The operating pressure is about 10^{-6} Torr and photoions were detected by the TOF detector FIG.E1-1. Molecular beam source is a heating alumina tubing with 4 cm long heating zone on the exit. In the heating zone the gas flow is fully developed laminar flow. Gas expands in the reactor continually and become free jet out of nozzle. At 20 mm downstream a skimmer picks up the core of free jet forming a molecular beam in the TOF chamber. The VUV photons are generated by tripling the third harmonic output of an Nd:YAG laser in a Xe/Ar tripling cell. the VUV light pulse width is about 5 ns and the fluctuation of VUV light intensity is monitored by a NO photogalvanic cell shot by shot. Both the static cell signal and beam signal are collected with a computer for further analysis.

3.1.3 Results and Discussion

The relative mole fraction in the beam does'nt change comparision with bulk

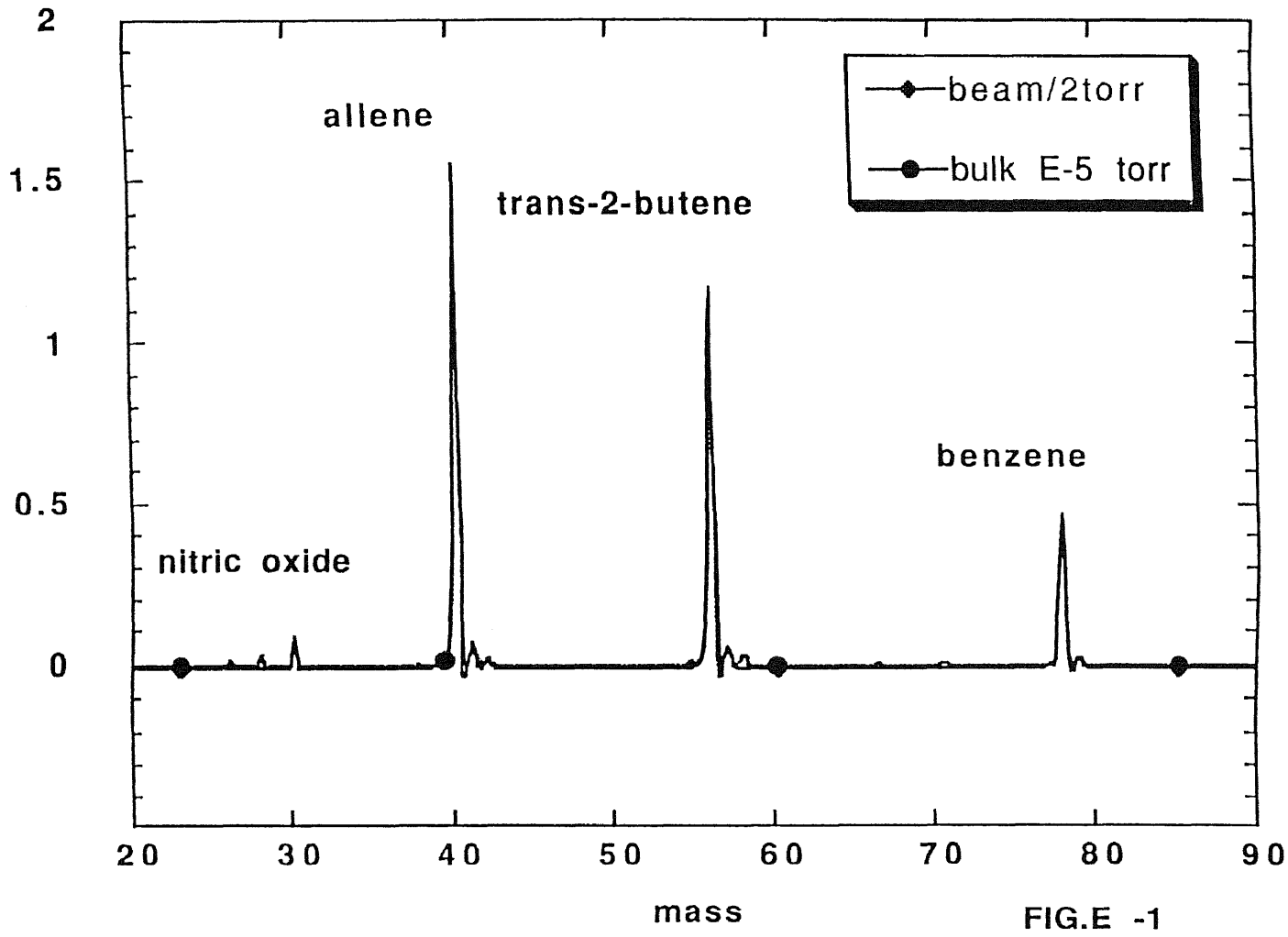

FIG.E -1

We sent about 5 sccm mixture into the reactor, because the correct index of mixture in unknown, we only measure the pressure on the inlet of the reactor. When the total flow rate was double, the pressure increases from 2 Torr to 2.6 Torr and the ions yield increased by a factor of 1.7, meanwhile the relative signal intensity keeps constant. The relative signal can be written as

$$R_{ij} = S_i/S_j = (m_i/m_j)^x \partial_i/\partial_j n_i/n_j \qquad \text{Eq 3.1.3.1}$$

where m is the molecular mass, ∂ is photoionization cross section and n is the density of molecule in the reactor.

In the static cell measurement we sent the mixture directly into the TOF chamber and measure the pressure by an ion gauge. The total pressure is in the range $1x10^{-6}$ Torr to $2x10^{-5}$ Torr. The relative signal is

$$R'_{ij} = S'_i/S'_j = \partial_i/\partial_j \; n_i/n_j \qquad \text{Eq 3.1.3.2}$$

The enrichment index x is defined as

$$\log (R_{ij}/R'_{ij}) = x \log (m_i/m_j) \qquad \text{Eq 3.1.3.3}$$

The results is in the table E.1 the four components average enrichment index is about 0.02. We can extend this to the mass region from 15 to 90. the maximum enrichment will be $E = 6^{0.02} = 1.036$. only 3.6 % change. From the static cell data we can estimate the sensitivity of our MBMS. It is clear that $1x10^{-10}$ Torr allene is

measurable which is about $3x10^{8}$ molecules per cc. The pressure at the exit of reactor is estimated about 10^{-2} Torr which agrees with theoretical predication. The conclusion of this work is that for a fully developed laminar flow molecular beam source the mole fraction enrichment in the beam is negligible.

Table E.1 Relative signal in bulk and molecular beam

molecular beam			static cell				
chamble pressure $3x10^{-7}$ Torr							
mixture 1							
species	reactor pressure Torr		chamble pressure $x10^{-5}$Torr				
	2	2.6	1	1.4	1.6	2	
NO	0.21	0.4	0.21	0.36	0.42	0.62	
C3H4	4.32	7.07	4.23	6.64	7.88	11.05	
2-C4H8	3.55	6.02	3.47	5.31	6.23	8.66	
benzene	1.25	2.06	1.21	1.89	2.33	3.28	
relative intensity as 2-C4 is 1	avg						avg
NO	0.06	0.07	0.06	0.06	0.07	0.07	0.07	0.07
C3H4	1.22	1.18	1.20	1.22	1.25	1.26	1.28	1.25
2-C4H8	1.00	1.00	1	1.00	1.00	1.00	1.00	1
benzene	0.35	0.34	0.35	0.35	0.36	0.37	0.38	0.36

mole fragment enrich ment index

	log (R/R")	log (Mi/56)	x %
NO	-0.067	-0.27	7
C3H4	-0.018	-0.15	14
2-C4H8	0	0	0
benzene	-0.012	0.14	-15

mixture 2

species	reactor pressure Torr				chamble pressure x10^{-6}Torr
	1.00	1.40	1.70	2.61	0.9
NO	0.06	0.12	0.21	0.32	0.82
C3H4	1.04	1.84	3.21	5.46	12.75
2-C4H8	0.84	1.45	2.54	4.48	10.35
benzene	0.27	0.46	0.80	1.25	3.05

relative intensity as 2-C4 is 1				avg	avg
NO	0.08	0.08	0.08	0.07	0.08	0.08
C3H4	1.24	1.26	1.26	1.22	1.24	1.23
2-C4H8	1.00	1.00	1.00	1.00	1	1.00
benzene	0.33	0.32	0.31	0.28	0.31	0.29

mole fragment enrichment index

	log (R/R")	log (Mi/56)	x %	vag x%
NO	-0.014	-0.27	1	4
C3H4	0.0035	-0.15	-3	6
2-C4H8	0	0	0	0
benzene	0.029	0.14	14	1

3.2 Relative 10.5 ev Photoionization Cross Section of Stable Species.

The results of the above work implied that the TOF mass spectrometer is ready to determinate the relative photon ionization cross section of stable species. The photoionization cross sections via photon energy of 1,3-butadiene, 1,2-butadiene, Allene, Propyne, Propene, Acetylene, Ethylene and Butene-1 are measured by

J.A.R.Samson [25], James C. Person [26, 27], and Albert C Parr [28]. They measured the photoionization cross section of these species individually and then compared them with nitric oxide. Because the measurement was not carried out simultaneously, the relative ionization cross section for some species can has a large deviation as much as 30%. Use our MBMS we can simultaneously measure the 10.5 eV photoionization cross sections of gas phase olefines, polylenes and aromatics. When well known mole ratio mixtures are sent in to the molecular beam, photoions are separated and detected according to their mass / charge ratio. The instrument response is true universal for all detectable species. First we chose propylene as internal standard and measure the relative ion yield of 1,3-butandiene.

3.2.1. The Relative Initial Mole Fraction Change

We keep laser power (30 mj a pulse) and the temperature (350 K) of reactor constant and varying the total flow rate and mixture mole ratio by changing the 1,3-butadiene's flow rate. The ratio of 1;1 was checked out directly by bubble flow meter. The result is on the table E 2. and the relative ion yield is linearly proportional to the relative flow rate, FIG. E2-1. Changing the total flow rate with 1;1 ratio dose not change the relative ion yield. The flow meter of 1,3-butadiene is checked out directly with 1,3-butadiene gas, and the propylene's flow meter in calibrated by the N2 gas and then corrected by the gas flow correct factor, the relative error is estimated about 5%. The relative 1 0.5 eV photoionization cross section of propylene

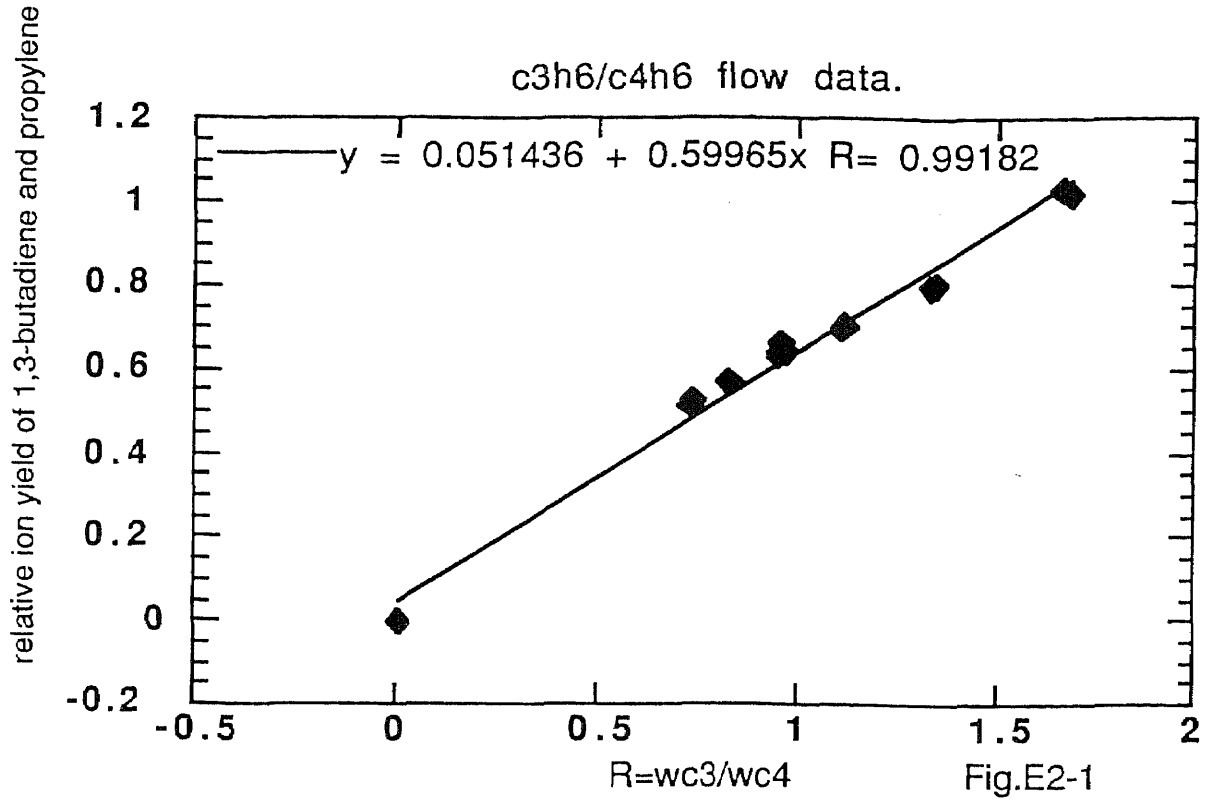

Fig.E2-1

Azo-methane 10.5 eV photon ionization cross section

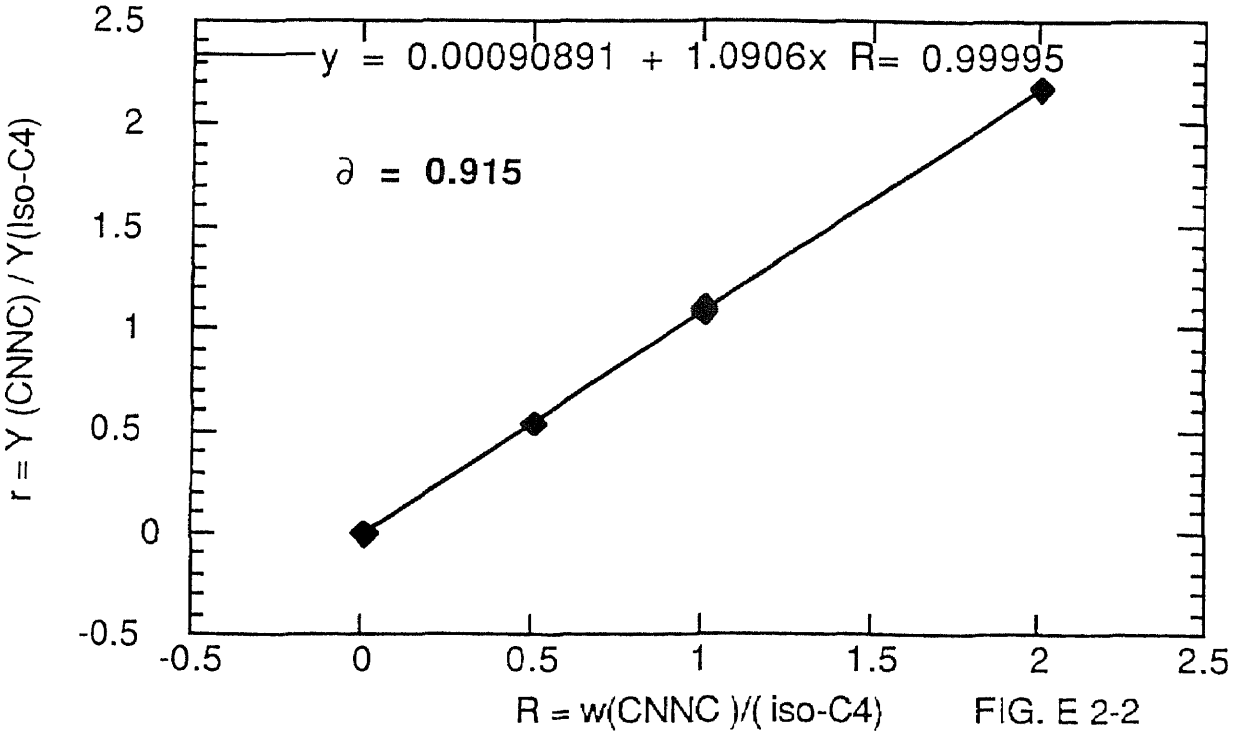

FIG. E 2-2

1,3-butadiene is 0.6.

FIG. E2-2 shows the relative ion yield of azomethane comparing with iso-butene. The relative ionization cross section turned out to be 0.92 which is very close to trans-2-butene.

3.2.2. Internal Energy Effect

James C. Person and Albert C. Parr showed the photoionization cross sections of propylene and 1,3-butadiene are photon energy dependent. From 10.5 eV the ionization cross sections are increasing with photon energy for both of them. When we heat up the reactor, there are two things will effect the ion yield. First the pressure factor, the backpresure is increasing with the reactor temperature, which in turn increase the intensity of molecular beam. The second factor is the internal energy. Both of these increase the ion yield, FIG. 2-3. However the pressure factor is universal for all the species in the flow and the internal energy is species dependent. If the rate are similar then the relative ionization cross sections will keep constant as the internal energy increase. We heat up the reactor and detect the changing of relative ion yield, FIG, E2-4. The decrease of 1,3-butadiene ion yield is due to the pyrolysis or the flow rate change. The changing of relative photoionization cross sections [FIG.2-5] is negligible because the photoionization cross sections of individual species is not sensitivity to the internal energy when the photon energy is 0.5 eV above the ionization potential. The increase of propylene ion yield with reactor temperature is due to the pressure factor only.

propylene 10.5 eV photoionization ion yield via temperature

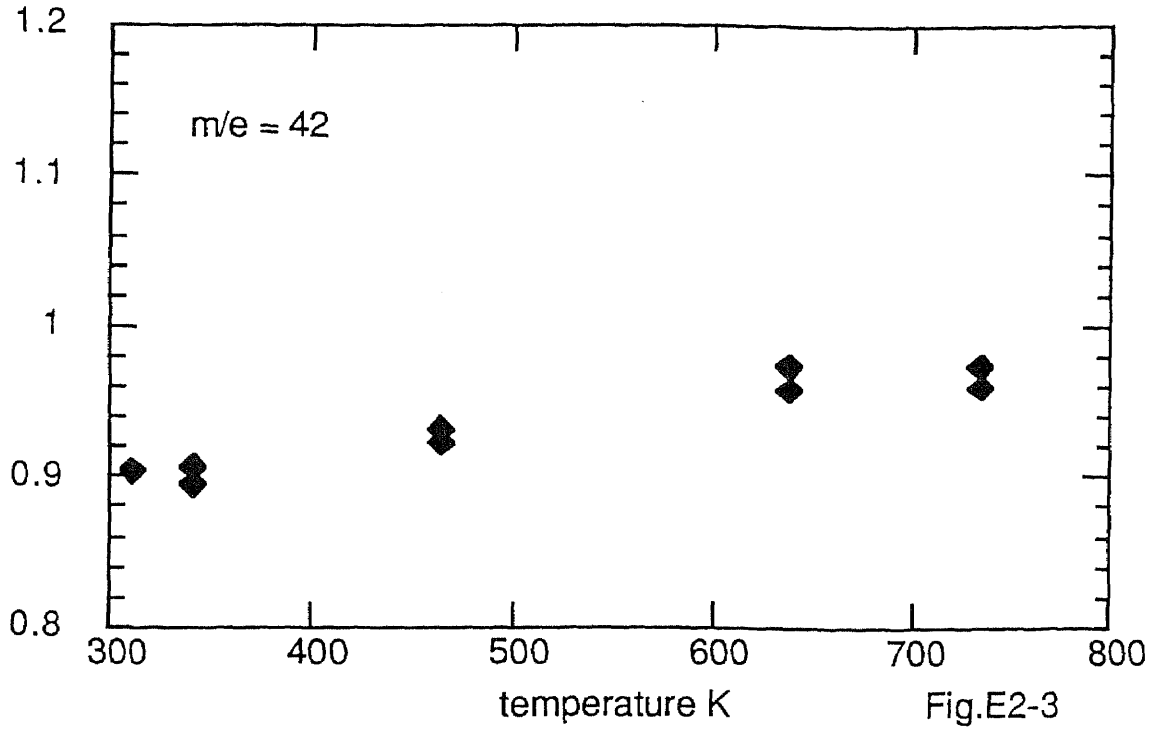

Fig.E2-3

relative ion yield of propylene and 1,3 butadiene in TOF. and Quad. detectors

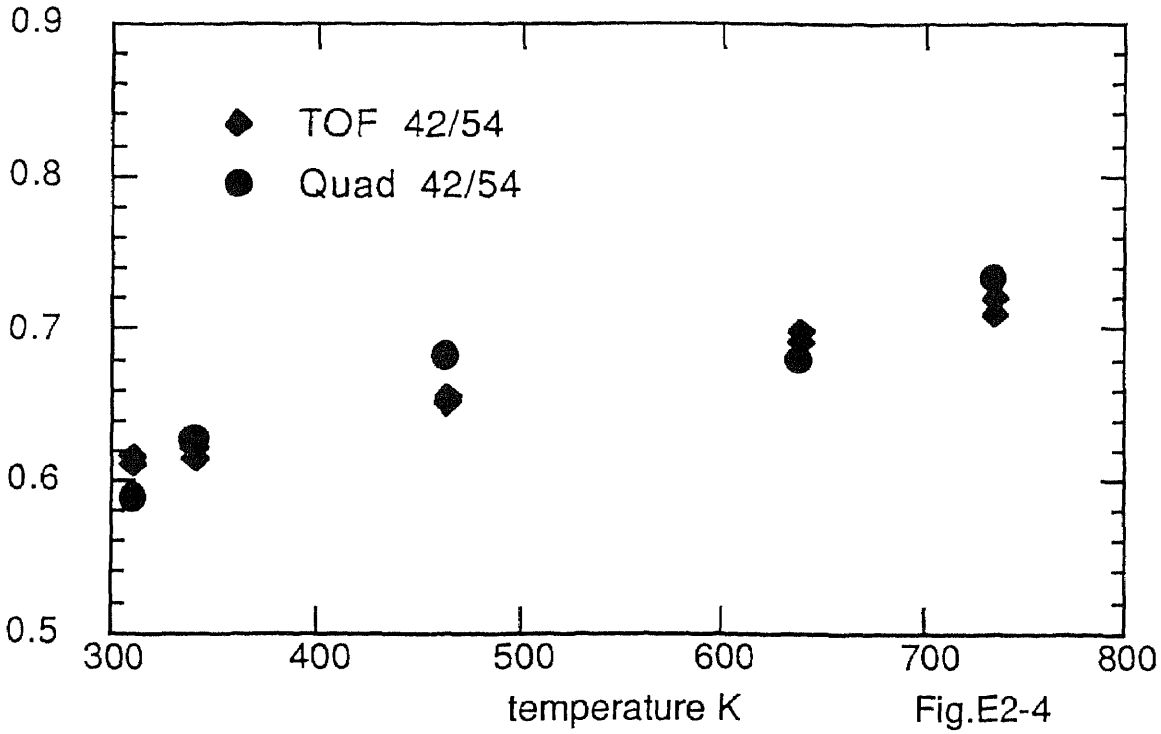

Fig.E2-4

relative 10.5 eV photoionization cross section of propylene and 1,3 butadiene

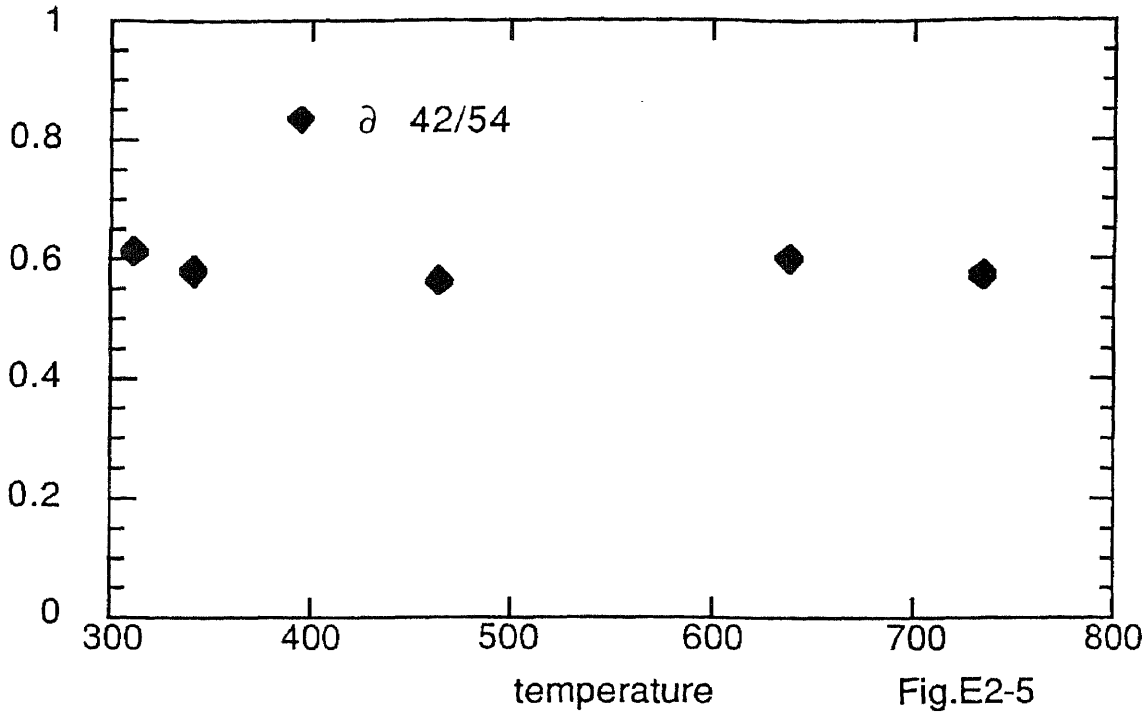

Fig.E2-5

relative ion yield of propylene and 1,3 butadiene via laser energy

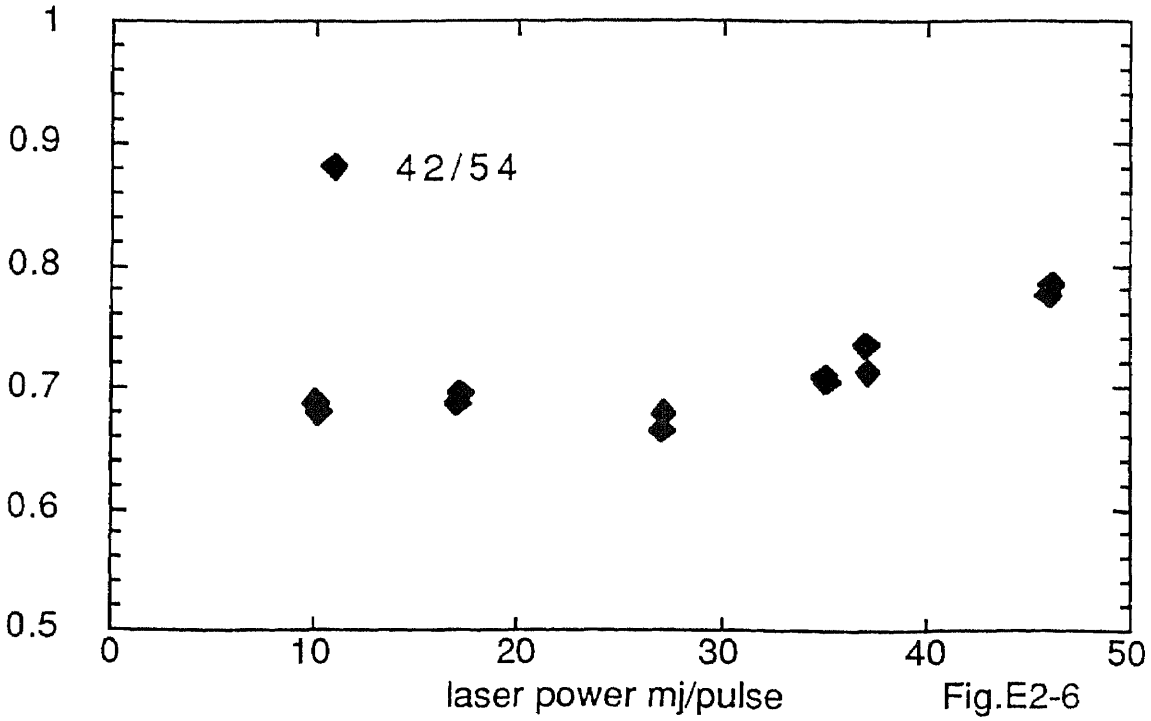

Fig.E2-6

Table E 2-1

Observed 118 nm photon ionization cross section ratio of stable species

photon energy 10.5 eV Feb.1.91

Molecule	IP (eV)	Ratio to			
		Propylene	1-butene	Propyne*	2-butene
Propylene	9.73	1	0.95		0.72
1,3 butadiene	9.07	1.67			1.20
1,2 butadiene	9.23		1.5		1.14
2-butene	9.13	1.39			1.00
1-butene	9.59	1.04	1		0.75
iso-butene	9.21	1.16			0.84
allene	9.62	1.43	1.34	0.96	1.02
ethylene	10.5		0.012		0.01
propyne	10.38			1	1.06
1-butyne	10.18			1.13	1.2
nitric oxide	9.26				0.14
benzene	9.2				2.16
aceton**	9.8				0.92
azomethane**	8.4				0.92

* Albert C Parr, J of Chem. Phys. Vol 49, No 6, 2659 (1968)
Toshio Nakayama, J of Chem. Phys. Vol 40, No 2, 558(1964)

** Measured with iso-butene.

3.2.3. Laser Intensity Effect

Because of our VUV light source is actually a two color light mixture source. The intensity of fundamental laser (355 nm) is 10^5 times stronger then VUV light (118 nm). The strong fundamental laser intensity may cause multiphoton (1 + 1) ionization and dissociation, FIG.E2-6. In our experiment condition the critical laser energy is about 35 mj / pulse.

The same approach can applied on other olefins and polylenes. The final results is on the table E2-1.

3.3 VUV Photoionization Cross Section Group Addition Theory and Group Assignment

3.3.1 The Theory of low Energy Photon Ionization Cross Section of π-electron System

L.L.Lohr, Jr., and M.B.Robin [24] had calculated VUV photoionization cross section for π-electron systems. The quantum-mechanical expression for the photoionization cross section ∂ is related to the Golden Rule rate, obtained from time-dependent perturbation theory.

$$w = h \, I \, H_{ab}'I^2 \, ç \, (E) \qquad \text{Eq 3.3.1.1}$$

where H_{ab}' is the interaction energy of the initial state < **a** I and final state I **b** > due to the presence of the radiation field and ç (E) is the density of final states with energy in the vicinity of Eb. We can

treat the interaction energy in electric-dipole momentum approximation for low photon energy. Where the photon momentum is neglected.

$$w = e^2 A_o^2/(h\ m^2 c^2)\ |\ \mathbf{u} < \mathbf{a}|\ \Sigma\ \mathbf{p}_n|\ \mathbf{b} >|^2\ ç\ (E) \quad \text{Eq 3.3.1.2}$$

where A_o is the magnitude of the vector potential, **u** is an unit vector in the polarization and $\mathbf{p}_n$ is the linear momentum operator for the n'th electron. The number rate is converted to cross section by multiplying the photon energy hv and equating the result to the product of the cross section ∂ and the magnitude $w^2 A_o^2 / (2\pi c)$ of the poynting vector. If the expression for ∂ is divided by 4π, the differential cross section for the producing photoelectrons in the solid angle dΩ is

$$d\partial/d\Omega = \pi\ e^2 / (m^2 cw)\ |\ \mathbf{u} < \mathbf{a}|\ \Sigma\ \mathbf{p}_n|\ \mathbf{b} >|^2\ ç(E) \qquad \text{Eq 3.3.1.3}$$

If the ground state <al is a determinant of double occupied molecular orbitals (MO's) and the excited state lb> is a spin singlet constructed by the promotion of one electron from the jth MO to an unbound orbital lk>, with no change in the shape of other MO's, then

$$<a|\Sigma\mathbf{p}_n|b> = 2^{1/2} <\mathbf{j}|\mathbf{p}|\mathbf{k}> \qquad \text{Eq 3.3.1.4}$$

The functions lk> for the ejected electron are assumed to be plane waves (PW's) normalized in the cubic box of length L

$$PW(k) = L^{-3/2} \exp(i\mathbf{Kr}) \qquad \text{Eq 3.3.1.5}$$

the accompanying density of states is

$$ç(E) = 2\ m\ k\ L^3 / h^2 \qquad \text{Eq 3.3.1.6}$$

the differential cross section is

$$d\partial/d\Omega = 4\ e^2\ k\ L^3\ \pi\ /(m\ c\ h^2\ w)\,|\mathbf{u} <\mathbf{j}|\mathbf{p}|\mathbf{PW(k)}>|^2 \qquad \text{Eq 3.3.1.7}$$

Since the **PW** is an eigenfunction of **p** with eigenvalue $hk/2\pi$, then we have

$$d\partial/d\Omega = e^2\ k\ L^3/(\pi\ m\ c\ w)(\mathbf{uk})^2 |<j|PW(k)>|^2 \qquad \text{Eq 3.3.1.8}$$

Each MO <jI is a linear combination of atomic orbitals (AO's) $<©_l|$ and $<j| = \sum_l C_{lj} <©_l|$ In Gaussian basis function a carbon $2p_z$ AO can be written as

$$<©_l| = \sum_s A_s\, N(a_s) z\, \exp[-a_s(\mathbf{r}-\mathbf{R}_l)^2] \qquad \text{Eq 3.3.1.9}$$

where each A_s is the coefficient of a Gaussian function with normalization constant $N(a) = 2a^{1/2}(2a/\pi)^{3/4}$ The vector Rl denotes the position of the lth carbon atom in the molecular xy plane. The overlap of an AO with a PW is readily evaluated in Cartesian coordinates and is

$$<\odot_l|\ PW(k)> = ik_z\,(2\pi)^{3/4}\,L^{-3/2}\,\exp(i\mathbf{K}\mathbf{R}_l)\Sigma_s A_s a_s^{-5/4}\exp(-k^2/4a_s)$$

Eq 3.3.1.10

now we get the final result

$$d\partial/d\Omega = \text{cont.}\ [\Sigma_l\, C_{lj}^2 + 2\Sigma_{l>m}\, C_{lj}\ C_{mj}\ \cos(\mathbf{k}\,\Delta\mathbf{R}_{lm})] \qquad \text{Eq 3.3.1.11}$$

where $\Delta\mathbf{R}_{lm} = \mathbf{R}_l - \mathbf{R}_m$. This equation tell us how the AO's $2p_z$ orbital on the carbon atom contribute to the total ionization cross section.

In our MBMS we use linear polarized VUV light and collect all the cations which equal to the total electrons ejected from the molecules. So the total ionization cross sections are measured. The ionization potential of olefin and plylene is in the range of 9 -10 eV. Table E3-2. The highest occupied molecular orbit [HOMO] is π orbit. 10.5 eV photon can only excite these π electron to infinite orbit and left a stable cation. If for all m orbital the product $\mathbf{k}\Delta\mathbf{R}_{lm}$ is a constant, then the total ionization cross section is simplified as

$$\partial = \text{cont.}[\Sigma_l\, C_{lj}^2 + 4\ \Sigma_l C_{lj} C_{kR}] \qquad \text{Eq 3.3.1.12}$$

Where C_{kR} is a constant and we used the relationship $\Sigma\ C_j = C$.

3.3.2 The Group Assignment

We can group atomically hybridizations as the bases of π orbital, so the ionization cross sections. The coefficient of these bases is list

in the table E3-1. as group assignment. Propylene, 2-butene and 1,3-butadiene have ideal conjugate π bond system. From these compound we can determinate the first three basic π bond system group, Cd/H2, C/Cd/H3 and Cd/C/Cd/H.

Molecule Propylene

group; Cd/H2, C/Cd/H3, Cd/C/Cd/H.

Molecule 2-butene

group; 2 x C/Cd/H3, 2 x Cd/C/Cd/H.

Molecule 1,3-butadiene

group; 2 x Cd/H2, 2 x Cd/C/Cd/H.

Iso-butene has two C/Cd/H3 group, one Cd/H2 group and a Cd/C2/Cd group. From molecular orbital structure the C-C bond is a ∂ bond in group Cd/C2/Cd and Cd/C/Cd/H have the same sp^2 hybridization so they may have same value. Benzene is a important aromatic compound with a good π bond system. The calculated cross section has very small deviation from observation. Part of this deviation may come from the ring contribution and another part do come from flow rate measurement. The vapor pressure of benzene at pumping condition is smaller then it saturate pressure at the same temperature. The unpaired electron on the hydrocarbon radical is likely be a $2p_z$ electron on the carbon atom. Our theory can expand to cover radical case and nitrogen and oxygen organic compound. Aceton has two C/Cd/H3 group, one CO/C2 group. The measured relative photoionization cross section is 0.92, so the coefficiency of carbonium group is 0.68.

Table E3-1

Calculated TOF sensitivuty of stable species and group assignments

Photon energy 10.5 eV

Group	Cross section	Group	Cross section
CD/H2	0.22	CD/C2	0.38
CD/C/H	0.38	CT/C	0.94
C/Cd/H3	0.12	ND/C/ND	0.34
Cß/C/H3	0.03	CO/C2	0.68
CA	0.5	C/ND/H3	0.12
C/Cd/C/H2	0.12	C_{2p} (CH3)	0.1

Table E3-2

Comparison of photoionization cross section of stable species

Molecule	Observed	Calculated	Deviation %
Propylene	0.72	0.72	0
1.3 butadiene	1.2	1.2	0
2-butene	1	1	0
1.2 butadiene	1.14	1.22	6.6
1 butene	0.75	0.75	-0.5
iso-butene	0.84	0.84	0.33
allene	1.02	0.94	-7.8
ethylene	0.01	-	-
propyne	1.06	1.06	0
1 butyne	1.2	1.09	-9.2
benzene	2.16	2.28	5.6
aceton	0.92	0.92	0
azo methane	0.92	0.92	0

Example: Propylene = CD/H2 + CD/C/H + C/Cd/H3

∂ = 0.22 + 0.38 + 0.12 = 0.72

3.4.Molecular Beam Velocity in Nitric Oxide, Trans-2-butene and Neon Three Components Mixture

The short residence time, low pressure flow tube reactor was widely used in experiment to obtain kinetic data on elemental reactions.[14,15] The fully developed theory of subsonic compressible flow of gases in small tubes with friction, heat transfer and chemical reactions can predicate the fluid dynamical properties.[18] We can use this theory to handle more complex reactions such as pyrolysis reactions and oxidation of hydrocarbons. Molecular beam sampling is a useful technique to obtain the reaction products and their temperature profiles. But the relationship of molecular beam dynamical properties and fluid's in the reactor can only be measured by the experiment.[29] In the long tubing type nozzle, the gas continually expands along the tube and absorb energy from the reactor. The real gas temperature is proportional to the reciprocal of heat capacity and total flow rate. The beam velocity is very important for understanding the beam dynamic properties. Based on our measurement above, we developed a experimental data base to convert the hydrocarbon's Quadruple mass and VUV (118.2 nm) photoionization TOF data to their relative concentrations in the reactor. Using our dual detectors molecular beam mass spectrometry

we find that for the VUV photoionization TOF signals the ion yield follow the linear function of flow rate.

$$S_{TOFi} = K W_i = K' N_i \qquad \text{Eq 3.4.1}$$

$$S_{TOFi}/S_{TOFj} = \partial i / \partial j \;\; W_i / W_j = \partial i/\partial j \;\; N_i/N_j \qquad \text{Eq 3.4.2}$$

$$S_{TOFi} = K W_i F(W) \qquad \text{Eq 3.4.3}$$

where Wi is the flow rate, K is the experiment constant, S is the signal of i'th species ∂i is the photoionization cross section and Ni is the number density of i'th species in the molecular beam. These three equation are used in one, two and more components mixture .

For the quadrupole mass data. we find that :

$$S_{Quadi} = K W_i \qquad \text{Eq 3.4.4}$$

$$S_{Quadi} / S_{Quadj} = Q_i / Q_j \; \beta i / \beta j \; \text{sqrt}(M_i/M_j) W_i/W_j \qquad \text{Eq 3.4.5}$$

These sqrt term indicate that the molecular beam has supersonic molecular beam behaviour. The internal energy of species was converted to traslation energy. In this case, The velocity of ntric oxide and trans-2-butene at 400 K are propertional to 0.68 and 0.488. The ratio of their velocities is 0.72. This is very close with their mass ratio square-root, 0.73. The detail velocity distribution via molecular weight is more complex. This is only a possible explanation of our experiment result. Combine the photoionization data and quadrupole data we find that:

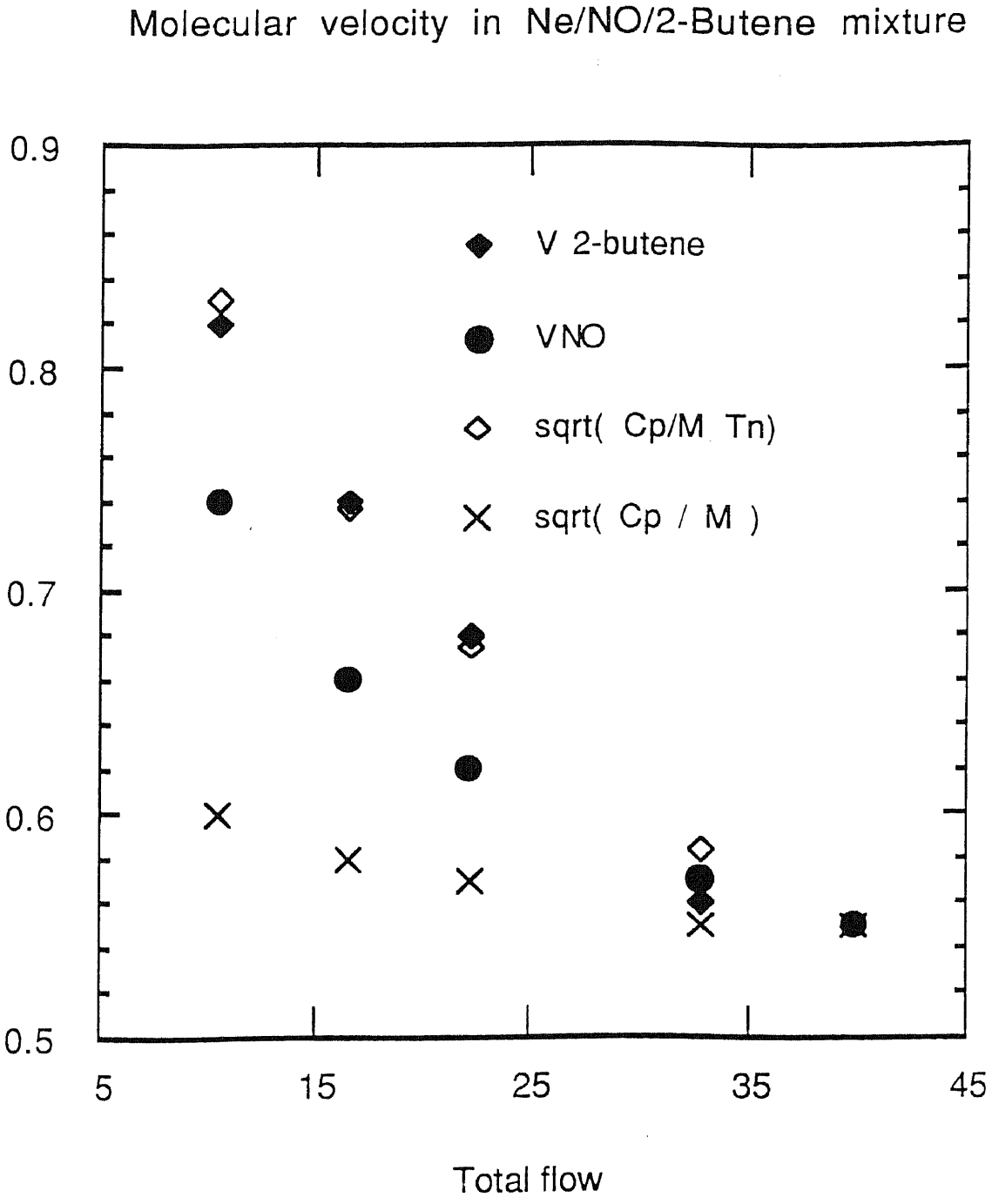
Molecular velocity in Ne/NO/2-Butene mixture
0.9
0.8
0.7
0.6
0.5
5
15
25
35
45
V 2-butene
VNO
sqrt(Cp/M Tn)
sqrt(Cp / M)
Total flow

Fig E 4-1

$$S_{Quad} / S_{TOF} = Qi * \beta i * V_0 * \sqrt{M}/\partial * K_Q/K_T = C_k V \qquad \text{Eq 3.4.6}$$

we know that the mole fraction in the beam is the same as it in the reactor[See part 1]. The velocity of i'th species is given by the supersonic beam velocity

$$V = \sqrt{2kC_p/R/M\ T_n} \qquad \text{Eq 2.4.4.6}$$

where T_n is the temperature at skimmer. The measured velocities of Nitric Oxide and Trans-2-butene in the molecular beam with various mixture ratio and total flow rate is tabulated in table.E 4-1. Because we can not measure T_n directly, we need make an assumption that T_n is proportional to the reciprocal of total flow rate. This is becuase the bigger flow rate the sharper pressure drop at reactor exit. If we assume that the velocity of trans-2-butene followed the mixture velocity that is the velocity calculated by the above equation is for the mixture and the Cp and M is the mixture heat capacity and average mass. We do see the beam temperature decreasing with increasing Ne flow rate.

The real velocity changing with total flow rate must be between sqrt(Cp/M) and sqrt(Cp/M T_n). as showed in FIG.E4-1.

Table E4-1 Ne/NO/2-Butene mixture velocity

Total flow	10.50	16.49	22.18	32.84	39.7
Pressure Torr	5.6	7.4	8.9	11.2	12.5
Ne flow	-	5.99	11.68	22.34	29.2
Xr NO	0.57	0.36	0.27	0.18	0.15
Xr 2-C4	0.43	0.27	0.20	0.14	0.11
Xr Ne	-	0.36	0.53	0.68	0.74
Sq Ne	-	5.77	9.39	15.97	19.46
Sq NO	29.85	30.28	29.51	27.78	26.97
St NO	0.71	0.80	0.83	0.85	0.86
Sq 2-C4	19.22	17.87	16.91	13.57	13.67
St 2-C4	4.62	4.38	4.55	4.4	4.56
∂	0.12	0.14	0.14	0.15	0.14
V no	0.74	0.66	0.62	0.57	0.55
V2-C4	0.82	0.74	0.68	0.56	0.55
Cp	15.04	11.39	9.74	8.19	7.63
M	41.14	33.47	30.01	26.76	25.59
sqrt(Cp/M)	0.6	0.58	0.57	0.55	0.55
sqrt(Cp/M T_n)	0.83	0.74	0.67	0.58	0.55
T_n/T_{nf}	1.9	1.6	1.4	1.1	1

These two velocity distributions are the limitation of real velocity. We assume that at very large Neon flow rate the velocities of nitric oxide and trans-2-butene will be the same [29]. This result again tells us that in the molecular beam the enthalpy is converted into molecules translational energy. The relative velocity changing

70 eV electron impact ionization cross section of gas phase hydrocarbon

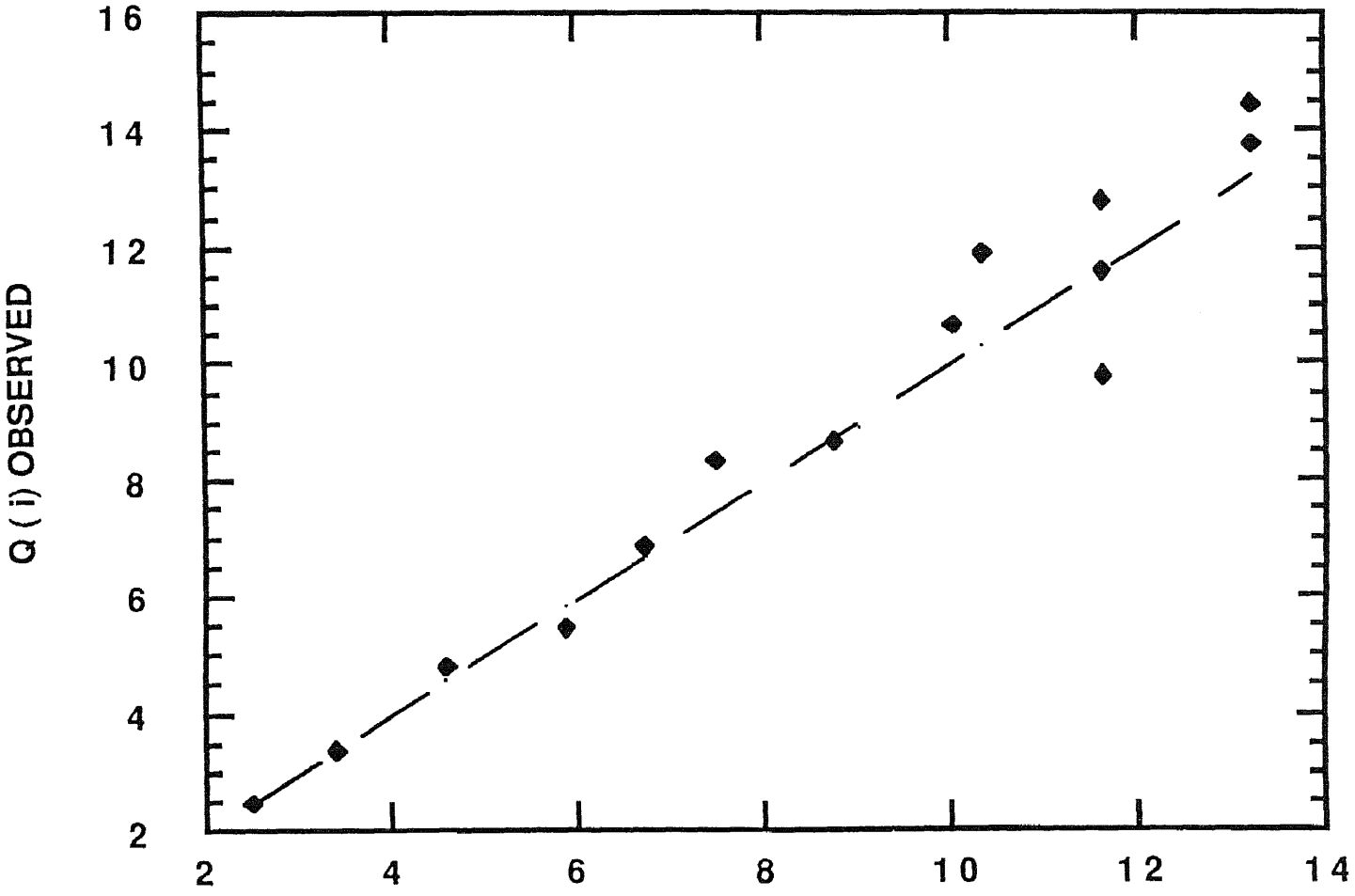

FIG. E 5-1

Table E 6-1

Cross Section = A*sp3+B*sp2+C*sp+D*h+0.943

molecule	sp3	sp2	sp	h	Cross Section
	2.12	1.7	0.85	0.38	
CH3		1		3	3.78
CH4	1			4	4.58
C2H2 (C#C)			2	2	3.40
C2H3		1	1	3	4.63
C2H4 (C*C)		2		4	5.86
C2H5	1	1		5	6.66
C2H6	2			6	7.46
C3H3		1	2	3	5.48
C3H4		2	1	4	6.71
C3H5		3		5	7.94
C3H6	1	2		6	8.74
C3H7	2	1		7	9.54
C3H8	3			8	10.34
C#CC#C			4	2	5.10
C#CC.*C		1	3	3	6.33
C#CC*C		2	2	4	7.56
C*CC.*C		3	1	5	8.79
C*CC*C		4		6	10.02
C*CC.C	1	3		7	10.82
C*CCC	2	2		8	11.62
CCC.C	3	1		9	12.42
CCCC	4			10	13.22
C#CC*CC.		3	2	5	9.64
C#CC*CC	1	2	2	6	10.44
C*CC*CC.		5		7	12.10
C*CC*CC	1	4		8	12.90
C*CC(C2)	3	2		10	14.50
benzene		6		6	13.42
C*CC*CC*C.		5	1	7	12.95
C*CC*CC*C		6		8	14.18

William L.Filch and Andrew D. Sauter (Anal.Chem. 1983 Vol 55 P-832)

as increasing Neon flow rate may be coming from the viscosity (380 x 10^{-6}) response. In the mixture the viscosity dependents on the collision partners, trans-2-butene viscosity(110 x 10^{-6}) is smaller than nitric oxide(240 x 10^{-6}) so it's effective viscosity will increase faster than nitric oxide in the mixture, which appears to be the velocity decreases faster than nitric oxide as showed in FIG.E4.1. The relative changing is about 10 % in the Neon mole fraction region from 0 to 0.74. In the Neon mole fraction region1/3 to1/2 , this increasing is only about 3% which can be negligible in the further experiment. From this poin we can assume that for the hydrocarbons which have the similar viscosities will has the same velocity response in mixture.

The relative 118.2 nm photoionization cross section of nitric oxide is about 0.14 as trans-2-butene was assigned to be one unit, Table E4-1. From two components mixture to three component mixture there is a jump in the relative sensitivity of nitric oxide and trans-2-butene. This jump may be comes from the mixture dynamical property, because the differential response of the viscosity of nitric and trans-2-butene in the mixture, but even so this jump was only a changing about 10 % in a very large flow region. If the Neon mole fraction is in 1/3 and 1/2 , this jump is only about 3 % which can be negligible in our pyrolysis and combustion work.

3.4.1 The 70 ev Electron Impact Ionization Cross Section of Trans-2-butene and Nitric Oxide

In the quadrupole mass spectrometer measurement the cracking pattern of molecule is varying from one ionizer to another, but the total ion yield will assumed to proportion to the total ionization cross section, that is say the fragments are forming from the unimolecular ion decomposition. Its well known that the fragment ions in the electron impact mass spectrum can contributed from various molecules. For example the allyl cation can come from either propylene or 1-butene. On other hand, the parent cations are unique. We can use parent ion to determinate the relative ionization cross section in the electron impact ionization mass spectrometer. First, we defined the ß factor which is a experiment constant, as the ratio of parent ion yield to the total ion yield of one species.

$$ß = S_p / \Sigma S_f \qquad \text{Eq 3.4.1.1}$$

Comparison this ß factor with its standard indicate that we need a calibrate factor. We find out that his calibration factor is proportional to the sqrt of molecule weight of organic molecules. The reason for this factor as we mentioned above is due to the velocity distribution. The relative cross section of trans-2-butene is 12.6 as nitric oxide is taking to be 2.5 as group additivity theorem predication [23].

3.5 Calibration of Electron Impact Ionization Cross Section of Organic Molecules and Cracking Pattern

Molecular beam ionizer is working on the 70 eV modal. Neon as the internal standard premixtured with the hydrocarbons. Use the same approach used above we get the relative ionization cross sections of small hydrocarbons. Table E5-1. Comparison of observed data and the calculated data is straight forward, FIG E5-1. We believe the atomically hybridization base is more accurate then simple atomic base. The deviations of C4 isomers indicated that the group base may be better than the hybridization base, but the hybridization base is very simple. Another byproduct of this work is that we get the cracking pattern of these species in our instrument which will be used to determine the concentration in the mixture.

6. Prediction of Hydrocarbon Radical Ionization Cross Section in Both 10.5 eV Photon Ionization and 70 ev Electron Impact Ionization.

The group addition theory works very well for the stable hydrocarbon species ionization procedure. We can simply extend this theory to radicals. The hydrocarbon radical has an unpaired $2p_z$ electron on the carbon atom sit. Our π bond system photoiozation theory indicate that this orbital can be an independent group. but the contribution of this electron to the total ionization cross section is unknown. Once we can determinate methyl radical photoionization cross section, we can simply add it to the parent species to estimate the cross section of it's radical.

7. 1-butene Pyrolysis

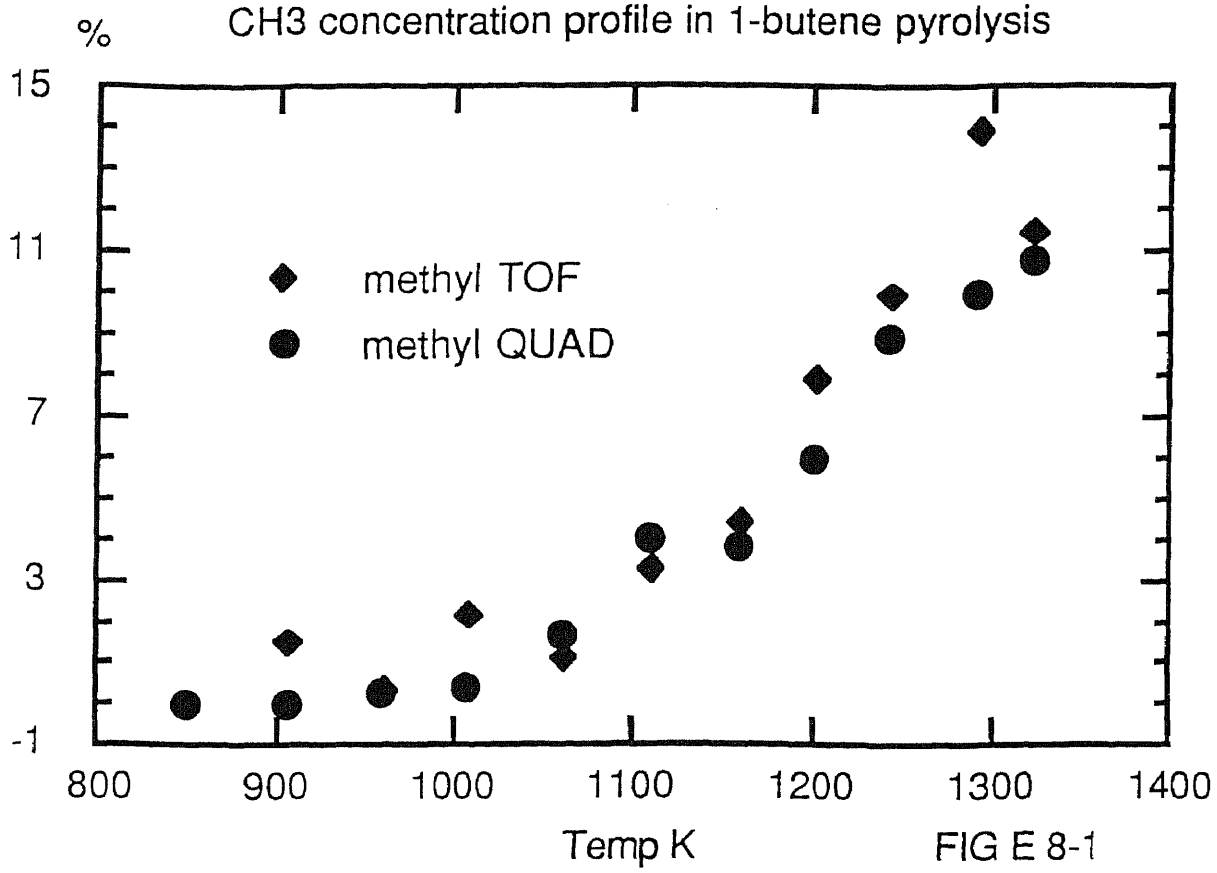

FIG E 8-1

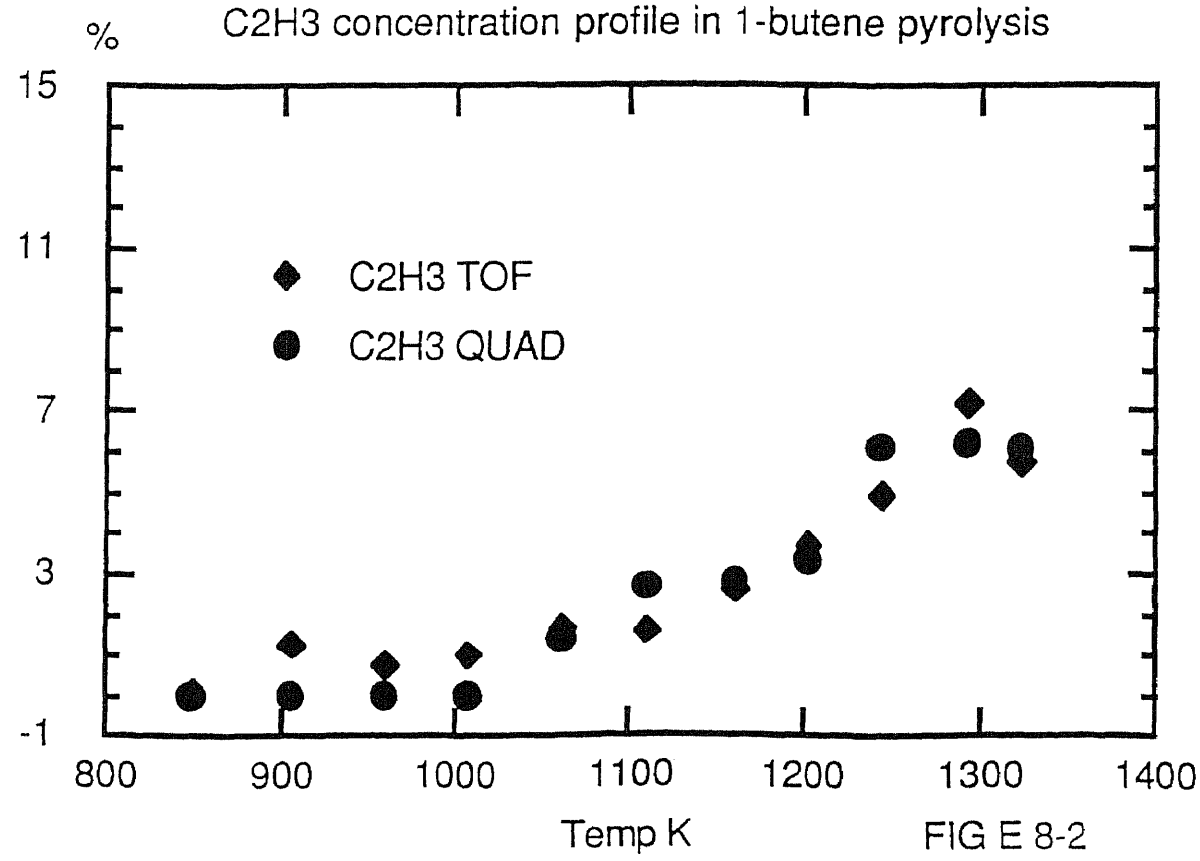

FIG E 8-2

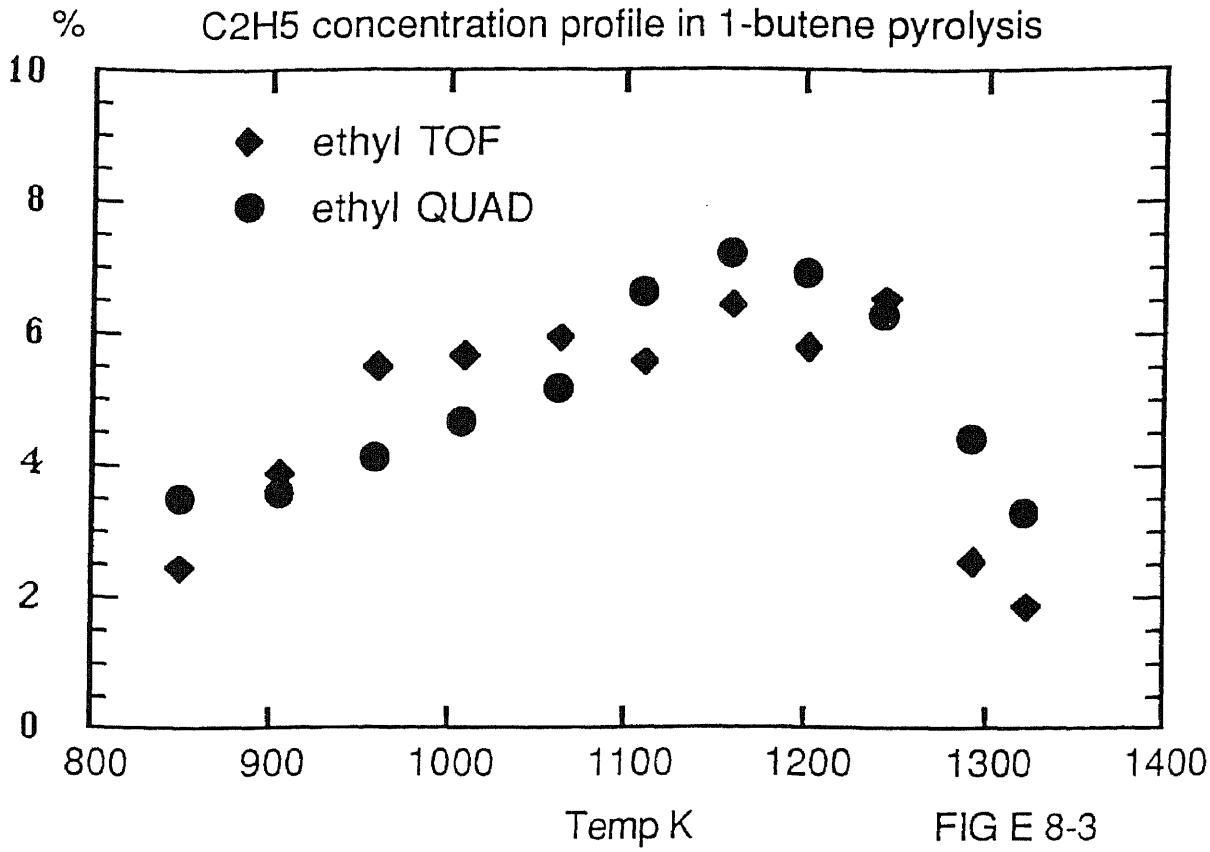

FIG E 8-3

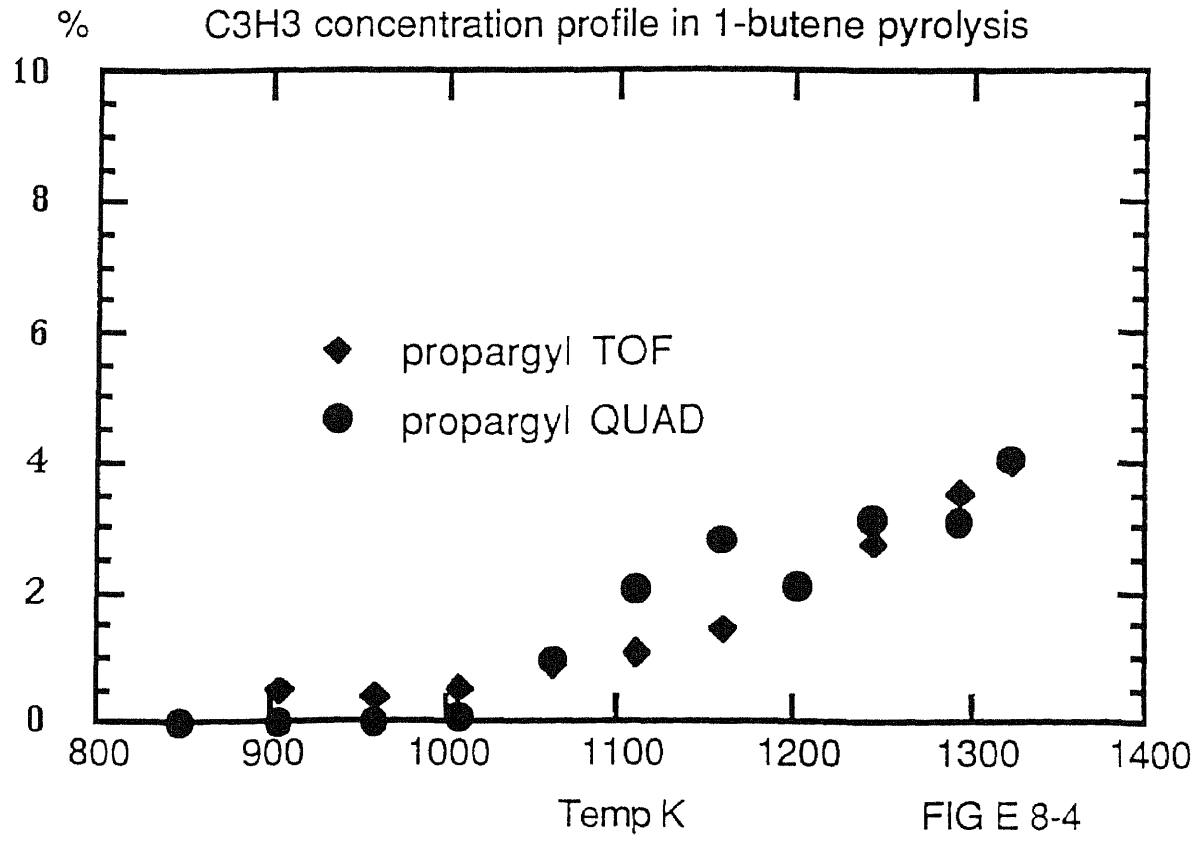

FIG E 8-4

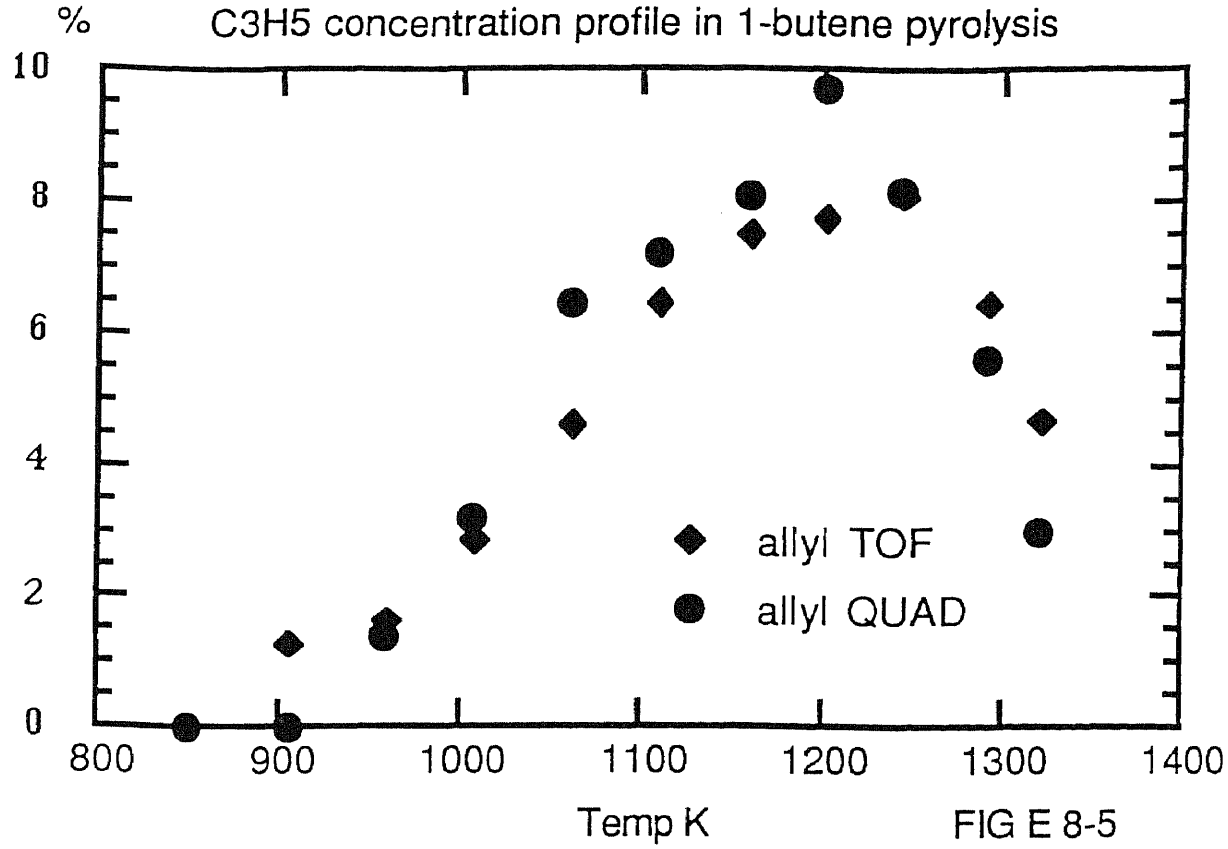

FIG E 8-5

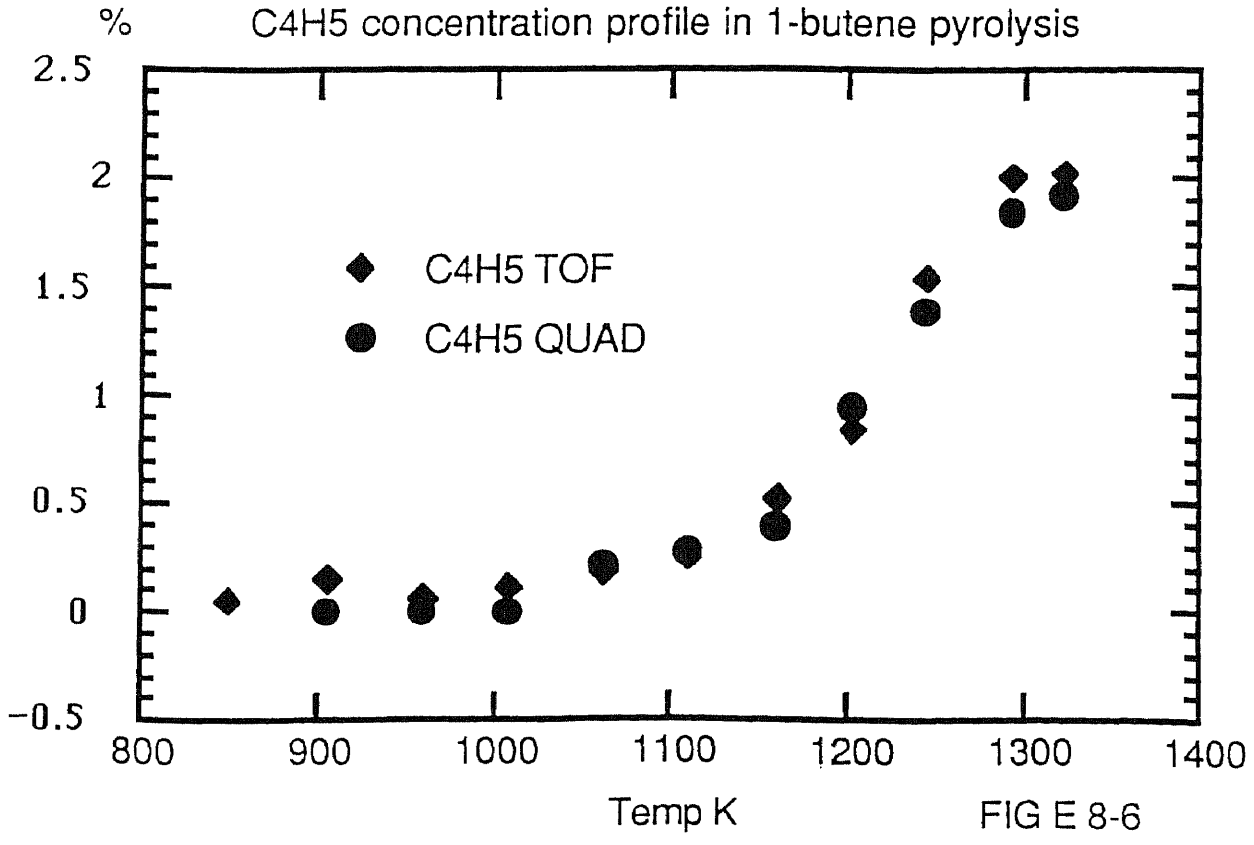

FIG E 8-6

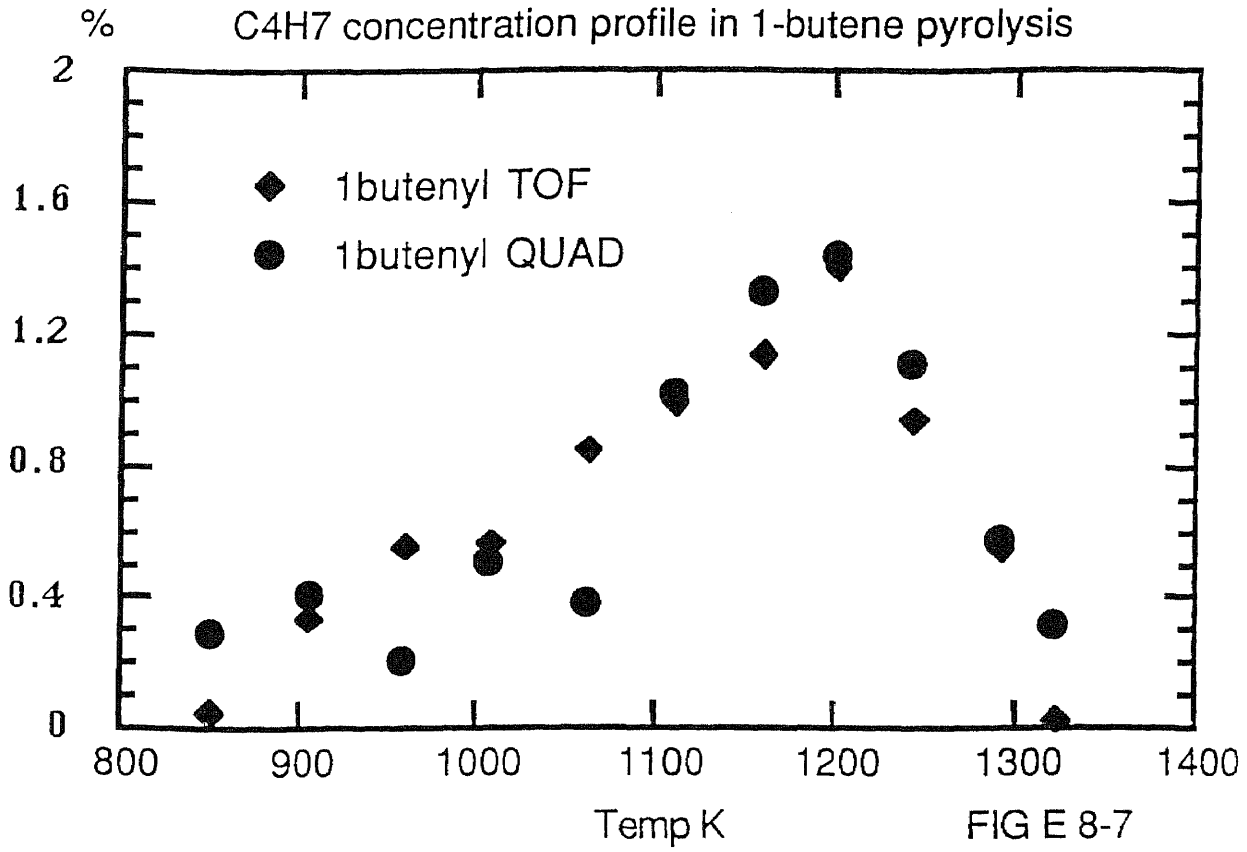

FIG E 8-7

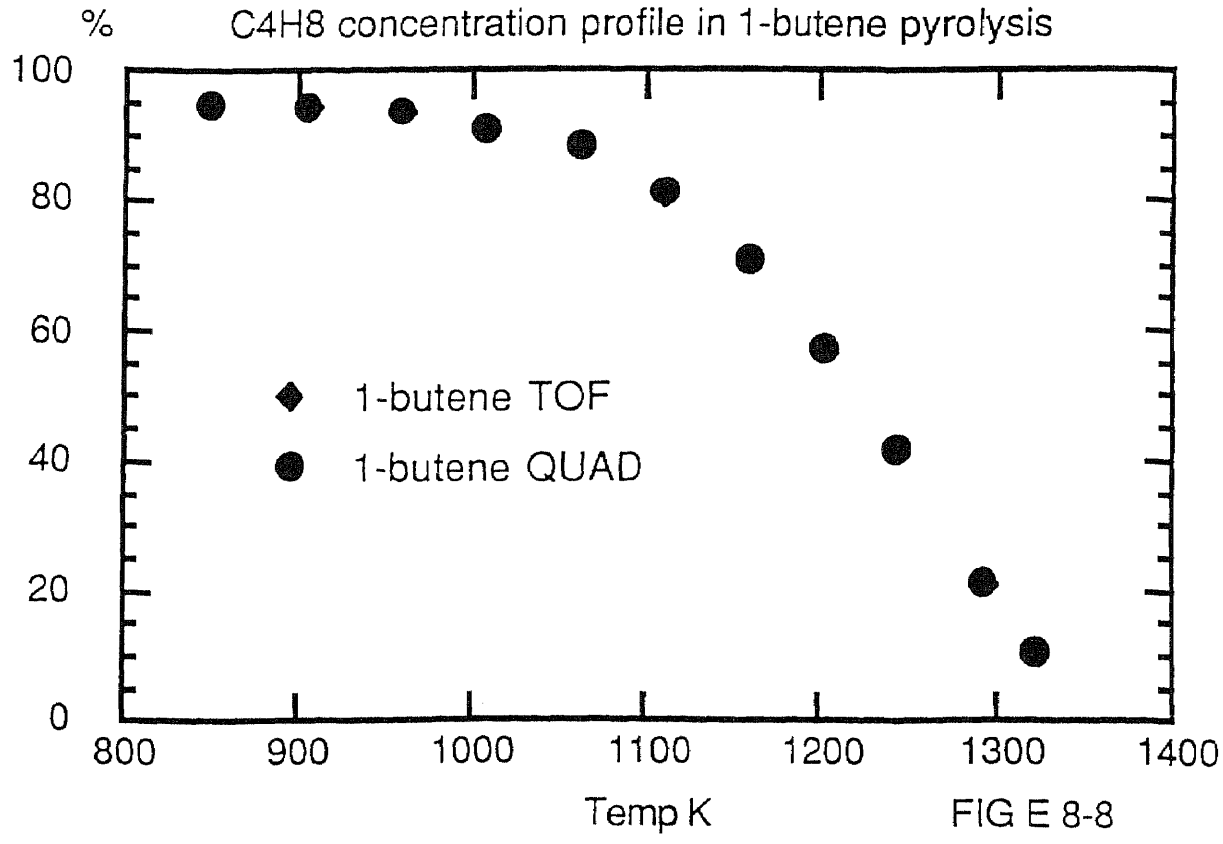

FIG E 8-8

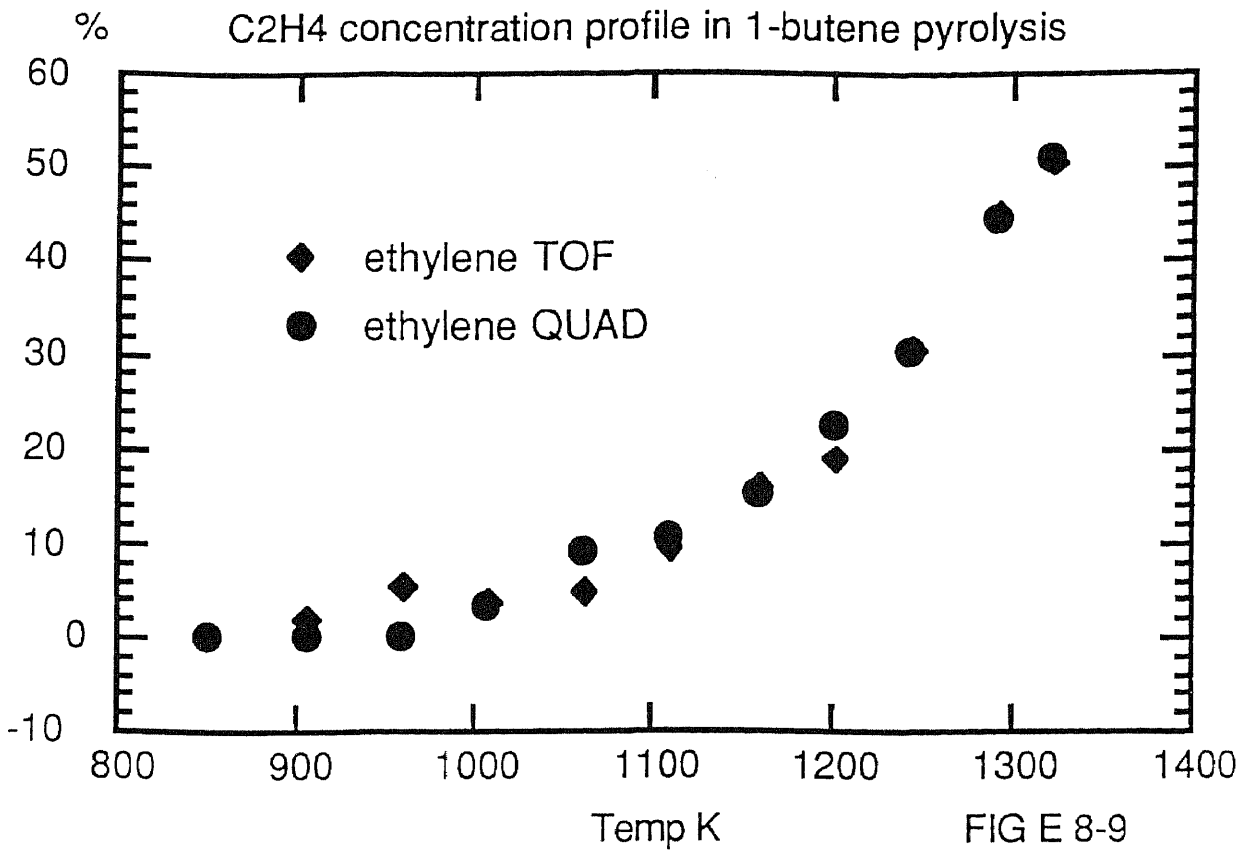

FIG E 8-9

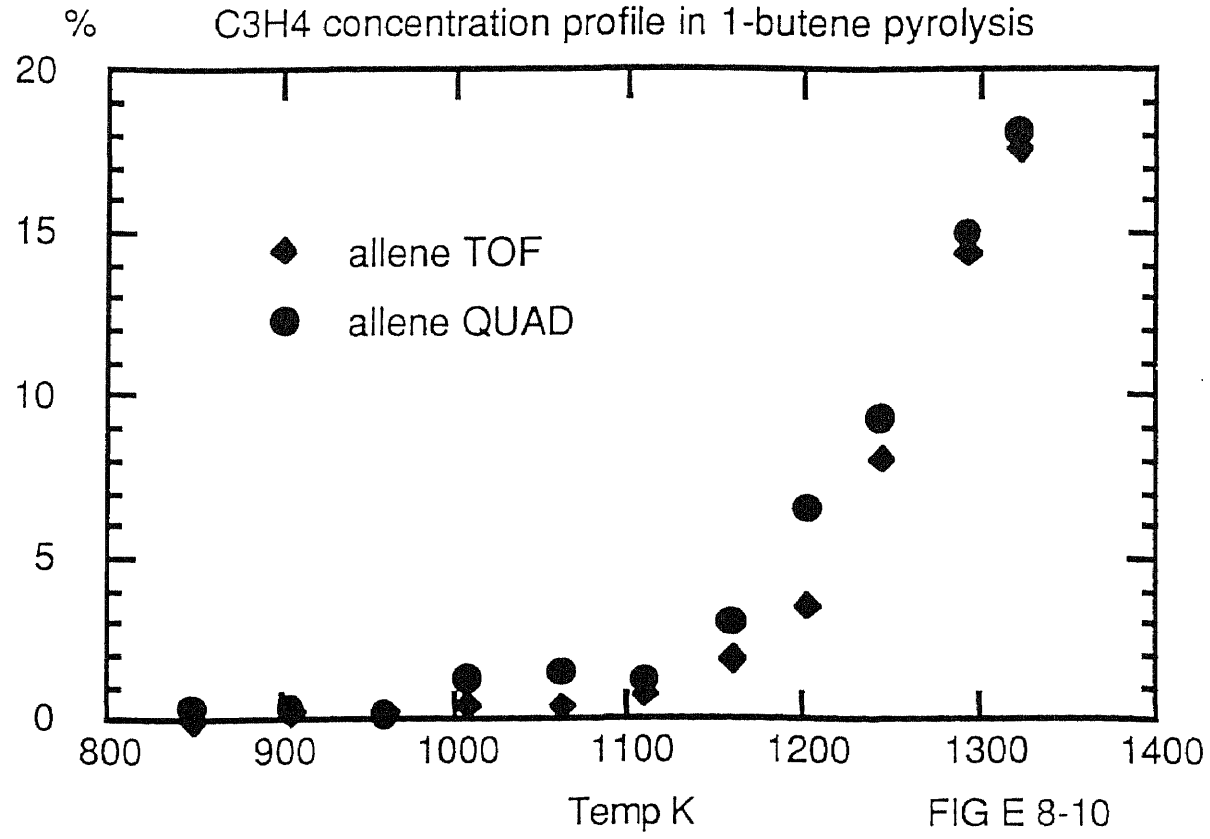

FIG E 8-10

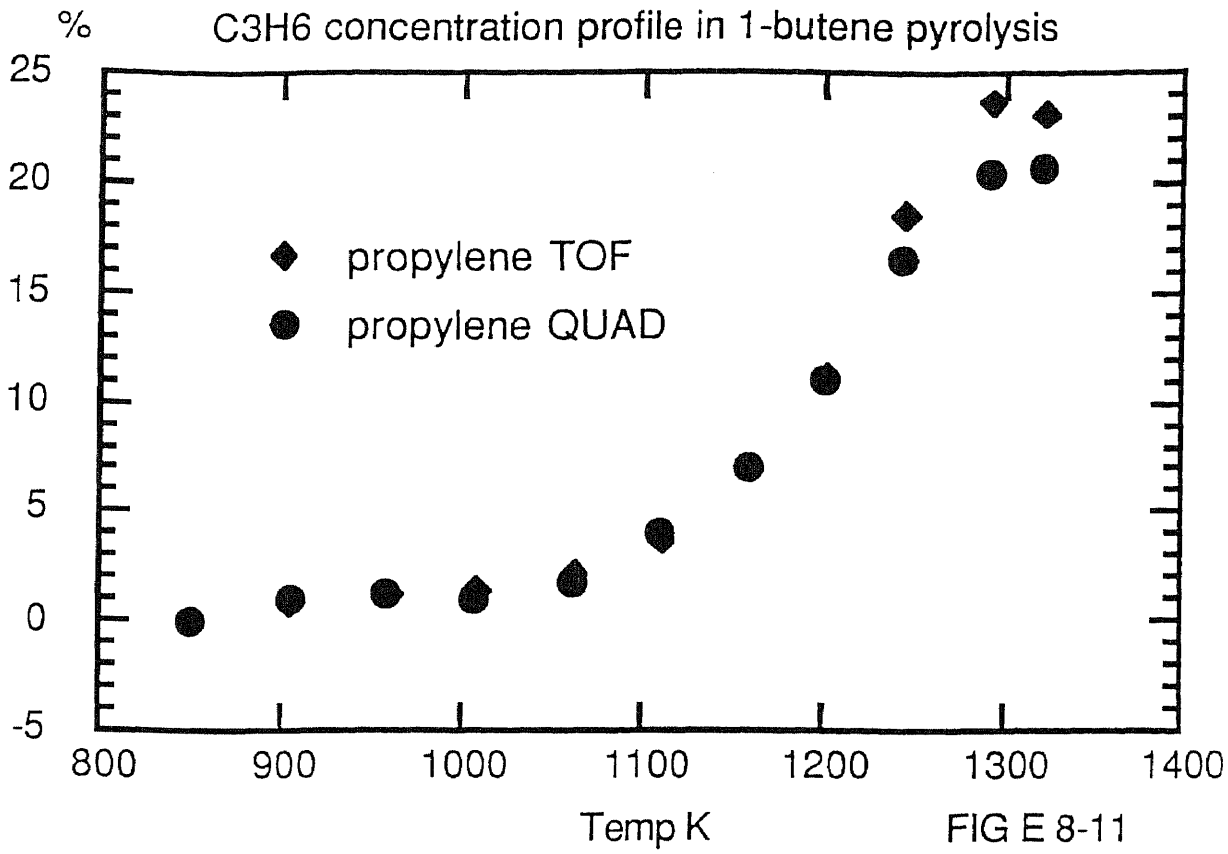

FIG E 8-11

60

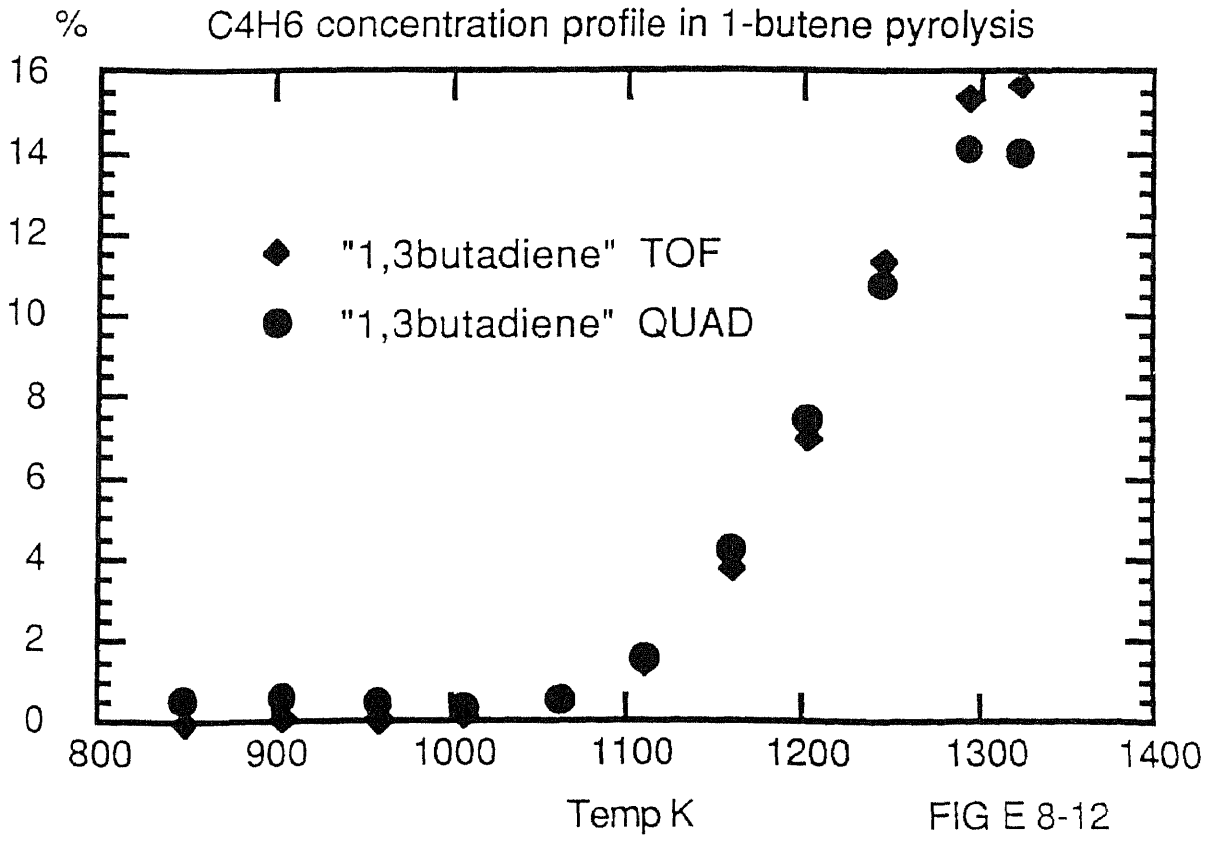

FIG E 8-12

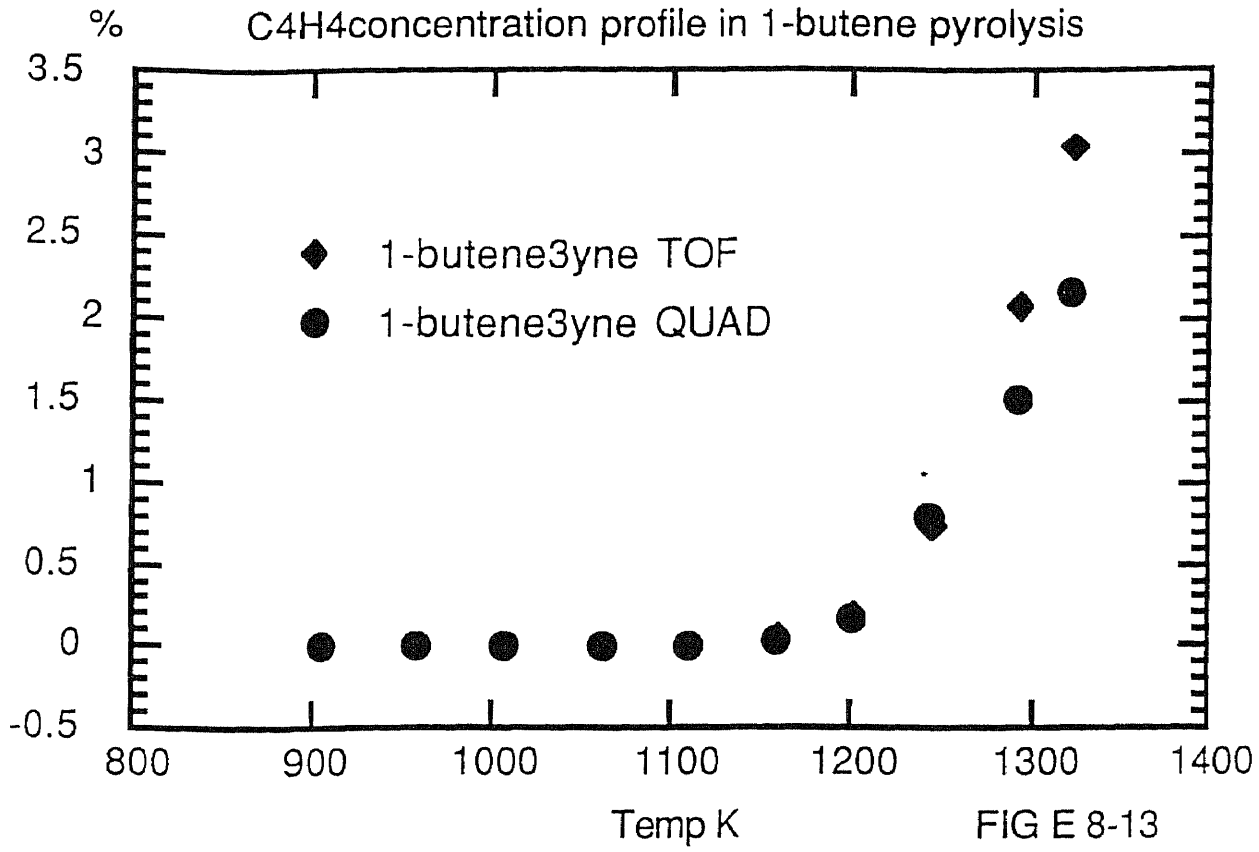

FIG E 8-13

61

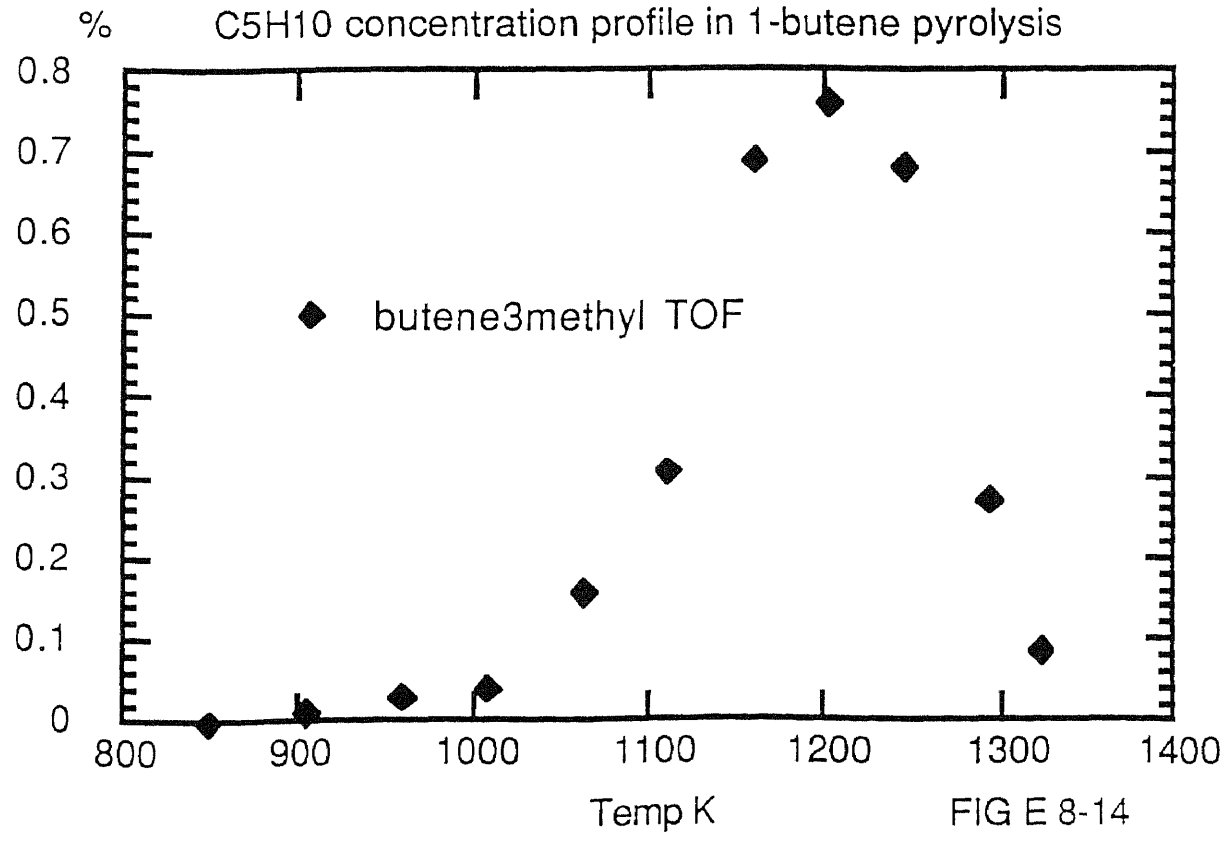

FIG E 8-14

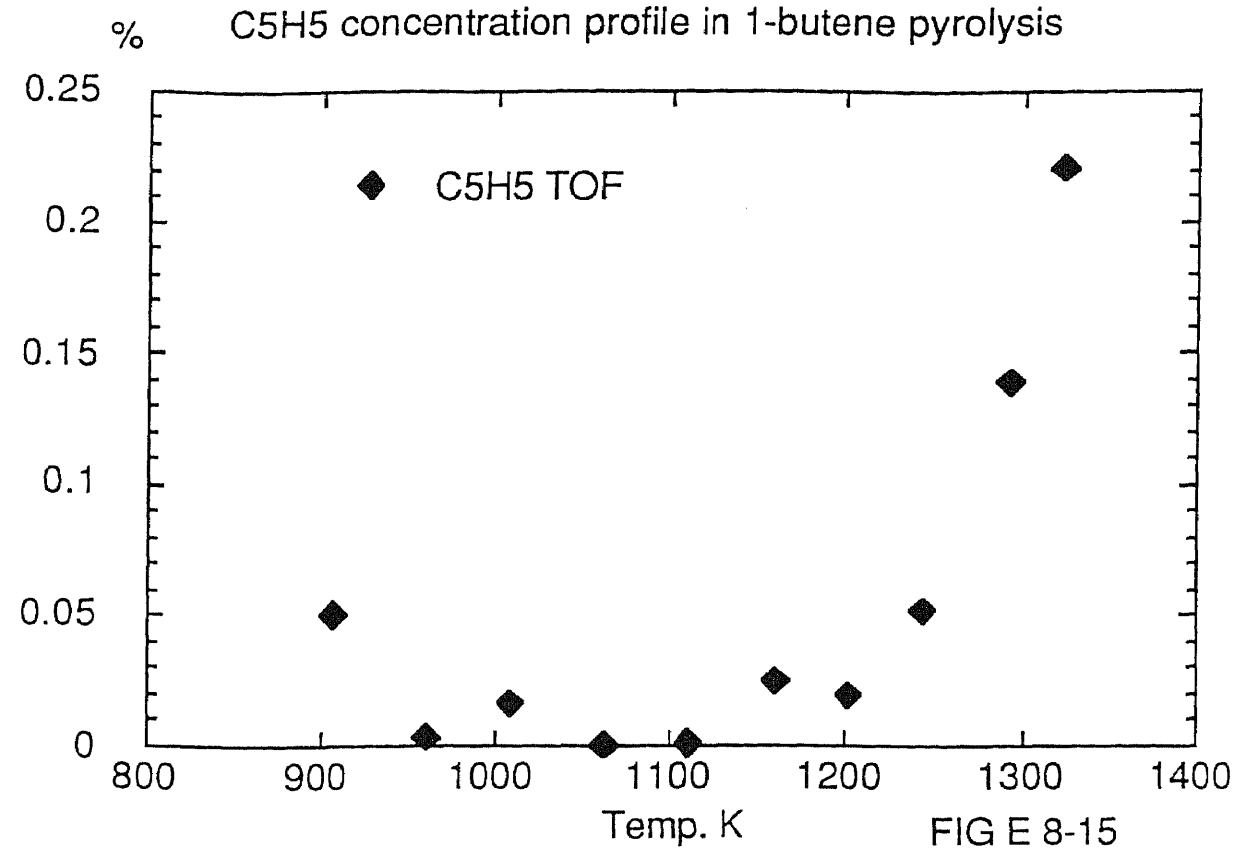

FIG E 8-15

62

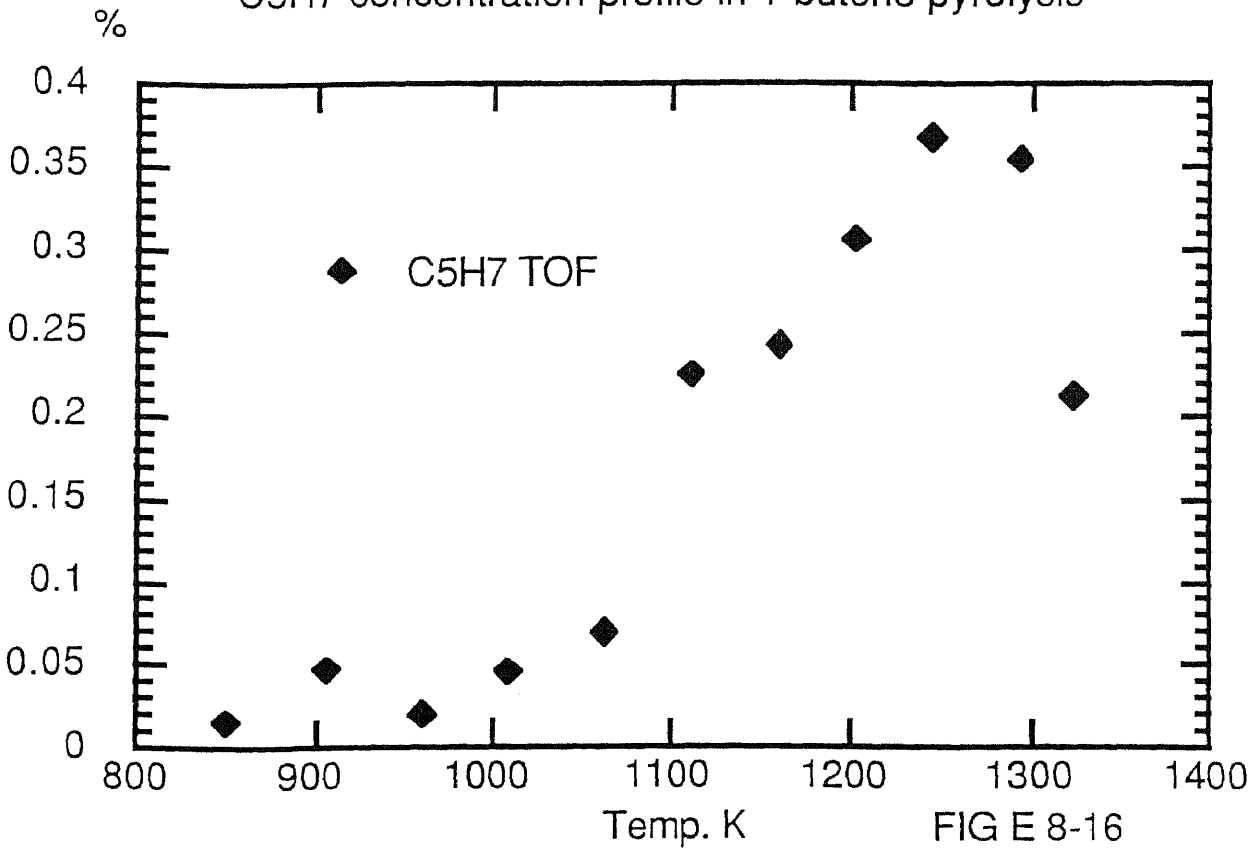

FIG E 8-16

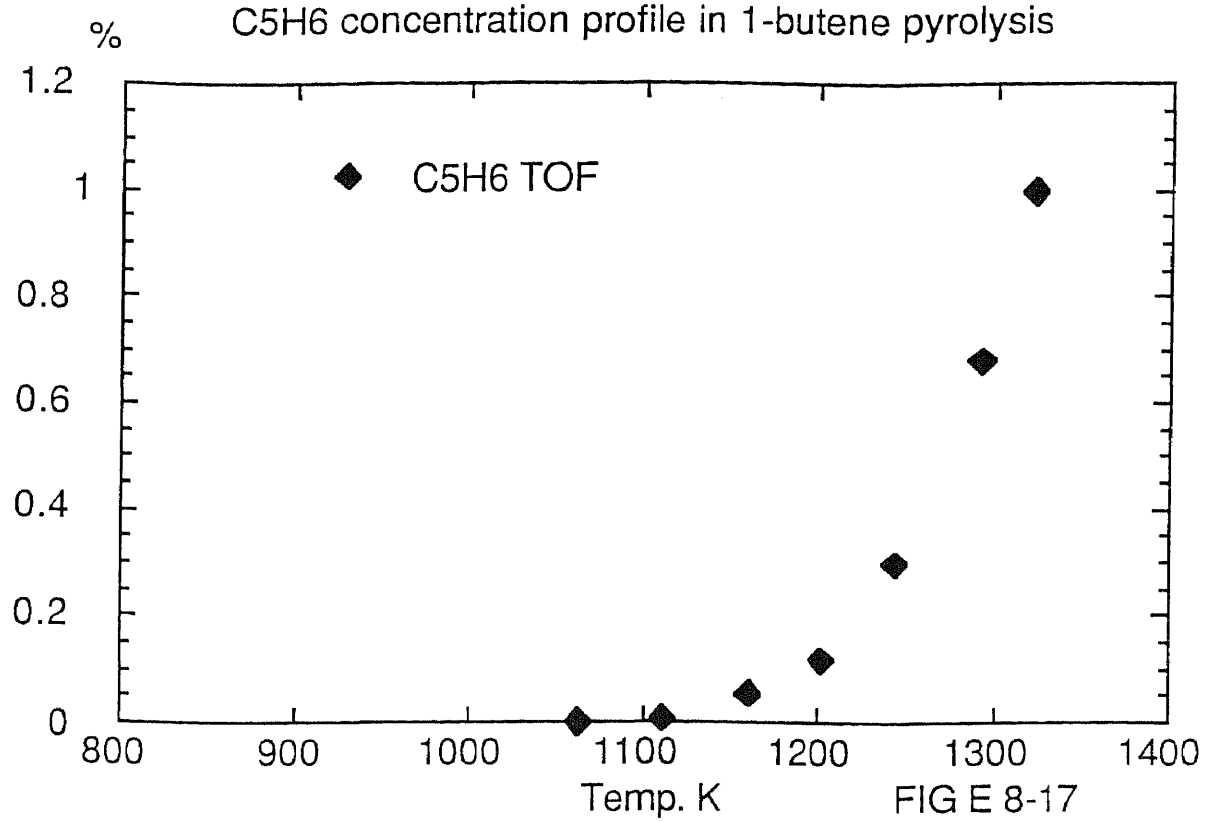

FIG E 8-17

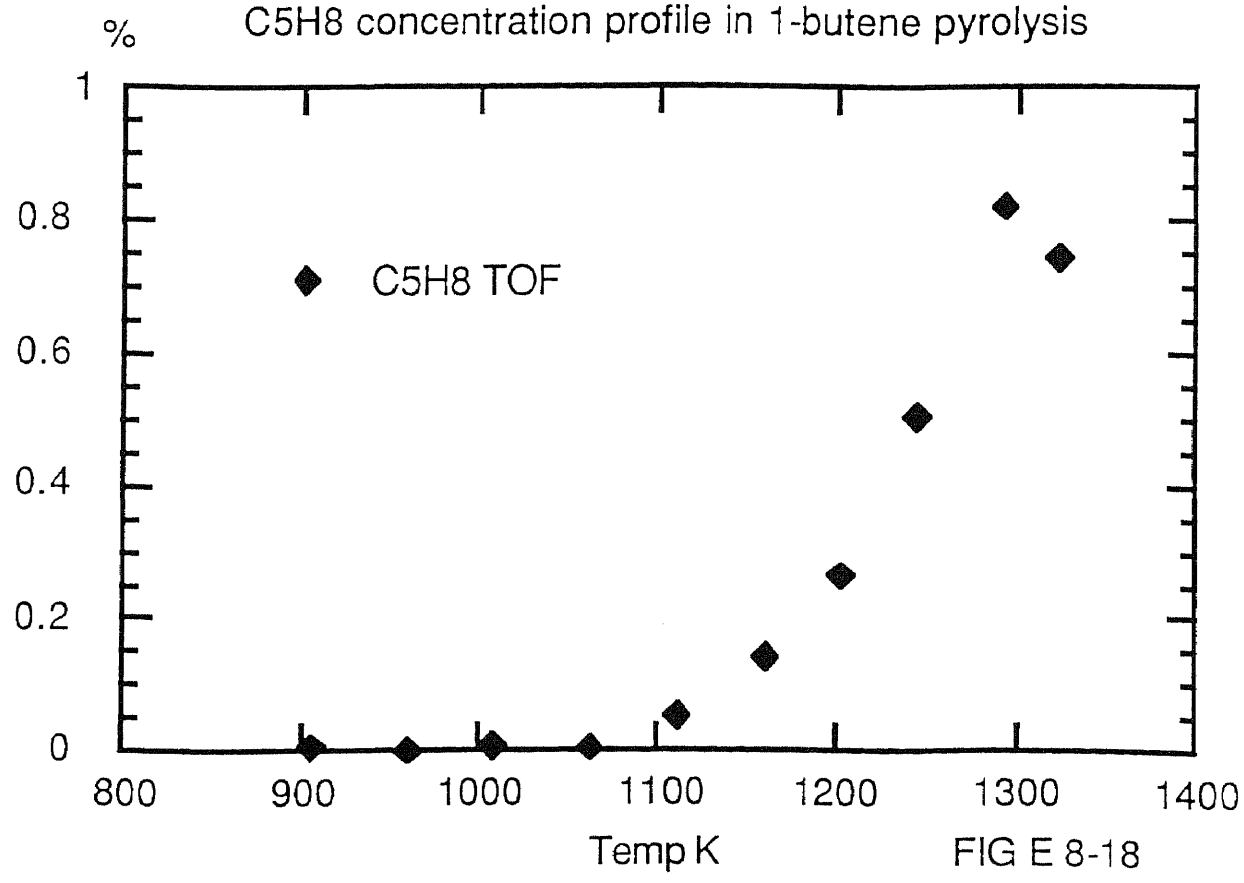

FIG E 8-18

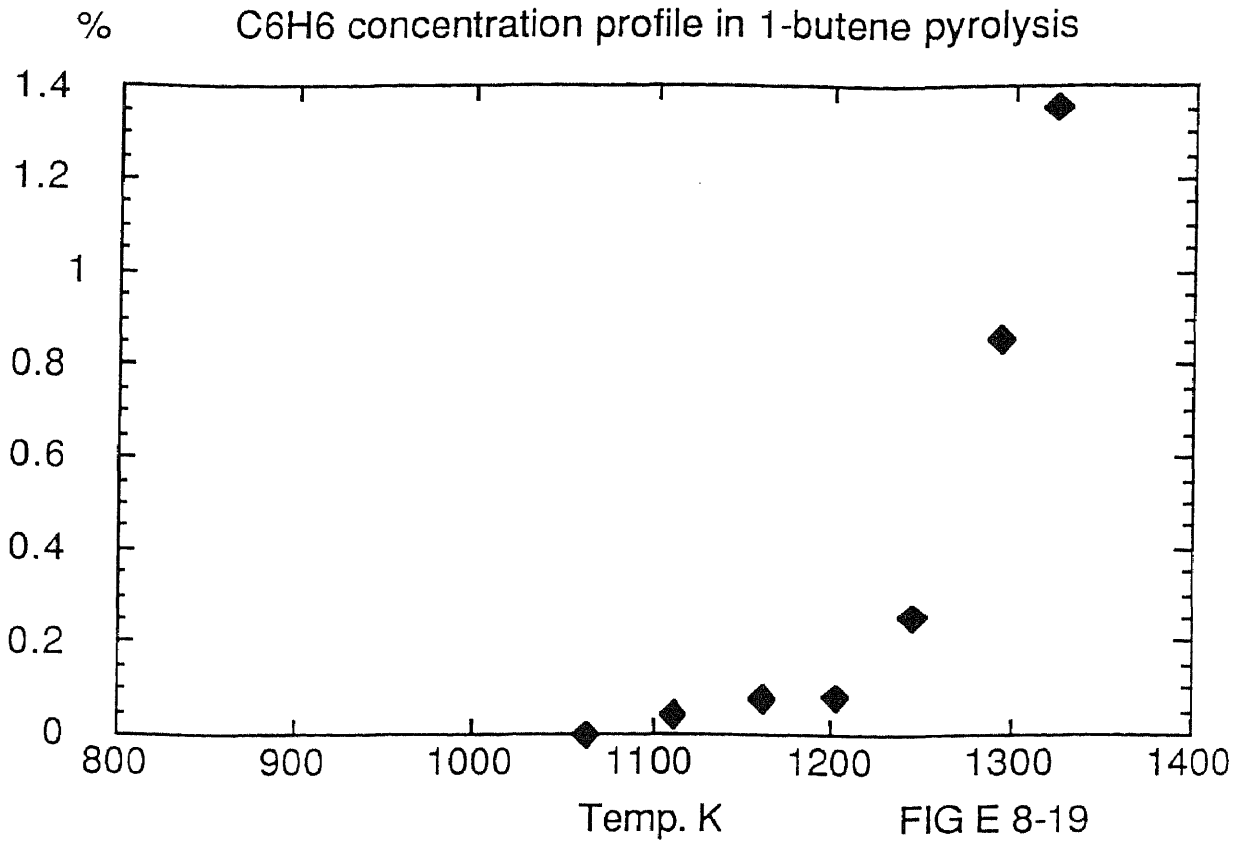

FIG E 8-19

64

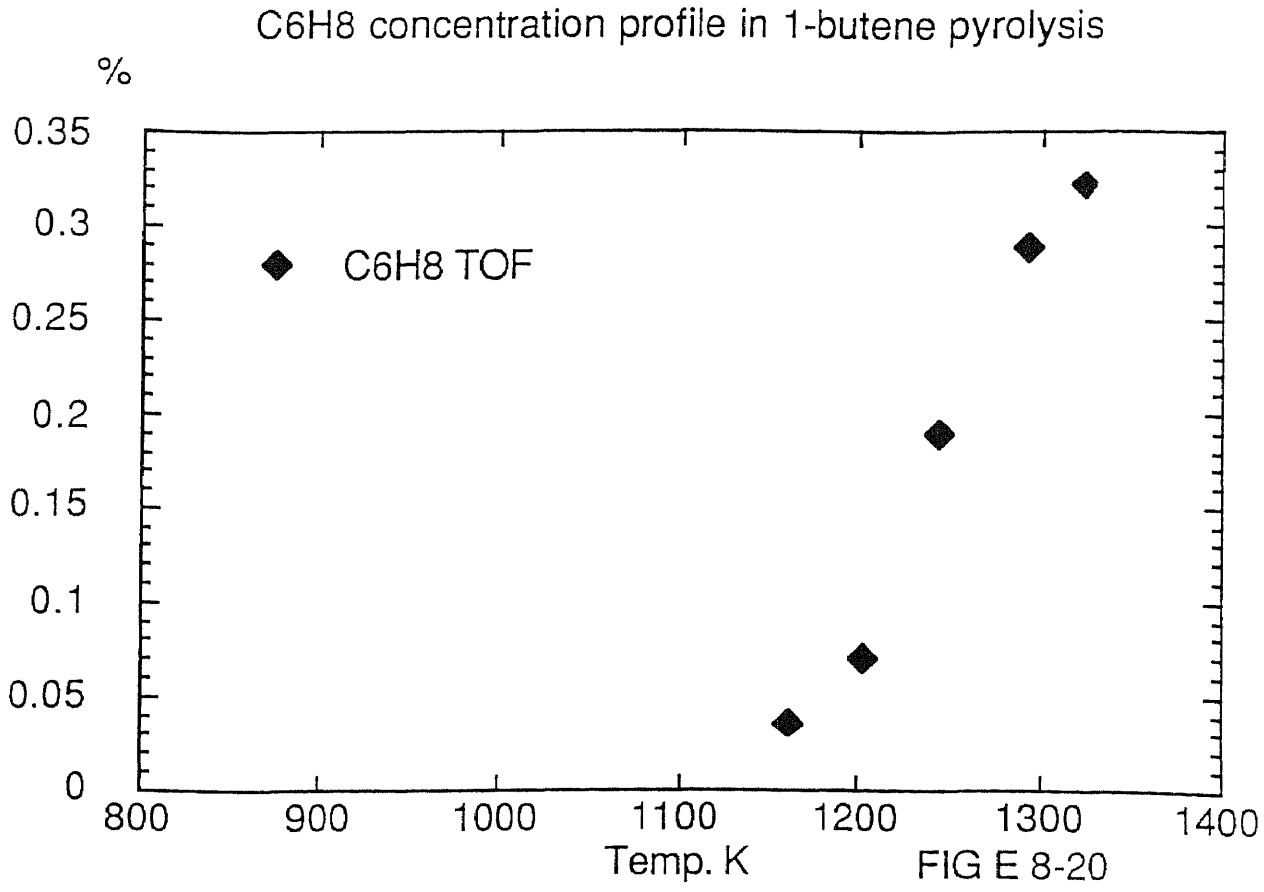

FIG E 8-20

Table E 8-1 1-butene pyrolysis products concentration profiles

temp K	methyl TOF	methane* TOF	ethyne*TOF	C2H3 TOF	ethylene TOF	ethyl TOF	propargyl TOF	allene TOF
850	0.03			0.12	0.08	2.45	0.00	0.01
906	1.53			1.29	2.11	3.91	0.51	0.28
960	0.37			0.80	5.50	5.53	0.41	0.26
1008	2.18			1.06	3.82	5.69	0.54	0.46
1062	1.14			1.71	4.88	5.97	0.90	0.41
1110	3.29			1.64	9.46	5.59	1.08	0.80
1160	4.42			2.64	16.09	6.45	1.45	1.90
1202	7.90	4.36	1.24	3.74	19.20	5.81	2.09	3.56
1244	9.95	16.62	15.03	4.97	30.82	6.55	2.76	8.07
1292	13.92	33.81	24.38	7.22	45.02	2.56	3.52	14.40
1322	11.47	32.40	25.34	5.78	50.67	1.88	3.99	17.61

the number is percentage of initial 1-butene flow rate

allyl TOF	propylene TOF	1,3butadiyne T	C4H3 TOF	1-butene3yne	C4H5 TOF	1,3butadiene T	1butenyl TOF	1-butene TOF
0.04	0.01				0.05	0.00	0.05	94.77
1.28	0.86				0.15	0.09	0.34	94.49
1.62	1.21				0.06	0.09	0.56	93.74
2.84	1.37		0.04		0.12	0.18	0.57	90.86
4.61	2.18		0.04	0.01	0.19	0.58	0.85	88.31
6.45	3.69		0.00	0.02	0.26	1.52	0.99	81.33
7.48	6.94	0.02	0.07	0.06	0.53	3.80	1.14	70.98
7.73	11.19	0.04	0.05	0.19	0.84	7.02	1.41	57.02
8.08	18.60	0.05	0.07	0.73	1.54	11.36	0.94	41.89
6.46	23.69	0.06	0.21	2.07	2.01	15.37	0.55	21.21
4.67	23.16	0.13	0.28	3.04	2.03	15.70	0.03	10.67

C5H5 TOF	C5H6 TOF	C5H7 TOF	C5H8 TOF	butene3methyl	C6H6 TOF	C6H7 TOF	C6H8 TOF	SUM(n) TOF
		0.02		0.00				97.64
0.05		0.05	0.01	0.01				106.96
0.00		0.02	0.00	0.03				110.20
0.02		0.05	0.01	0.04		0.01		109.83
0.00	0.00	0.07	0.01	0.16	0.00	0.00		112.00
0.00	0.01	0.23	0.05	0.31	0.04	0.02		116.78
0.03	0.06	0.24	0.14	0.69	0.08	0.04	0.04	125.29
0.02	0.12	0.31	0.27	0.76	0.08	0.02	0.07	135.04
0.05	0.30	0.37	0.51	0.68	0.26	0.12	0.19	180.52
0.14	0.68	0.36	0.82	0.27	0.86	0.16	0.29	220.03
0.22	1.00	0.21	0.74	0.09	1.36	0.15	0.32	212.93

Table E 8-2	1-butene pyrolysis products concentration profile in quadrupole detector							
temp K	methyl QUAD	methane*QUA	ethyne*QUAD	C2H3 QUAD	ethylene QUAD	ethyl QUAD	propargyl QUA	allene QUAD
850	0.00	0.68	0.00	0.00	0.00	3.49	0.00	0.36
906	0.00	0.80	0.46	0.00	0.00	3.59	0.00	0.29
960	0.23	0.89	2.62	0.00	0.00	4.14	0.00	0.14
1008	0.41	0.77	1.83	0.00	3.43	4.66	0.08	1.28
1062	1.68	1.63	2.38	1.42	9.09	5.19	0.95	1.48
1110	3.98	3.40	4.96	2.71	10.57	6.62	2.04	1.21
1160	3.79	4.69	4.84	2.83	15.29	7.20	2.78	3.02
1202	5.96	9.01	6.44	3.37	22.53	6.94	2.07	6.53
1244	8.84	15.27	12.53	6.12	30.68	6.28	3.11	9.32
1292	9.93	23.44	19.57	6.22	44.64	4.43	3.06	14.98
1322	10.74	28.25	26.36	6.07	50.96	3.29	4.03	18.11
ionization cross section is calculated from group addition theory for radical experiment for stable species								
ß is determinated by fitting for radicals and measured for stable species.								
the number is percentage of initial 1-butene flow rate								

allyl QUAD	propylene QUA	1,3butadiyne C	C4H3 QUAD	1-butene3yne	C4H5 QUAD	1,3butadiene C	1butenyl QUAD	1-butene QUA
0.00	0.00					0.53	0.29	94.77
0.00	0.96	0.00	0.00	0.00	0.00	0.60	0.41	94.49
1.37	1.18	0.01	0.00	0.00	0.00	0.45	0.21	93.74
3.16	1.00	0.02	0.00	0.00	0.00	0.34	0.51	90.86
6.42	1.65	0.03	0.00	0.00	0.22	0.54	0.39	88.31
7.15	3.97	0.04	0.00	0.00	0.27	1.54	1.02	81.33
8.07	6.96	0.05	0.00	0.02	0.39	4.20	1.32	70.98
9.67	11.03	0.07	0.07	0.16	0.94	7.44	1.44	57.02
8.15	16.46	0.08	0.13	0.78	1.39	10.75	1.11	41.89
5.57	20.38	0.07	0.20	1.49	1.84	14.10	0.58	21.21
2.96	20.68	0.12	0.19	2.15	1.92	14.02	0.31	10.67

C5H5 QUAD	C5H6 QUAD	C5H7 QUAD	C5H8 QUAD	butene3methyl	1,5hexadiyne (	C6H7 QUAD	C6H8 QUAD	SUM(mass c)
0.05	0.11	0.19	0.00	0.00	1.29	0.17	0.18	94.279
0.01	0.03	0.15	0.00	0.01	0.50	0.10	0.15	100.56
0.08	0.15	0.07	0.00	0.03	1.02	0.15	0.03	107.73
0.07	0.11	0.04	0.00	0.04	1.21	0.10	0.07	110.96
0.10	0.04	0.08	0.00	0.15	0.95	0.11	0.02	124.39
0.03	0.12	0.15	0.18	0.29	0.54	0.02	0.12	129.89
0.01	-0.03	0.25	0.24	0.64	0.02	0.06	0.04	134.5
0.04	0.15	0.31	0.15	0.71	0.28	0.09	0.07	152.34
0.08	0.19	0.30	0.46	0.64	0.41	0.09	0.17	184.87
0.05	0.50	0.37	0.40	0.25	0.55	0.08	0.19	240.22
0.14	0.74	0.44	0.56	0.08	1.09	0.19	0.25	244.13

1-butene pyrolysis provides a rich radical pool. 35 species are detectable by the photoionization TOF mass spectrometer, FIG.1-1b. Under very low pressure and short residence time condition, the unimolecular dissociation, H atom abstraction, addition and radical recombination reaction are dominant reaction channels. Mass 56 represents 1-butene at low temperature and butenes at higher temperature. Unimolecular dissociation is predominant at low temperature, at high temperature the stable species are in the rich radical pool, the H atom abstraction reaction become dominant reaction channels. This concentration profile , FIG.E8-14, is very important, it serves as an internal standard for other species as well as the reagent decay process. Mass 55 is butenyl radical, when photon excited the single unpaired electron to infinity, most extra energy was carried out by the electron and the left cation was stabilized. At high temperature butenyl go through the ß scission reaction and radical-radical recombination reaction. Butadiene is a stable molecule. It's produce reaction channels are butenyl's ß scission, H atom abstraction and disproportion reactions. If 1,3-butadiene is the dominant product, we can calculate it's concentration relative to the initial reagent flow rate. Later on we will see this data can be used to figure out the electron impact ionization cracking pattern of butenyl radical in the quadrupole mass spectrum. The good agreement between TOF measurement and quadrupole measurement are fully expected. Mass 42 is an unique product in 1-butene pyrolysis, propylene has only one isomer. Because it's relative ionization cross section in both of VUV photon ionization and 70 ev electron impact ionization are known, it's

absolute concentration in the reactor is determined from both of these two detectors individually FIG.E 8-11. Beside the stable species we can see the clear radicals signal. mass 15 is refereed to methyl radical, mass 29 the ethyl radical and mass 41 the allyl radical. These radicals have similar electron structure as 1-butenyl radical, after the 2p electron be excited to infinity the carbonium are very stable. These radicals concentration can be well estimate by assuming the methyl radical has the same scale photoionization cross section of nitric oxide (0.14). Because this is contributed from the single unpaired 2p electron on the carbon atom, if group theory is valid, big radicals concentration will be estimated within a 20 % uncertainty. Molecular weight growth is clearly in the pyrolysis reaction. Pentene, pentadiene and benzene (FIG. E8-14, 17, 19) are formed in this reaction through well known mechanism. Once benzene formed in the rich radical pool the aromatic compound grows up. At high temperature methyl radical and propargyl radical are dominant and propargyl look like response for benzene formation and methyl radical for molecular weight growing up. Toluene, xylenes and their radicals are observed in TOF spectrum.

8. Comparison of Photoionization and Electron Impact Data

We use Neon (mass 20) as internal standard in the quadrupole measurement, because Neon does not do any chemical reaction, but response for all flow dynamical parameter change and instrumental response changing. From early work we know that when the mole

fraction of Neon is in the range 1/2 and 1/3, all of the hydrocarbons will have similar behavior in the molecular beam. Using Neon as internal standard and buffer gas we can get the 1-butene concentration profiles from both measurement FIG E8-8. Because the Neon flux measured from quadrupole mass spectrometer is increased as the total mole number increase when molecule pyrolysis occurring, a normalization is need before comparison these two profiles. (equation E 8-1) The normalization factor is temperature dependent. After this normalization the two profiles of any other stable species must has a temperature independent normalization factor which comes from the two ionization cross sections. Except this constant factor the profiles of any stable species both in photoionization and electron impact ionization must be the same, FIG.E8-9, 10, 11, 12. For the radical their ß factor in quadrupole detector and photoionization cross section are unknown. But here have two important rules applied on all the species. Rule one is the ß factor of any species in quadrupole detector can not be greater than one, rule two, the group addition theory can applied to low energy photoionization cross section of π-electron system. The first step is make a best fit between QUAD. and TOF. signal profile. We would like to start from the butenyl radical FIG.E8-7. From simple unimolecular ion decomposition theory, we know that only butene and petene can contribute to this ion in both TOF and Quad. spectra. These fragment are ease be abstracted from the total signal by using the standard cracking pattern generated by our instrument. the result is good, the two profiles march very well. However to calculate the concentration of this radical we need to know it's ß

factor in quadrupole spectra. Unimolecular ion decomposition mechanism tell us that this ion can decay by å cleavage to generate mass 15, 27, 28 and 40. At high temperature the butenal radical was gone and not affect on the mass 54 ion. The best march between the two spectrum determined the contribute of butenyl on the mass 54 in electron impact ionization process. Heavier species formed at higher temperature are small amount so we do not account on them at this time. Check mass 54,(FIG.E8-12) we assume 1,3-butadiene is dominant. The concentration profiles both in TOF and in Quad. can get immediately from their ionization cross sections, the result is good also. For mass 53 ion the two profile march very well. For mass 42 ion FIG. E8-11, the propylene ion, this molecule is unique in 1-butene pyrolysis. This ion can generated from propylene it-self both in TOF and Quad. spectra. These data will not be interfered by other species, so it is a good check for our measurement. Allyl radical mass 41 is the major product of 1-butene pyrolysis the signal is very strong the contribution from other radical is negligible, FIG E 8-5. The ion mass 39 is propargyl, FIG E 8-4. After the abstraction of stable species fragment we need abstract the fragments from other radicals, the major part of them is come from allyl radical. Allyl radical ion lost a neutral molecule H2 is the major decay channel in ionizer. This part in turn reduced ß factor of allyl. For mass 27 ion FIG E 8-2, we find out that both allyl and C4H5 radical have fragment contribute to it. The a cleavage from allyl radical produce the ion mass 27, and C4H5 lost a neutral species C2H2 is the major decay channel of it in the electron impact ionizer. When we reach to mass 15 ion, the methyl radical, the work

is almost down. Both TOF and Quad. data show there are no appreciable mass 14 left. The ß factor of methyl radical is about 1 even we cumulated bigger error on low mass side, the mass 15 is ease to handle because the fragments from stable species is abstracted and the unknown cracking pattern of other radicals do not contribute to it at high temperature. The two possible radicals ethyl and butenyl radical already vanished at high temperature. Azomethane pyrolysis experiment also shows that methyl radical do not have appreciable fragmental ion in quadrupole mass spectrum.After the whole approach we can find out the ß factors for these important radicals, methyl radical, propargyl radical, allyl radical and butenyl radical. Because the radical signal is much weaker than their adjacent species, the bigger deviation in quadrupole signal is expected. If our basic assumption on the 70 eV electron impact ionization and VUV photoionization cross section group addition theory is right, the product of ß and conjugate ionization cross section will fill in a range predicated by this theory, Table.E.8-4. The data are very good except propargyl. We do understand that this deviation is acceptable because the error cumulated in the fragment subtraction process. The ratio of Quad. and TOF signal gives a constant for these species.

$$K(Q,T)_i = Q_i \beta_i / \partial_i \times (\partial/Q\ \beta)_s F \qquad \text{Eq 3.8.1}$$

where Q is the electron impact ionization cross section ∂ is the photoionization cross section and s here indicate the internal standard species or 1-butene. F is the experimental constant which

Ethylene concentration in 1-butene combustion

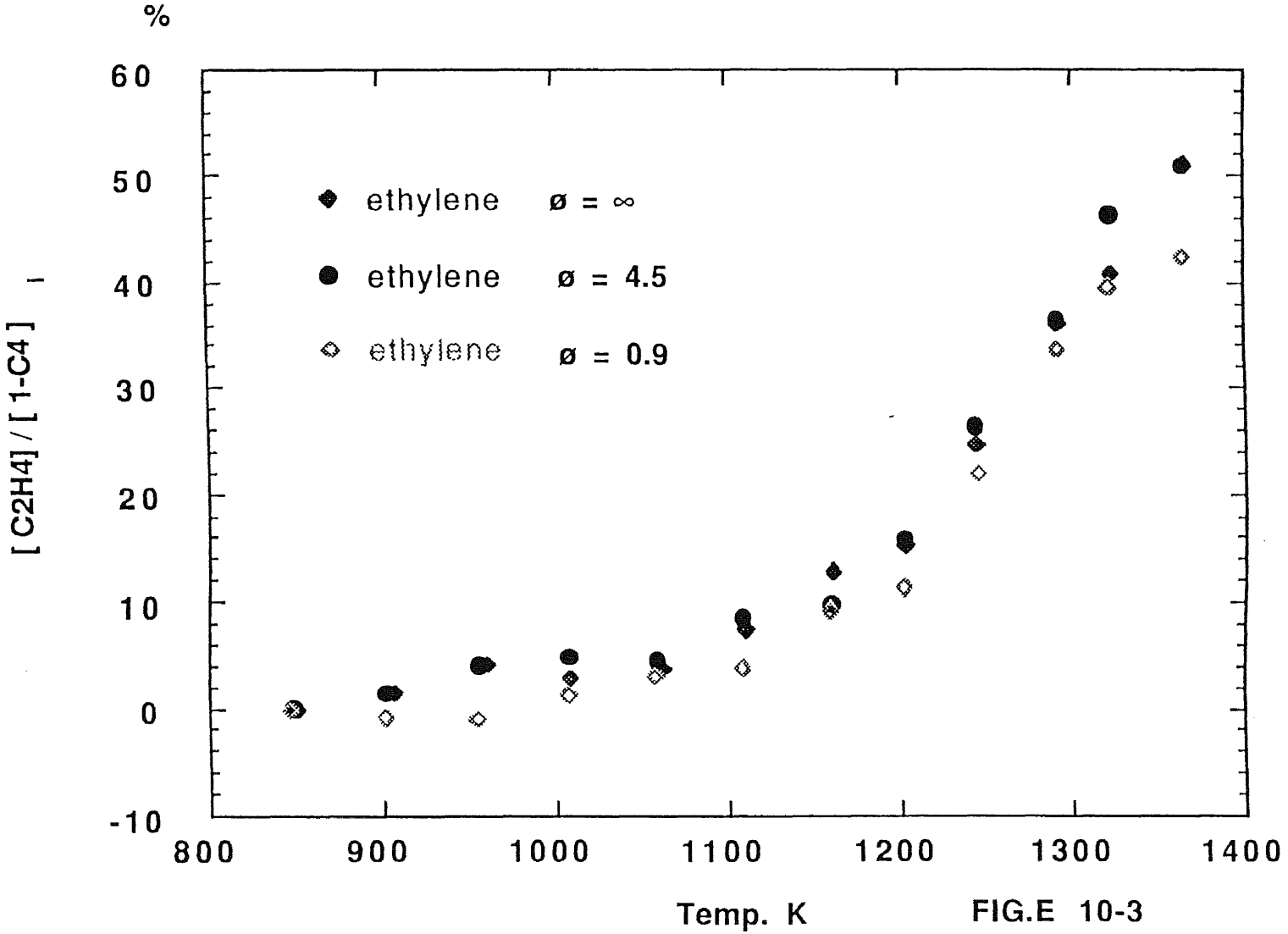

FIG.E 10-3

Ethyl radical concentration in 1-butene combustion

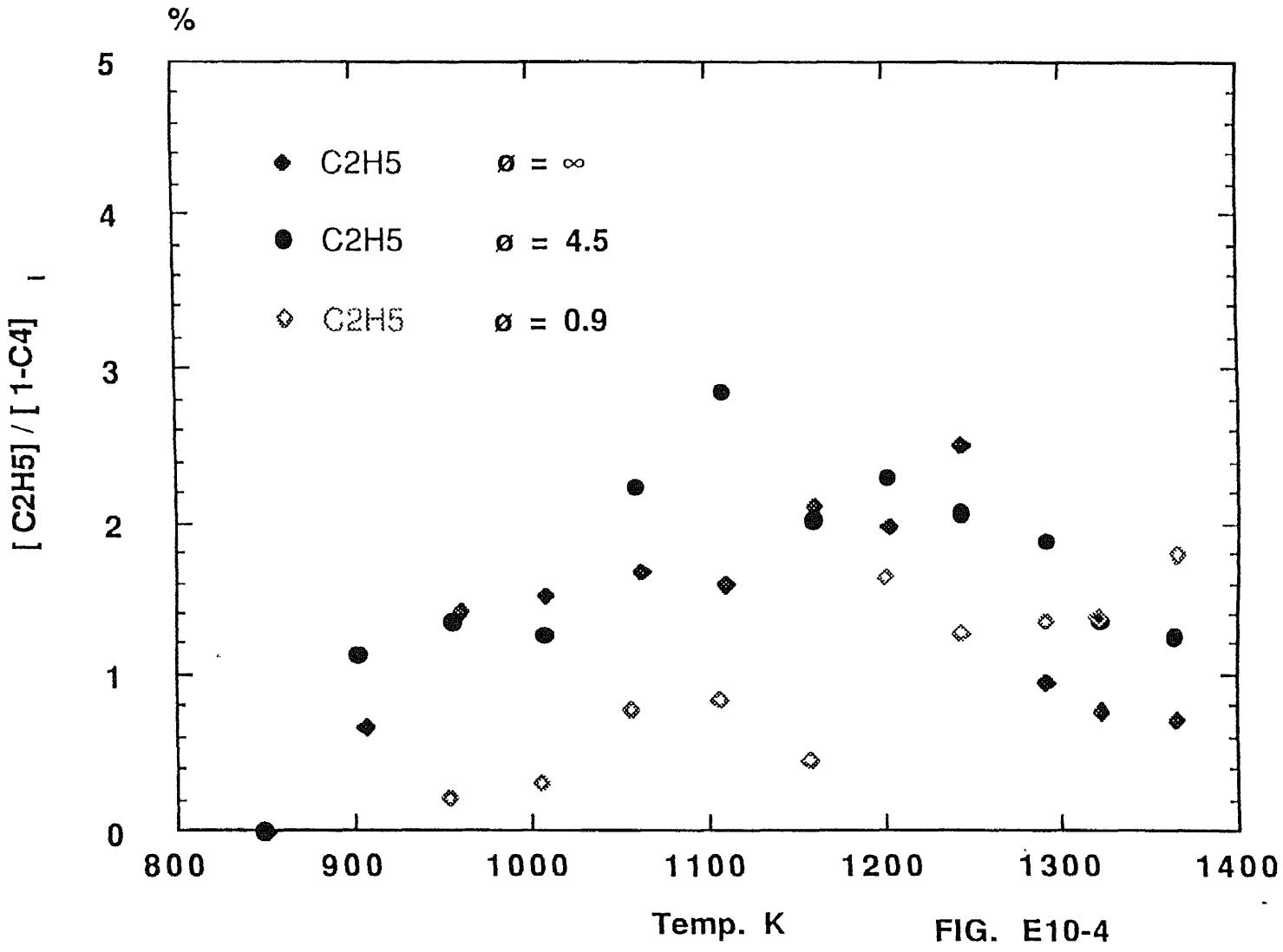

FIG. E10-4

Propargyl radical concentration in 1-butene combustion

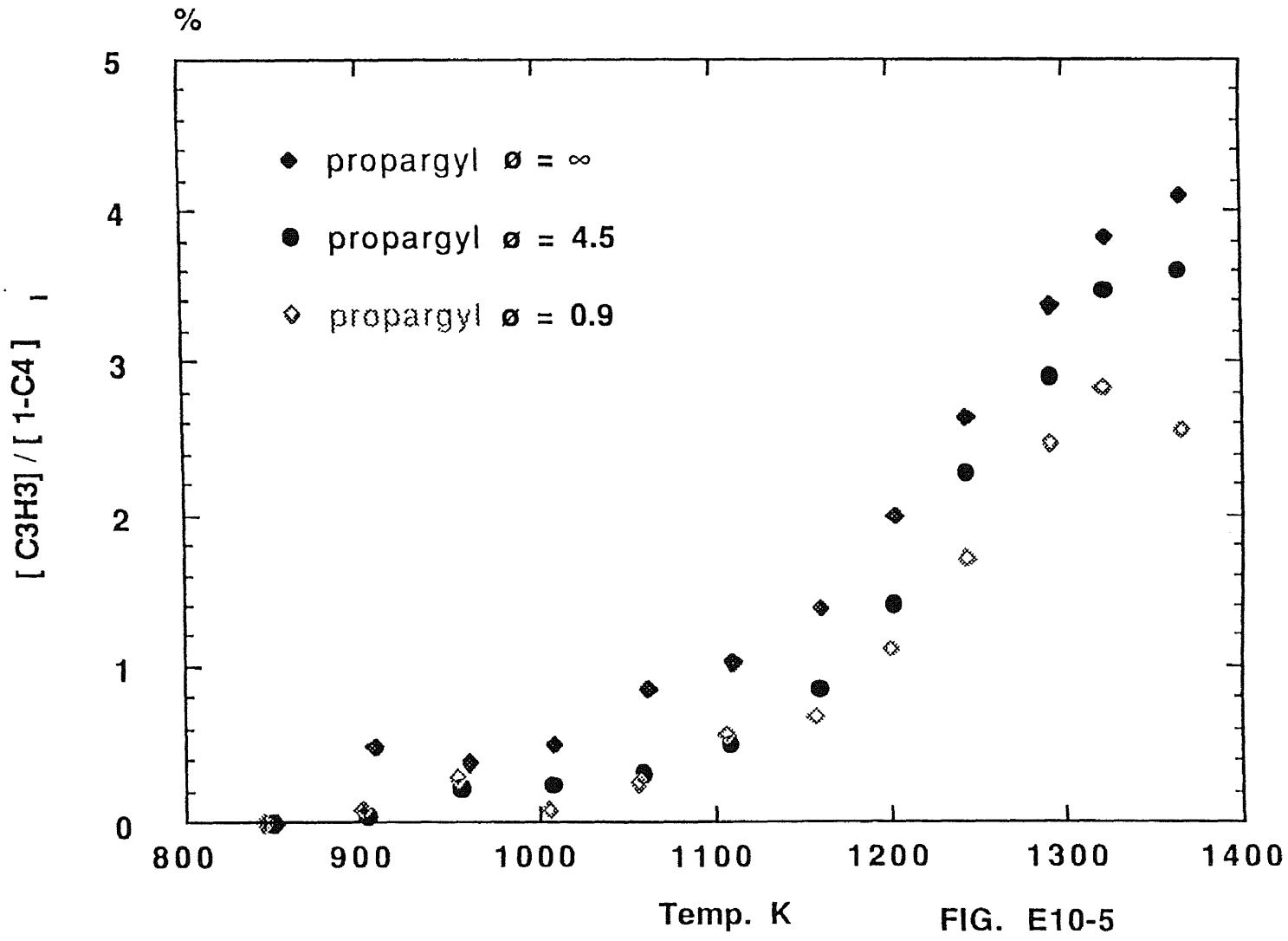

FIG. E10-5

Propargyl radical concentration in 1-butene combustion

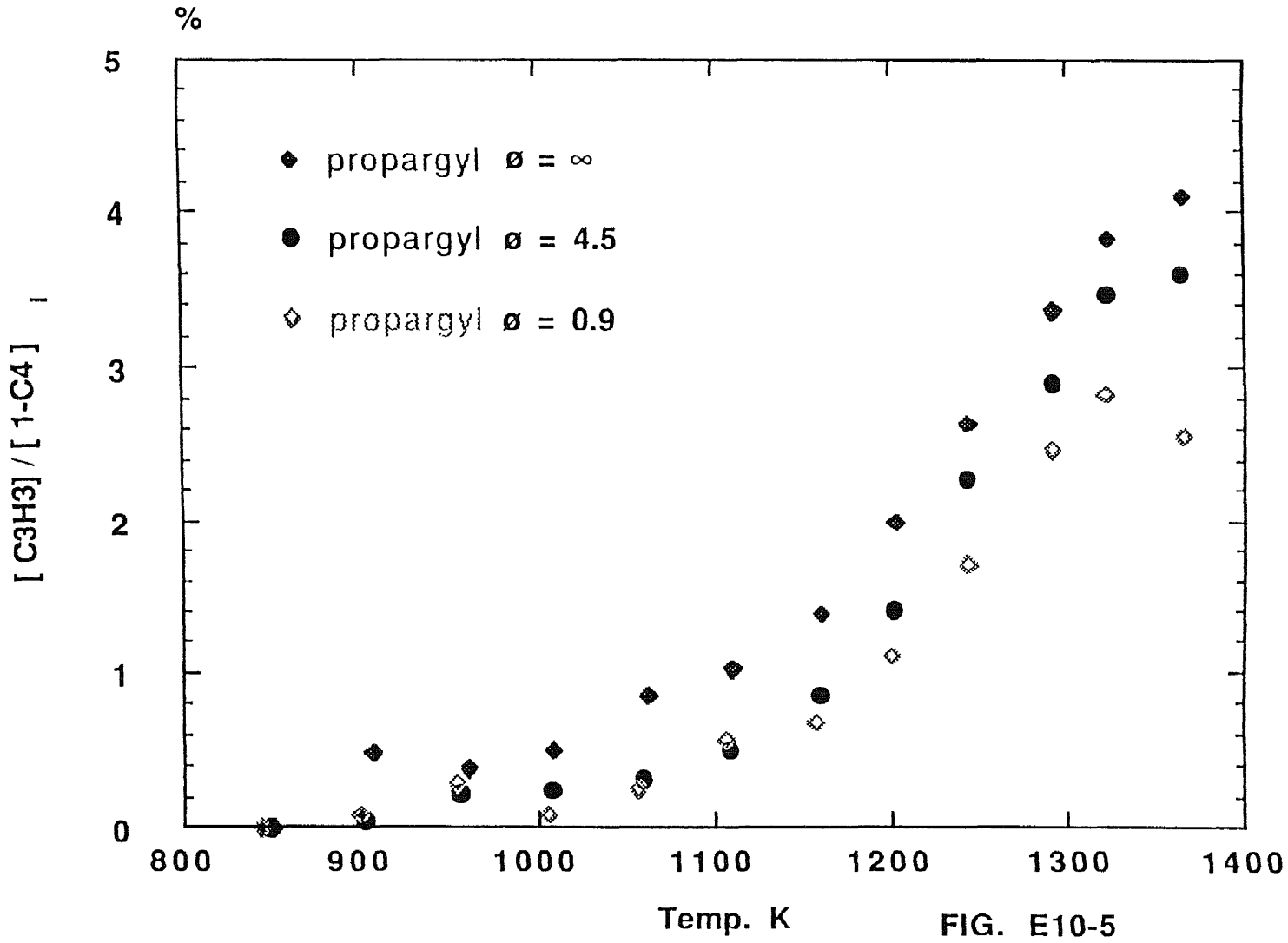

FIG. E10-5

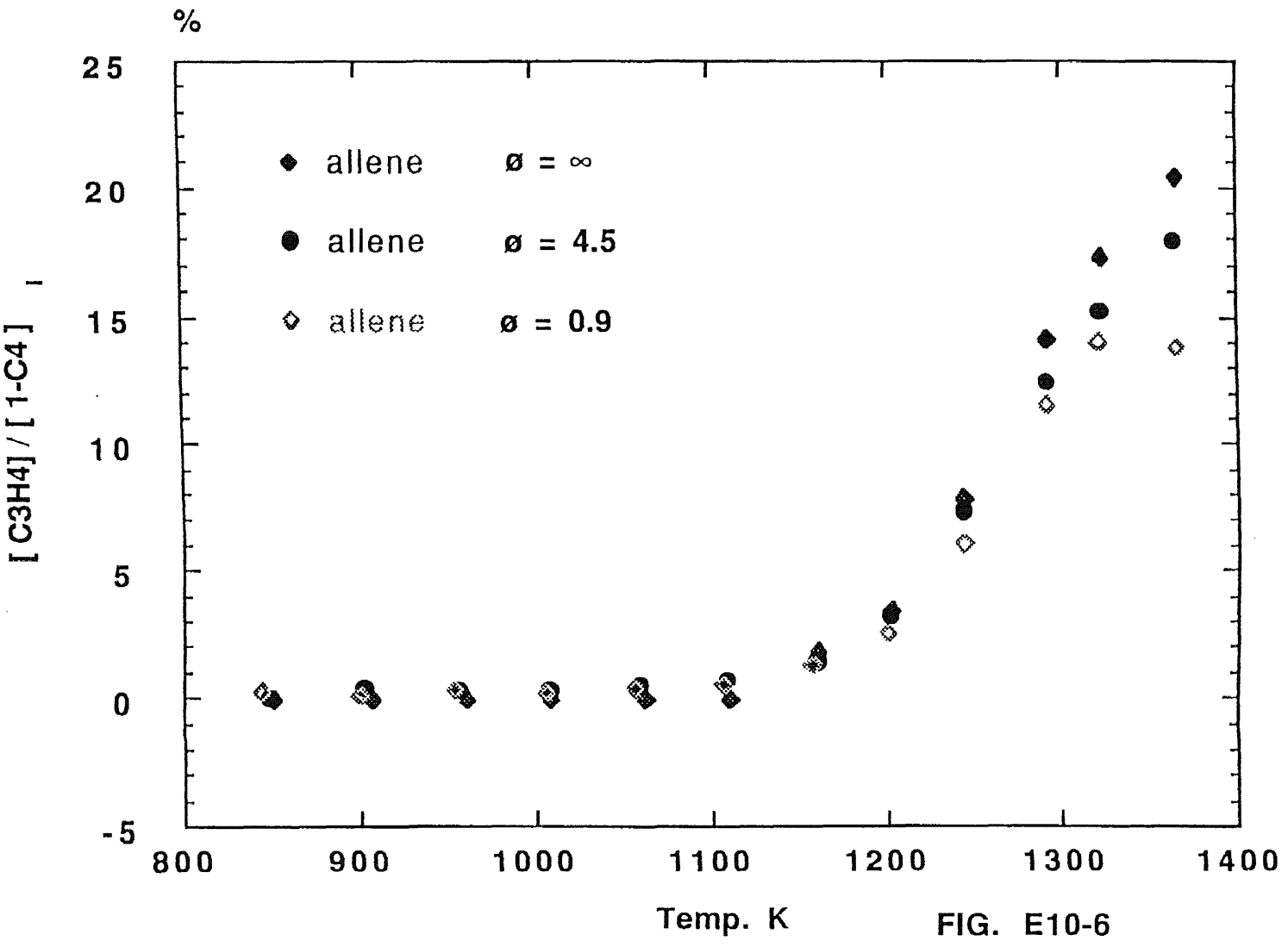
Allene concentration in 1-butene combustion
%
25
20
15
10
5
0
-5
[C3H4] / [1-C4]
allene ø = ∞
allene ø = 4.5
allene ø = 0.9
800
900
1000
1100
1200
1300
1400
Temp. K

FIG. E10-6

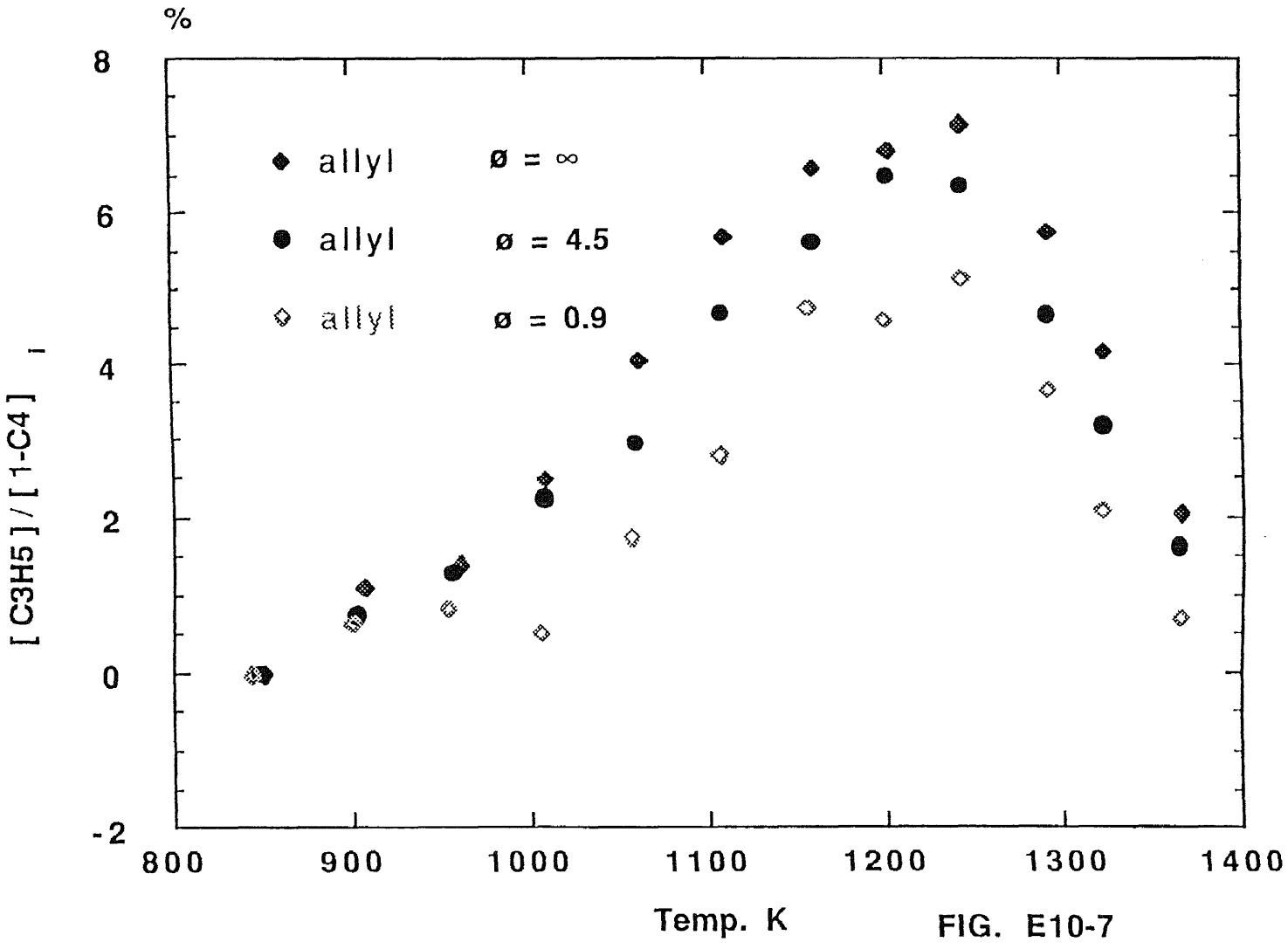
Allyl concentration in 1-butene combustion
%
8
6
4
2
0
-2
[C3H5]/[1-C4]i
allyl ø = ∞
allyl ø = 4.5
allyl ø = 0.9
800
900
1000
1100
1200
1300
1400
Temp. K

FIG. E10-7

Propylene concentration in 1-butene combustion

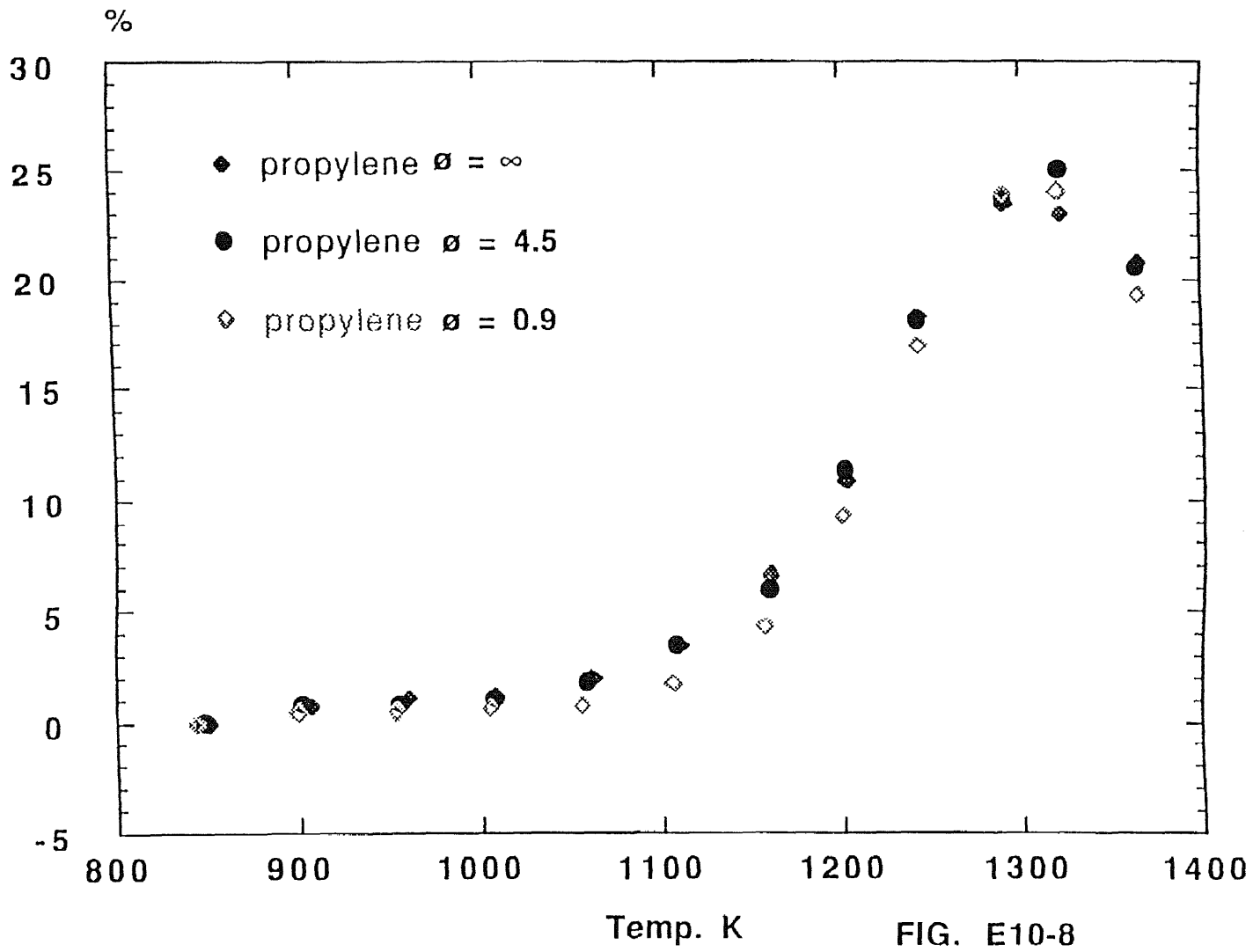

FIG. E10-8

Acetaldehyde concentration in 1-butene combustion

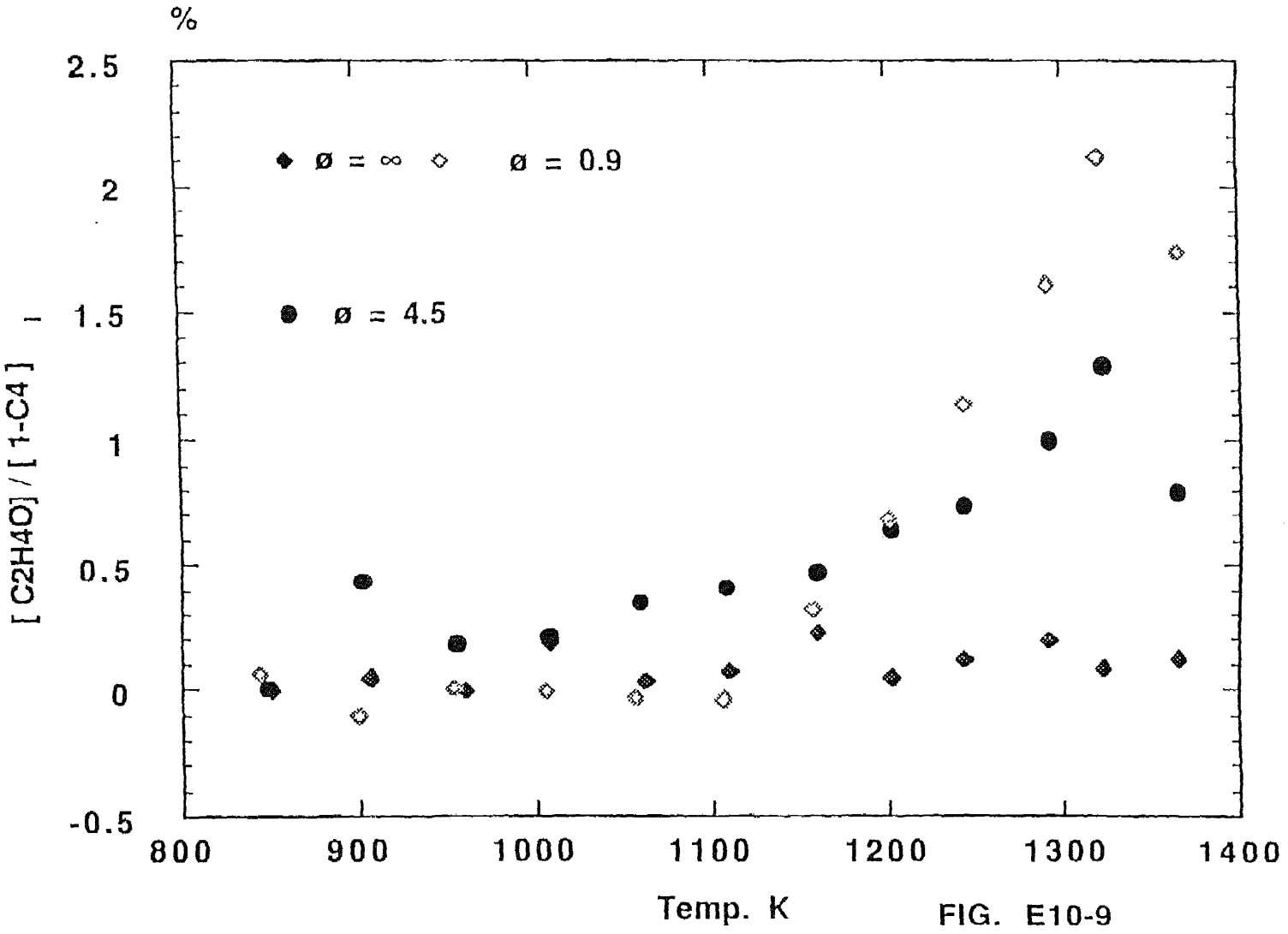

FIG. E10-9

C4H5 radical concentration in 1-butene combustion

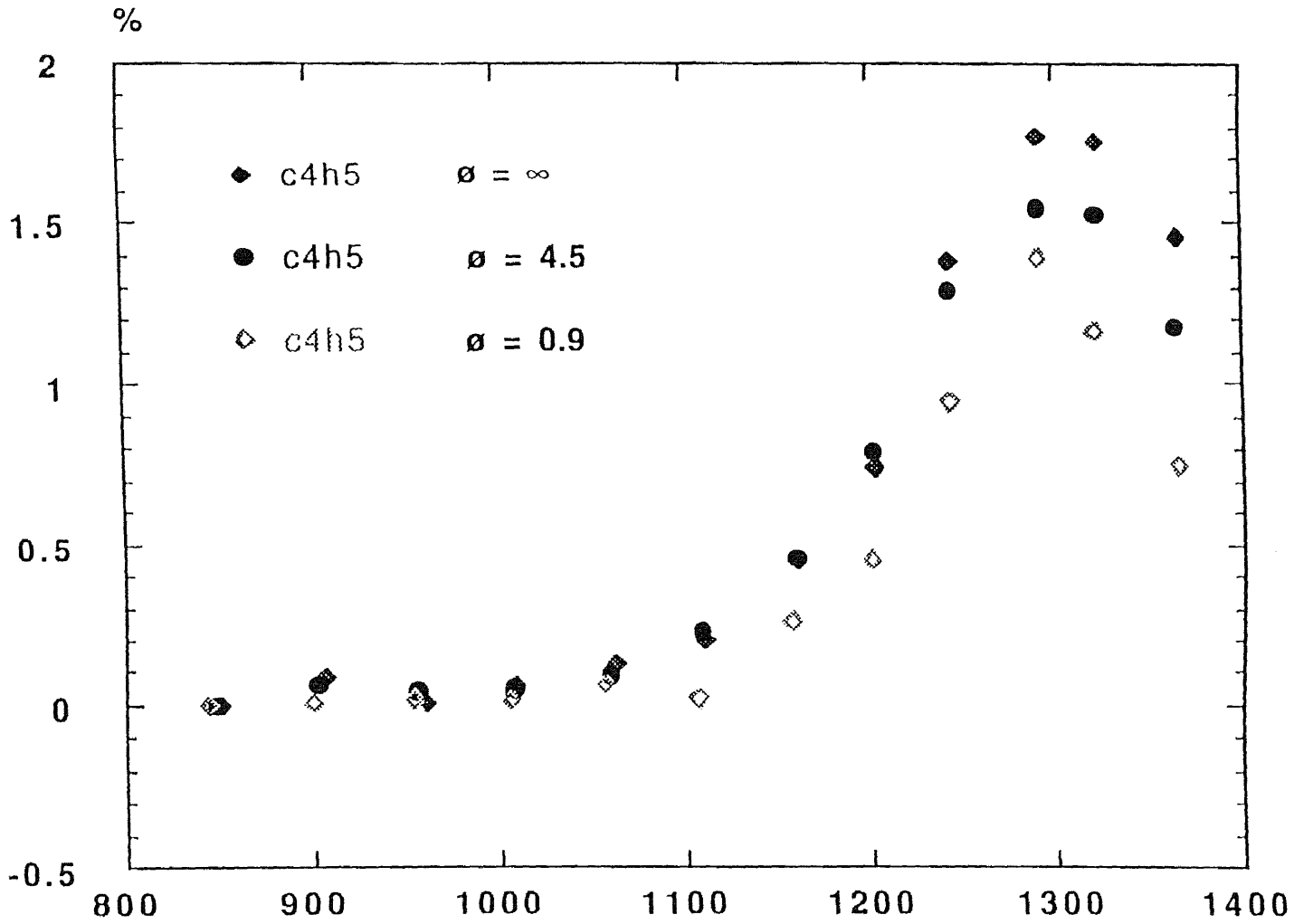

FIG. E10-10

butadiene concentration in 1-butene combustion

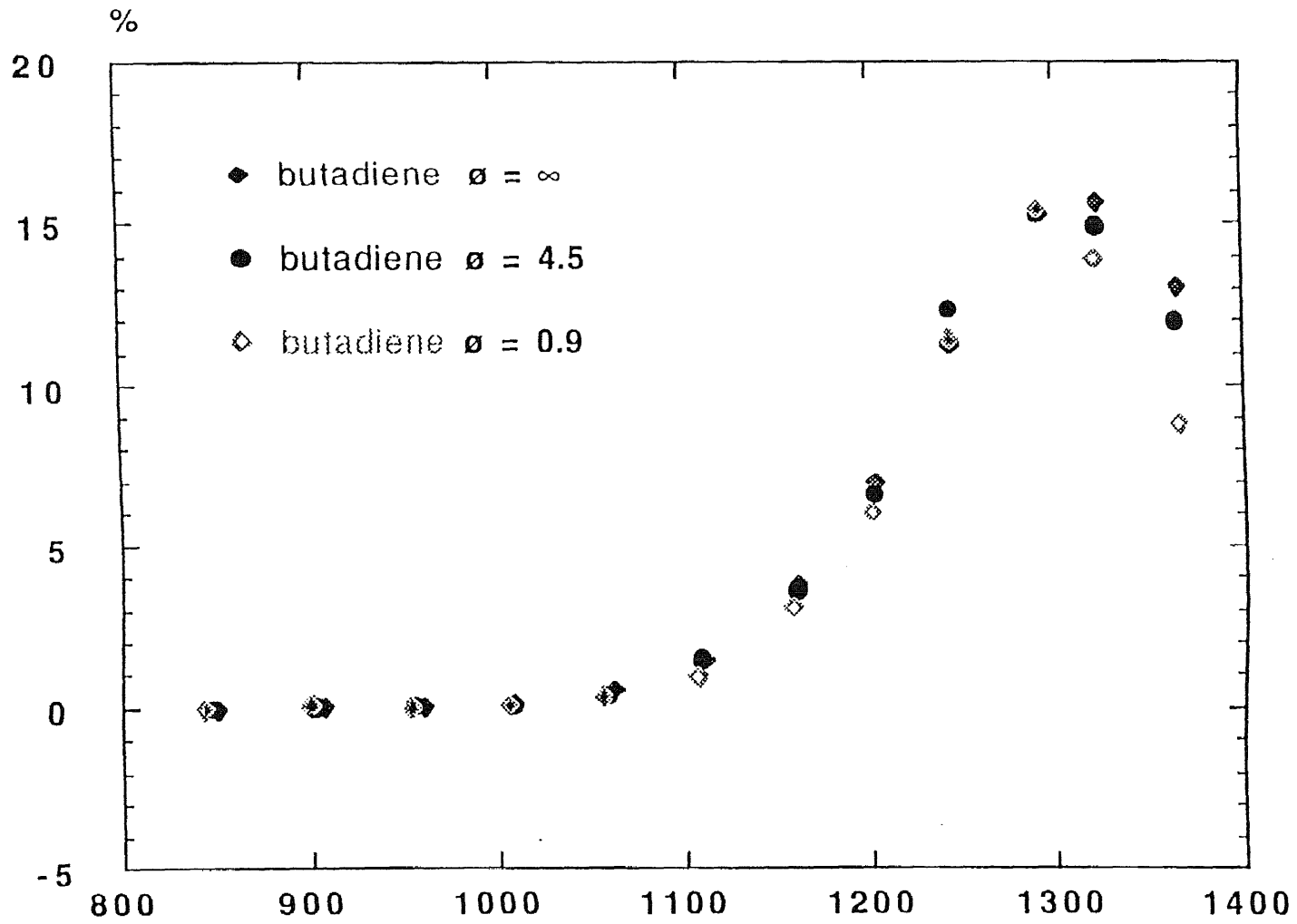

FIG. E10-11

butenyl radical concentration in 1-butene combustion

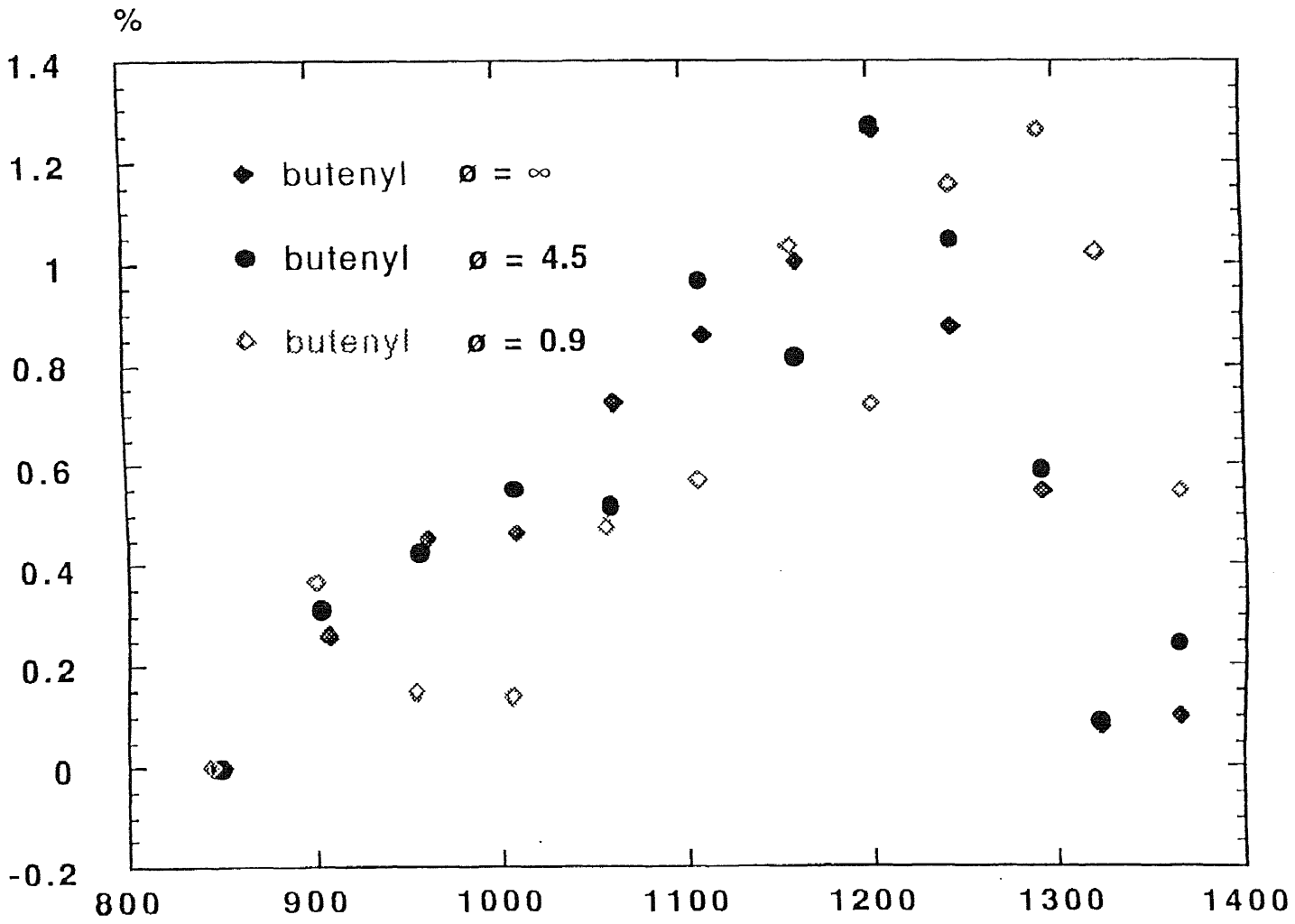

FIG. E10-12

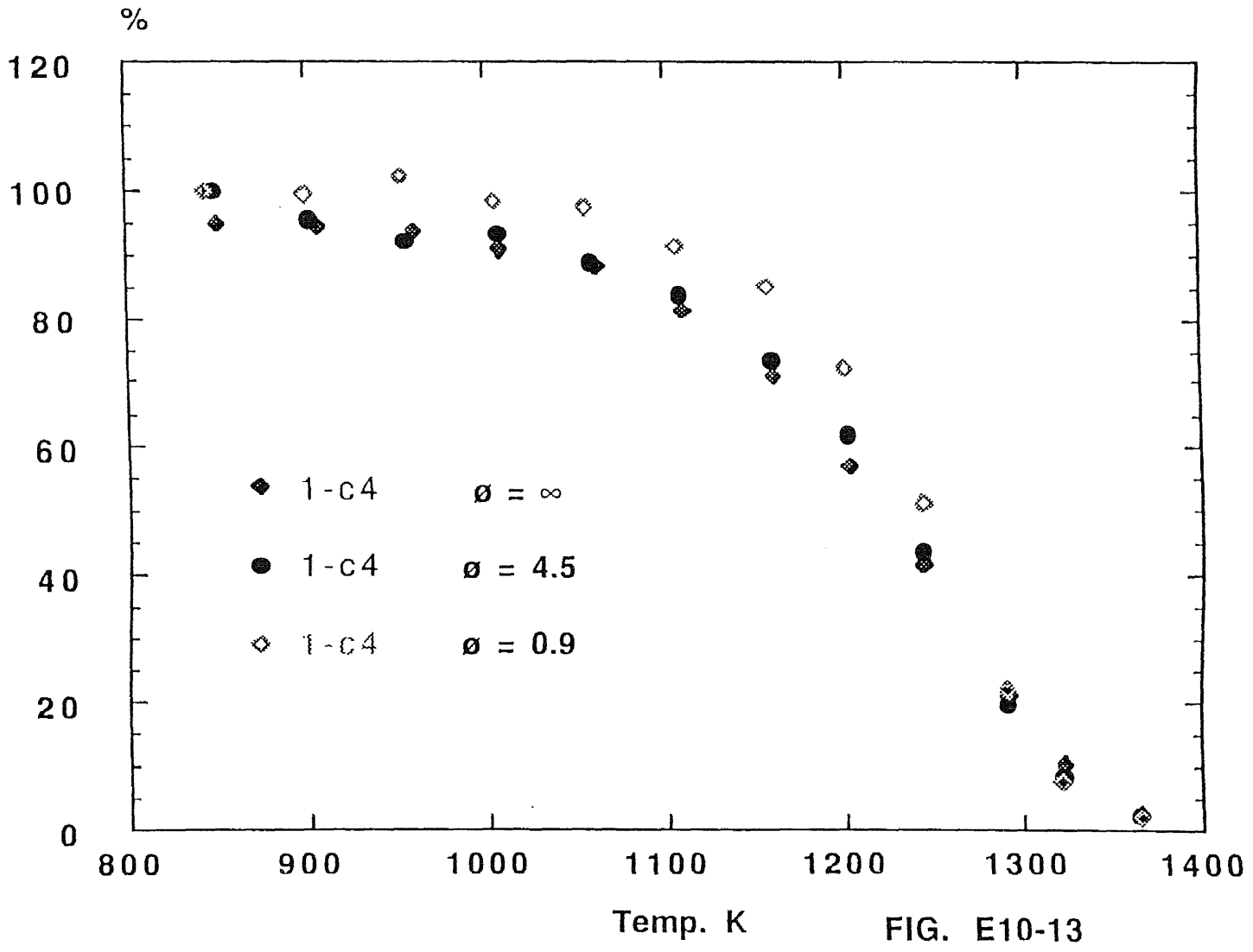
1-butene concentration in 1-butene combustion
%
120
100
80
60
40
20
0
800
900
1000
1100
1200
1300
1400
Temp. K
1-c4 ø = ∞
1-c4 ø = 4.5
1-c4 ø = 0.9

FIG. E10-13

pentadienyl radical concentration in 1-butene combustion

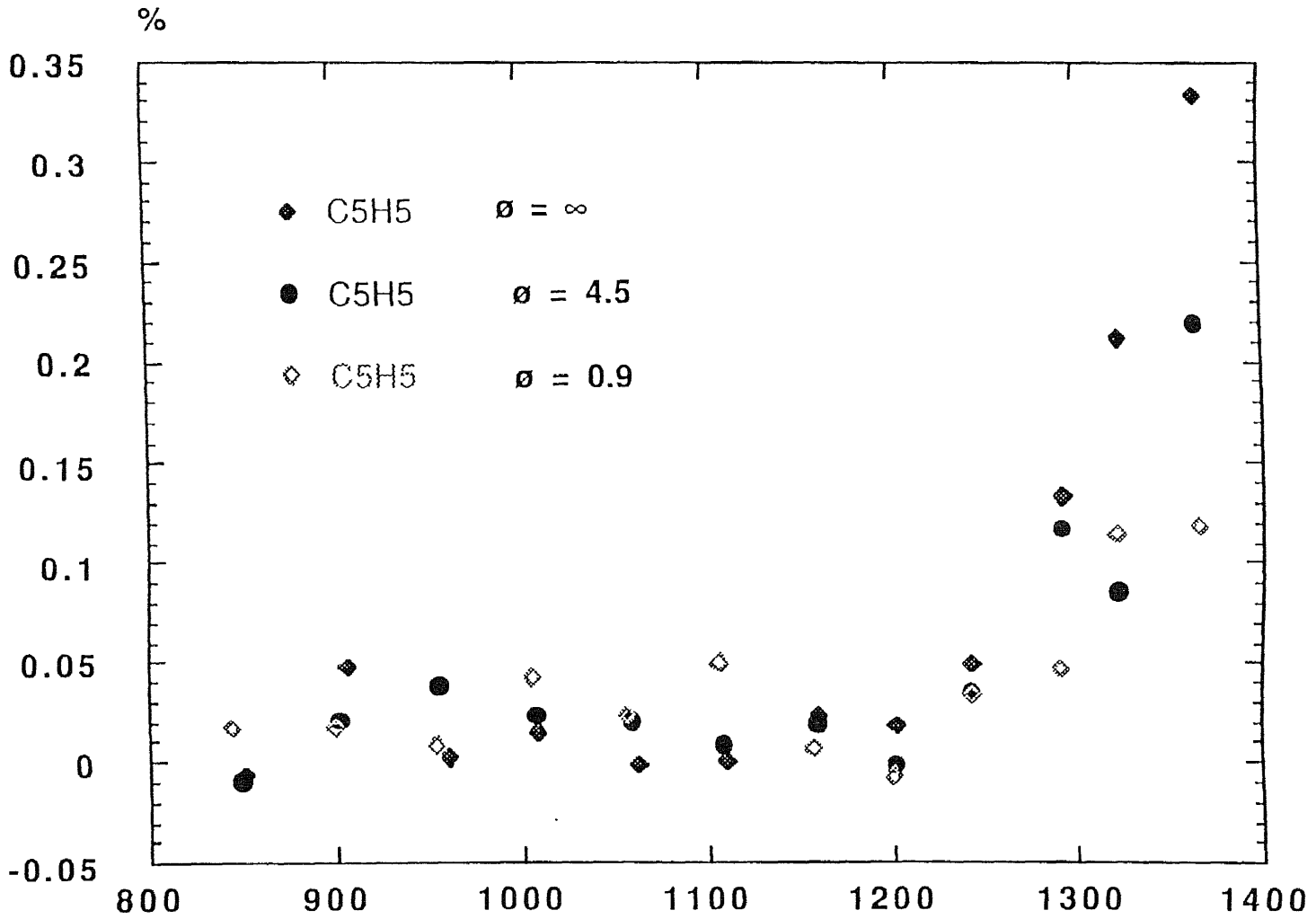

FIG. E10-14

pentadiene concentration in 1-butene combustion

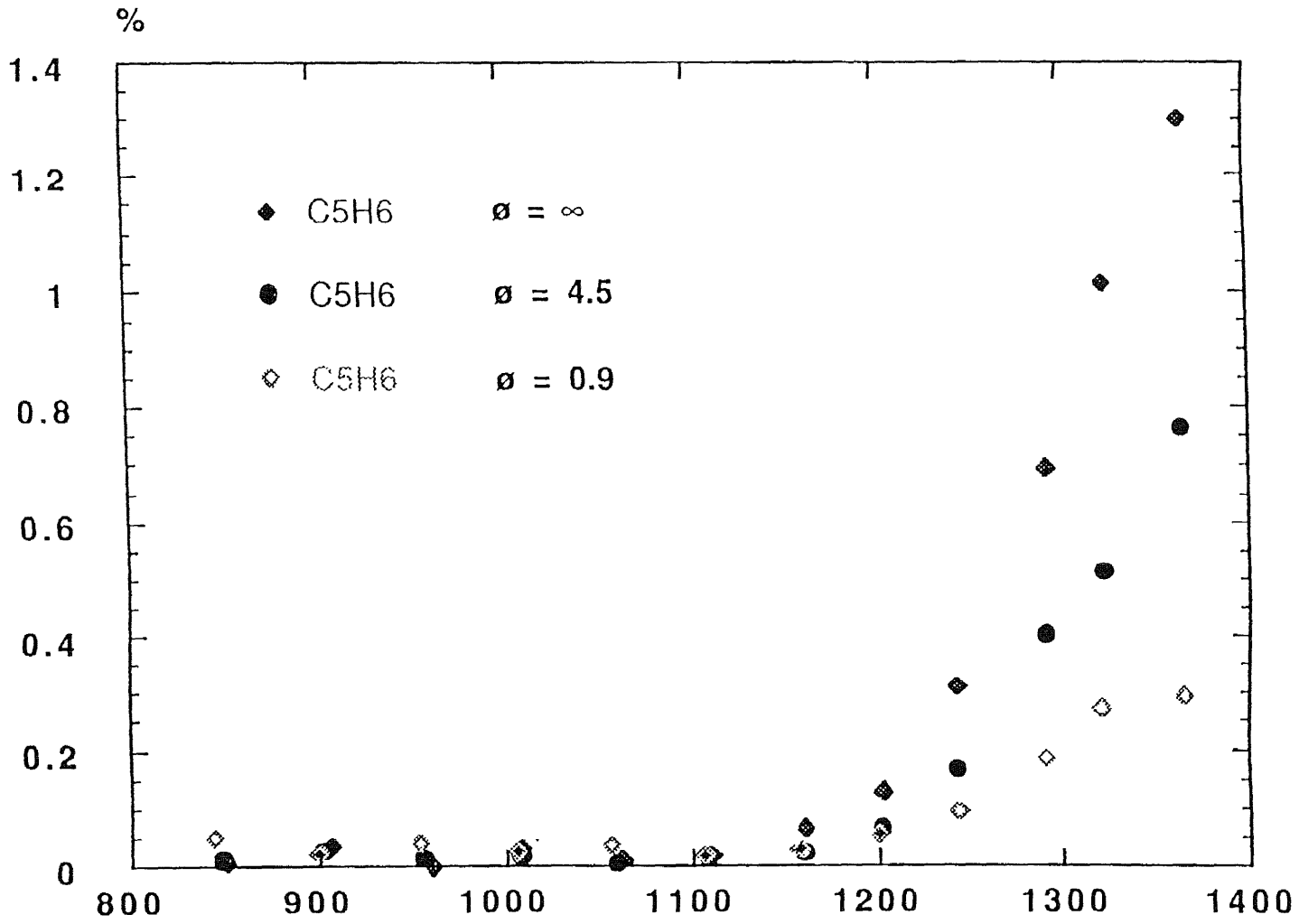

FIG. E10-15

cyclopentene concentration in 1-butene combustion

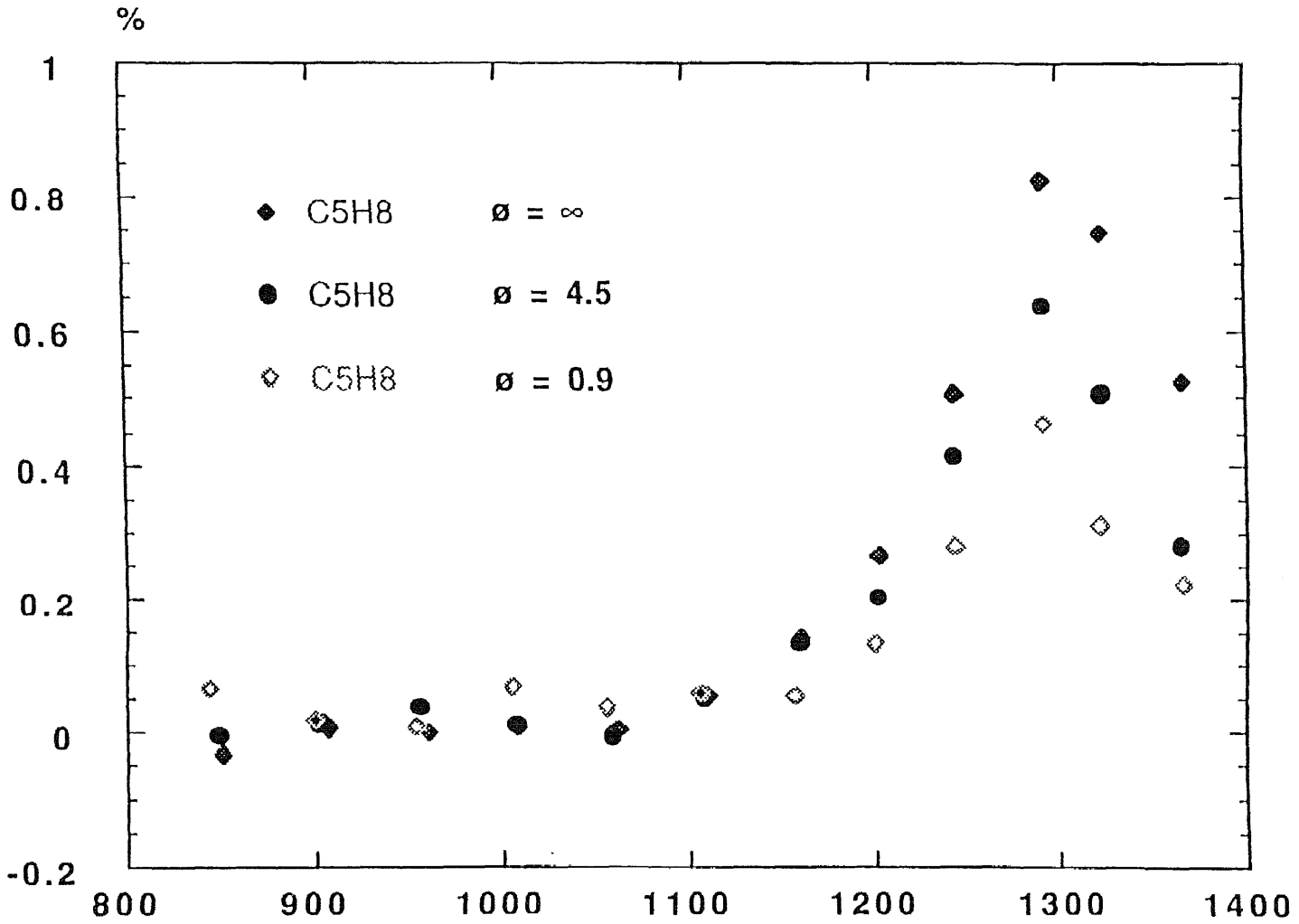

FIG. E10-16

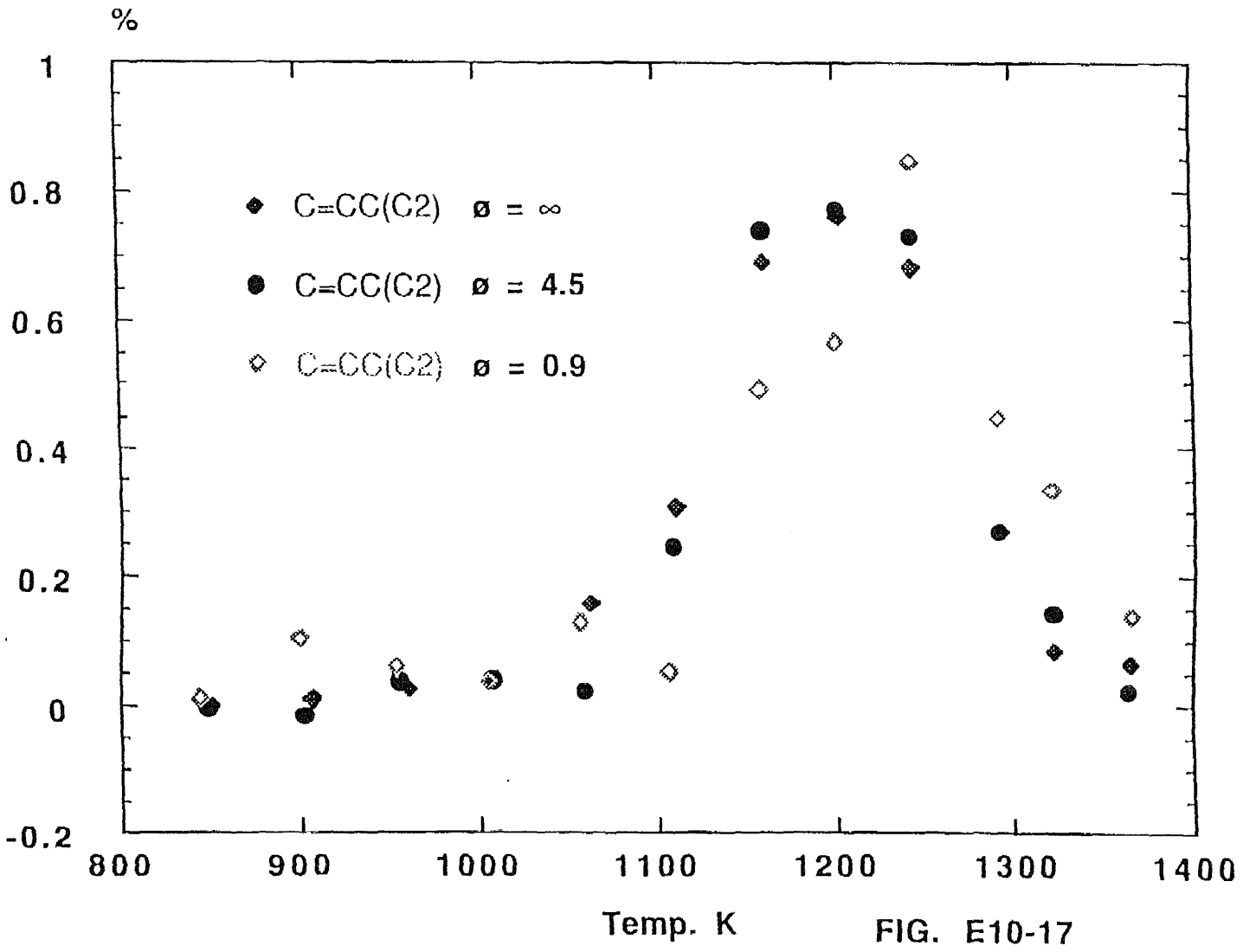
pentene concentration in 1-butene combustion
%
1
0.8
0.6
0.4
0.2
0
-0.2
C=CC(C2) ø = ∞
C=CC(C2) ø = 4.5
C=CC(C2) ø = 0.9
800
900
1000
1100
1200
1300
1400
Temp. K

FIG. E10-17

benzene concentration in 1-butene combustion

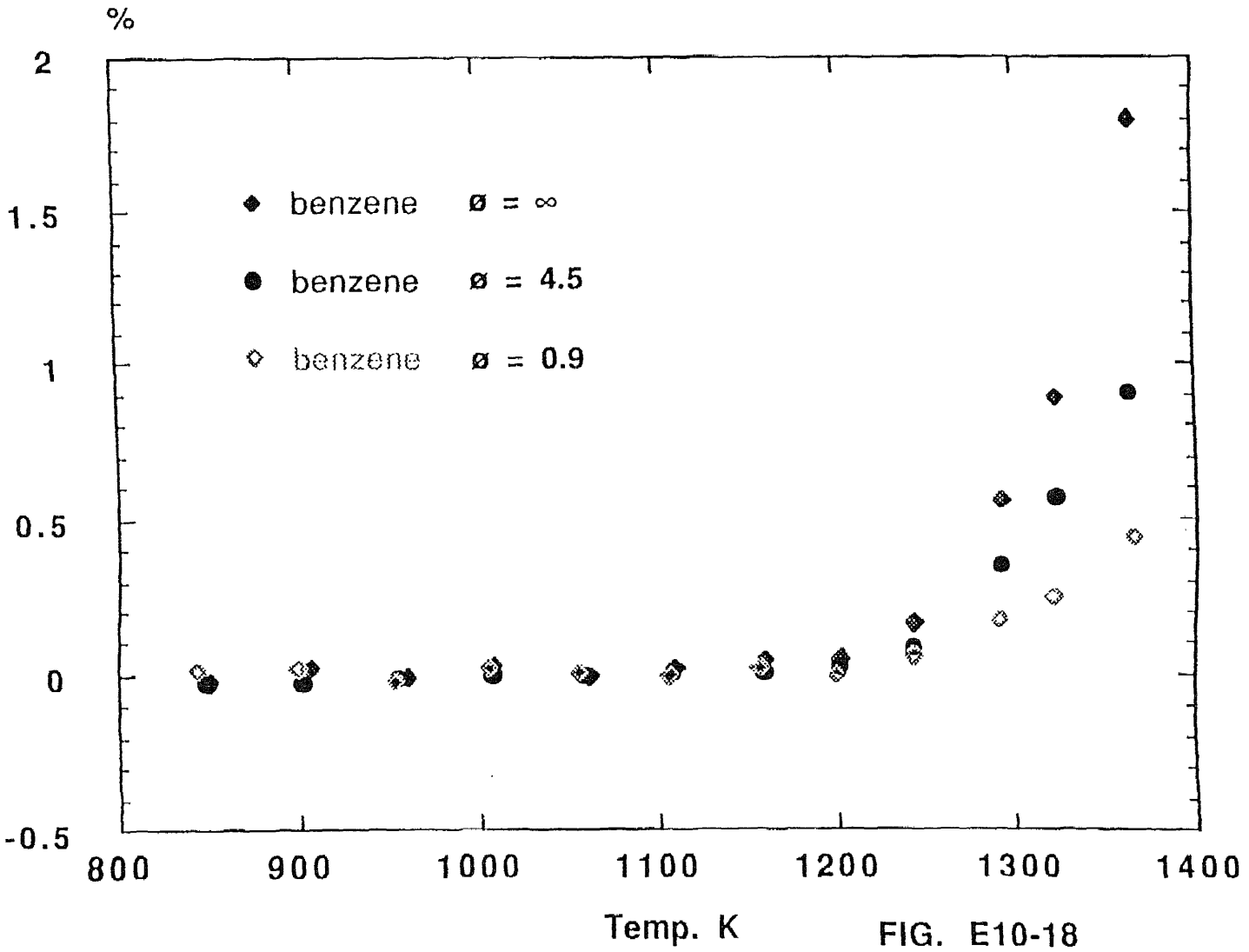

FIG. E10-18

Cyclohexene concentration in 1-butene combustion

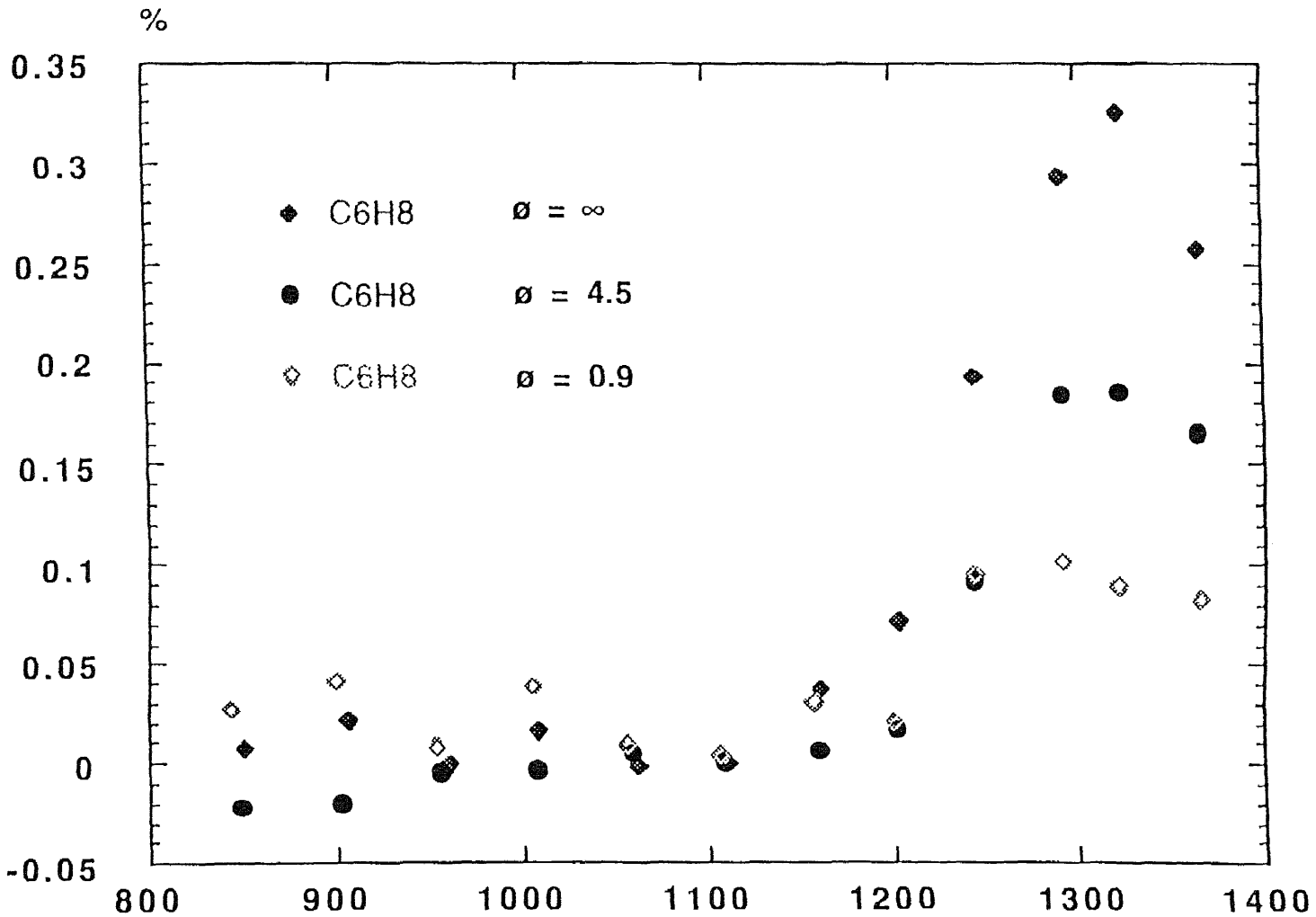

FIG. E10-19

C4H4 concentration in 1-butene combustion

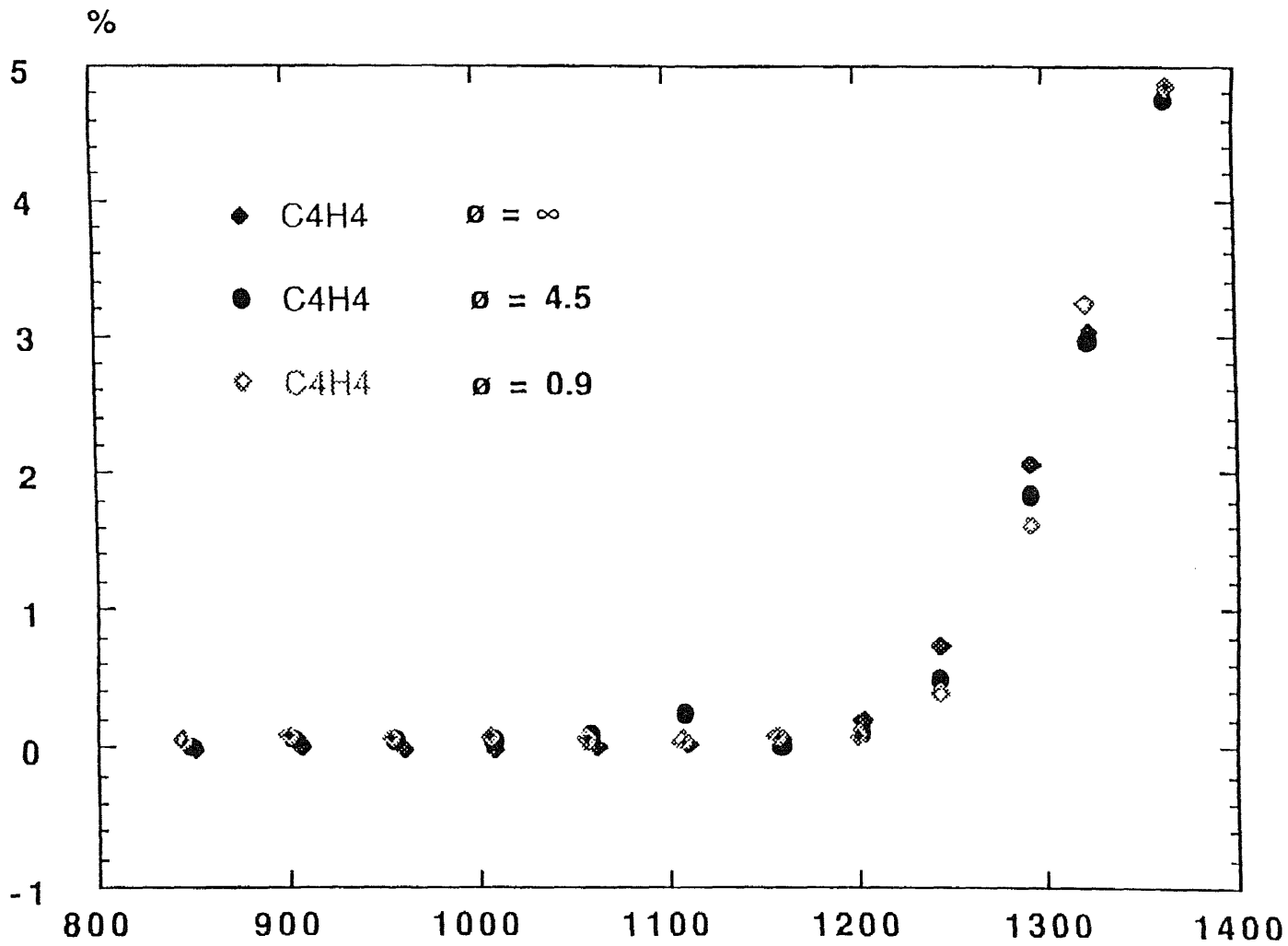

FIG. E10-20

was determinated by the internal standard species. For the stable species 1,3-butadiene, propylene, allene this equation just tell us what is the F factor and gives a proof of our basic concept. For ethylene we do not know it's photoionization cross section at high temperature, From this equation we can determinate that at 800 K to 1400 K the averaged relative photoionization cross section of ethylene is 0.1. For the radical we can apply the addition theory to calculate the Q from atomic data base. For the methyl radical we can determinate it's photoionization cross section by this equation. This data is actually a ensemble average. Once we assume this cross section coefficient is for the unpaired 2p electron on the carbon atom, we can apply the group addition theory to calculate the photoionization cross section of other radicals. We should understand that the ß factor determinated from data fitting would be the up limit and ∂ is the low limit. For the bigger radicals the photoionization cross section is not sensitive to the coefficient of the unpaired 2p electron on the carbon atom. Based on these parameter we can find the electron impact ionization cross section of radicals Table E 8-3. The agreement between group addition theory and experiment is very good. Now We can confidently say that we can measure the absolute concentration profile of radicals as well as stable species by the low energy photoionization cross section which given by the group addition theory. We will check the photoionization cross section of methyl radical again in azomethane pyrolysis both from the detail reaction model and experiment measurement.

Table.E 8-3

species	∂	β	Q (Obe)	Q (Cal)
CH3	0.1	1	3.7*	3.78
C2H3	0.1	1	4.58	4.63
C2H5	0.1	0.65	7.5	6.7
C3H3	1.12	1	6.9	5.5
C3H5	0.82	0.53	8.58	7.94
C4H5	1.3	0.65*	8.79	8.79
C4H7	0.86	0.25	10.28	10.82

9. Molecular Weight Growth

Radical-radical recombination reaction was dominate at high temperature radical pool. pentenes FIG. E 8-14 are formed from methyl radical and butenyl radical recombination and the cyclopentene formed from pentenyl. The reaction chain went down to cyclopentadiene FIG. E 8-17. Cyclopentenyl will equilibrium with cyclopentadiene in the rich H and methyl radical pool. At relative low temperature allyl radical recombination will produce cyclohexene, which will decay to benzene. at high temperature on the other hand propargyl radical will directly recombine to forming benzene. Once benzene state in the rich radical pool the H atom abstraction will form benzenyl radical, which in turn will reacted with methyl radical forming toluene. Xylenes are observed as this growth chain reaction.

10. Combustion

Oxidation products are observed in fuel lean ø = 0.86 (fuel/ oxygen (real) / fuel/ oxygen (stoichiometry)) condition. Mass 30, 42, 44 and 70 are observed in combustion reaction. The molecular weight growth procedure was slow down by the oxidation reaction. The flowing reaction channels are important to interpret the experiment results.

reaction channels:

H + O2 = O2H	1
52.1+ 0 3.5	
O2H + CH3 = CH3OOH	2
3.5 34.8 -32.68	
O2H + C2H5 = C2H5OOH	3
3.5 28.3 -40.8	
O2H + C4H7 = C*CCOOHC	4
3.5 32.2 -25.39	
O2H + C2H3 = C*COOH	5
3.5 66 -12.64	
O2H + C3H5 = C*CCOOH	6
3.5 41 - 14.28	

It is clear that reaction 1 is the initial chain reaction channel and when H atom was generated from pyrolysis reactions, the H atom was in the surrounding of O2, so this reaction channel will be the main consumption path of H atom. Reaction 2 to 6 are radical-radical recombination reactions which terminate the molecular weight growth reaction channels. The C5 and C6 products are reduced by these reactions (FIG. E 10- 14, 15, 16, 18, and 19). FIG.E

10-9 shows the Acetaldehyde formation in fuel lean combustion. However, mass 44 can also come from C2H5OOH, the VUV photon ionization procedure of C2H5OOH may be like this:

$$C2H5OOH + hv = [\ C2H5OOH^{+}\ ]\# + e \quad (\ m/z = 62\ )$$

$$[\ C2H5OOH^{+}\ ]\# = H2O + C2H4O^{+} \quad (\ m/z = 44\ )$$

Table E 5-1 gas phase hydrocarbon 70 eV electron impact ionization cross section

molecule	mass	Q(i) cal.	Q(i) obs.	Δ %
CH4	16	4.58	4.83	5.5
C2H2	26	3.4	3.4	-
C2H4	28	5.86	5.48	-6.5
C2H6	30	7.46	8.36	12
C*C*C	40	6.7	6.87	2.4
C*CC	42	8.74	8.68	-0.7
C3H8	44	10.34	11.92	15
C*CC*C	54	10.02	10.68	6.5
C*CCC	56	11.62	11.61	-
C*C(C2)	56	11.62	9.8	-15
CC*CC	56	11.62	12.8	10
CCCC	58	13.22	13.76	4
CC(C2)	58	13.22	14.45	9.3
NO [23]	30	2.5	2.5	-

BIBLIGRAPHY

1. Miller,J.A.; Bowman,C.T.Prog. Energy Combust. Sci. 1989, 15, 287-338

2. Wilk, R.D.; Pitz, W.J.; Westbrook, C.K.; Addagarla, S.; Miller, D. L.; Cernansky, N.P.; Green, R. M. In twenty-Third Symposium (International) on Combustion; The Combustion Institute: 1990; pp 1047-1053

3. Dean,A.M. J. Phys. Chem. 1990,94, 1432-39

4. M.S. Chou, Chem.Phys. Lett., 114, 279-281 (1984)

5. D.W. Squire, C.S.Dulcey and M.C.Lin, Chem. Phys. Lett., 116, 525-528 (1985)

6. D.S. Bomes, S. Dougal and R.L.Woodin, CR. 5B. 85

7. F.P Tully and J.E.M. Goldsmith, Chem.Phys. Lett., 116, 345-352 (1985)

8. J.W. Hastie, Pure and Appl. Chem., 56, 1583-1600 (1984)

9. J.B. Jeffries, J. A. McCaulley and F.A. Kaufman, Chem. Phys. Lett., 106, 111-116 (1984)

10. J.C. Brordi, C.P. Lazzara and J.F. Papp, Comb. and Flame, 23, 73-82 (1974)

11. A. Hoglund and L.G. Rosengren, Int. J. Mass Spectrom. Ion Proc., 60 173-187 (1984).

12. M. Kaufman and C.E. Kolb, Chem. Instrum., 3, 175-189 (1971)

13. J.D. Bittner, Ph.D. Thesis, MIT, 1981

14. K.H. Hoyermann, in " Physical Chemistry, " Vol. VIB, Ed. W. Jost, Academic, New York, 1975

15. C.J. Howard, J. Phys. Chem., 83, 3 (1979)

16. K.H. Homann and Ch. Wellmann, Ber. Bunsenges. Phys. Chem. 87, 527 (1983)

17. M.B. Colket, III, D.W.Neageli, and Glassman, Int. J. Chem. Kinet., 7, 223 (1975)

18. G.Rotzoll Int.J. Chem. Kine., 16, 1401-1426 (1984)

19. G.Rotzoll Int.J. Chem. Kine., 17, 637-653 (1985)

20. J.B.Anderson, R.P.Anders, and J.B.Fenn, Adv. in Chem .Phys . Vol.X Molecular beam

22. P.W.Geno Int J mass Spectro. and Ion Processes 92 (1989 195-210)

23. Willam L. Fltch, Andrew D. Sauter, Anul. Chem. 1983,55,832-835

24. L.L.Lohr,Jr., and M.B.Robin, J .Amer.Chem.Soc., Vol 92.No 25,1970

25. J. A. R. Samson, F.F. Marmo, and K. Watanabe, J. Chem. Phys. Vol.36,No.3, 1961

26. James C. Person and Paul P. Nicole, J. Chem. Phys. Vol.49,No.12, 1970

27. James C. Person and Paul P. Nicole, J. Chem. Phys. Vol.53,No.5, 1970

28. Albert C. Parr and Fred A. Elder, J Chem. Phys. Vol.49,No 6, 1968

29. G.Rotzoll, Int. J. Chem. Kinet., Vol. XIII, 39 (1981)